Afdelingen for Bærende Konstruktioner
Department of Structural Engineering
Danmarks Tekniske Højskole · Technical University of Denmark

A Failure Criterion for Normal and High Strength Concrete

Kaare K. B. Dahl

Serie R No 286 1992

A Failure Criterion for Normal and High Strength Concrete

Kaare K. B. Dahl

Juli 1992

A Failure Criterion for Normal and High Strength Concrete

Tryk:
Afdelingen for Bærende Konstruktioner
Danmarks Tekniske Højskole
Lyngby
ISBN 87-7740-106-9

Preface

This report has been prepared as one part of the thesis required to obtain the Ph.D. degree.

The thesis consists of the following three reports:

- **The Calibration and Use of a Triaxial Cell**
- **A Failure Criterion for Normal and High Strength Concrete**
- **A Constitutive Model for Normal and High Strength Concrete**

The thesis has been carried out at the Department of Structural Engineering, Technical University of Denmark, under the supervision of Professor, Dr.techn. M. P. Nielsen.

I wish to express my sincere thanks to my supervisor and the entire staff at the Department for their help during the time I have been here.

Finally I gratefully acknowledge the financial support granted by the structural research program 'High Performance Concretes in the 90'ies', which in turn is financed by the Danish Industri- og Handelsstyrelsen.

Frederiksberg 1992

Kaare K. B. Dahl

Summary

The Calibration and Use of a Triaxial Cell

This report describes in detail the equipment and techniques used for testing concrete in a triaxial cell. In a triaxial cell it is possible to induce a well defined triaxial stress field in a cylindrical test specimen. Not all possible combinations of stress fields can be generated in a triaxial cell, only stress fields where two of the three principal stresses are equal.

The subjects described in this report are the observations and conclusions, concerning the test equipment, of a major research program aimed at testing concrete under triaxial stresses. The major problems encountered were primarily how to generate a well defined triaxial stress field in a concrete cylinder, with the minor principal stresses in the range 0 to 140 MPa, and secondly how to measure the concrete strains at the same range of stresses.

The report pays particular attention to the following subjects:

1/ Describing the equipment needed for testing.
2/ Calibration of the test equipment.
3/ Preparing test specimens.
4/ Describing the adopted testing procedure.

A Failure Criterion for Normal and High Strength Concrete

This report deals with the strength of concrete subjected to stresses in more than one direction. The report describes a large test program aimed at determining a failure criterion for concrete, including high strength concrete. The concretes investigated were ordinary concretes with a varying uniaxial strength between 10 and 110 MPa.

A total of 240 test specimens were tested with the minor principal stress ranging between 0 and 140 MPa. All tests were conducted with all principal stresses compressive and the two minor principal stresses being equal. The tests were performed using a triaxial cell. The construction and use of this cell is described in detail in ***The Calibration and Use of a Triaxial Cell.***

The test results showed a large difference between the ultimate strength of low and normal strength concretes, especially for high relative stress loadings. The difference in ultimate strength of normal and high strength concrete was not large but still noticeable. The test results showed also a drastic change in the failure envelope when testing mortars and pastes, as compared to ordinary concrete.

The test results are compared to the Ottosen model, and the Mohr-Coulomb model. Both models are changed in order for them to reflect the new knowledge found in this investigation.

A Constitutive Model for Normal and High Strength Concrete

This report deals with the deformations of concrete subjected to stresses in more than one direction. The report describes a large test program aimed at determining a constitutive model for concrete, including high strength concrete. The concretes investigated were ordinary concretes with a varying concrete strength between 10 and 110 MPa.

The experimental investigation is an integral part of an investigation into the strength of concrete under multiaxial stresses as reported in ***A Failure Criterion for Normal and High Strength Concrete.*** In this investigation a total of 240 test specimens were tested with the minor principal stress ranging between 0 and 140 MPa. Of these 240 test specimens 91 were tested with strain gauges mounted. All the tests were conducted with the principal stresses compressive and the two minor principal stresses being equal. The tests were performed using a triaxial cell. The construction and use of this cell is described in detail in ***The Calibration and Use of a Triaxial Cell.***

The test results showed a surprisingly plastic behavior of the concretes under triaxial stresses. In the case of low strength concretes, deformations of more than 20% were experienced, and in the case of very high strength concretes, deformations of more than 8% were experienced.

Based on these test results an improvement of the Ottosen constitutive model is presented. The model is based on the non-linear elastic theory and is very simple and easy to use. The model has also been compared to experimental results from other investigations. Although widely different concrete strengths, test rigs, and load paths have been used in these investigations, it has been found that the model predicts the deformational behavior of concrete well within acceptable limits.

Resumé

The Calibration and Use of a Triaxial Cell

Denne rapport indeholder en detaljeret beskrivelse af det udstyr, og de teknikker der behøves for at kunne prøve beton i en triaxial celle. I en triaxial celle er det muligt at udsætte en beton cylinder for en forud fastlagt tre-akset spændingstilstand. Det er dog ikke muligt i en sådan celle, at frembringe en hvilken som helst tre-akset spændingstilstand, idet cellens opbygning gør, at to af de tre hovedspændinger altid vil være lige store.

I denne rapport er beskrevet de observationer og de konklusioner vedrørende forsøgsopstillingen, der er fremkommet under et større forskningsprogram rettet mod betons styrke og tøjningsforhold under tre-aksede spændingstilstande. De største problemer der opstod var, dels at kunne sikre en forud fastlagt spændingstilstand, hvor de mindste hovedspændinger var i området 0 til 140 MPa, og dels at kunne måle de tilsvarende tøjninger i betonen.

Rapporten beskriver indgående følgende emner:

1/ Beskrivelse af forsøgsopstillingen.
2/ Kalibrering af udstyret i forsøgsopstillingen.
3/ Den nødvendige forberedelse af prøvelegemer.
4/ Proceduren for den egentlige prøvning.

A Failure Criterion for Normal and High Strength Concrete

Denne rapport omhandler betons styrke, når denne er udsat for spændinger i mere end én retning. Rapporten beskriver et stort forsøgsprogram rettet mod at bestemme et brudkriterium for beton, inklusiv højstyrkebeton. De anvendte beton var normale betoner, med en én-akset styrke på mellem 10 og 110 MPa.

I alt blev 240 prøvelegemer afprøvet med den mindste hovedspænding varierende mellem 0 og 140 MPa. Alle forsøgene blev udført med trykspændinger overalt, og med de to mindste hovedspændinger lige store. Forsøgene blev udført i en triaxial celle. Opbygningen og brugen af denne celle er udførligt beskrevet i ***The Calibration and Use of a Triaxial Cell.***

Forsøgsresultaterne viste en afgørende forskel i den tre-aksede styrke for lavstyrke beton contra normalstyrke beton, specielt når de mindste hovedspænding steg i styrke. Forskellen mellem normal og højstyrke betoner viste sig ikke at være særligt stor, men dog ikke uden betydning. Sammenlignende forsøg med beton, mørtel og cement pasta viste, at der sker en drastisk forandring i brudfladens udseende når indholdet af det grove tilslag mindskes.

Forsøgsresultaterne er slutteligt sammenlignet med Ottosens brudkriterium, samt Mohr-Coulomb brudkriteriet. Begge brudkriterier er foreslået ændret, således at de nu reflekterer den nye viden fremkommet i dette projekt.

A Constitutive Model for Normal and High Strength Concrete

Denne rapport omhandler betons deformationer, når denne er udsat for spændinger i mere end én retning. Rapporten beskriver et stort forsøgsprogram rettet mod at bestemme en konstitutiv model for beton, inklusiv højstyrkebeton. De anvendte beton var normale betoner, med en én-akset styrke på mellem 10 og 110 MPa.

De, i denne rapport beskrevne forsøg, er en integreret del af en undersøgelse af betons styrke under fleraksede påvirkninger, som rapporteret i ***A Failure Criterion for Normal and High Strength Concrete***. I denne undersøgelse blev i alt 240 prøvelegemer afprøvet med den mindste hovedspænding varierende mellem 0 og 140 MPa. Af disse 240 prøvelegemer var 91 bestykket med strain gauges for at måle deformationerne. Alle forsøgene blev udført med trykspændinger overalt, og med de to mindste hovedspændinger lige store. Forsøgene blev udført i en triaxial celle. Opbygningen og brugen af denne celle er udførligt beskrevet i ***The Calibration and Use of a Triaxial Cell.***

Forsøgsresultaterne viste en overraskende plasticitet hos beton udsat for treaksede belastninger. Således blev der for lavstyrke beton målt deformationer over 20%, og for højstyrke beton målt deformationer over 8%.

På baggrund af resultaterne fra forsøgene er der foreslået en forbedring af Ottosens konstitutive model. Modellen er baseret på den ikke-lineære elasticitetsteori og er simpel i sin opbygning, samt nem at anvende. Modellen er også blevet sammenlignet med andre publicerede forsøgsresultater. Selvom der i disse undersøgelser er blevet benyttet meget forskellige betoner, forsøgsopstillinger samt belastningmåder, er det konstateret, at modellen forudsiger betons deformationer med meget begrænsede afvigelser.

List of contents

Notation

In this report standardized SI units and European symbols have been used. Any deviations from this are described in the text when they occur.

A	Parameter in the Ottosen model
B	Parameter in the Ottosen model
c	Cohesion
e	Unit vector along the hydrostatic axis
f_c	Uniaxial concrete strength
f_{cc}	Equal biaxial concrete strength
f_t	Uniaxial tensile strength
f_{tt}	Equal biaxial tensile strength
i	Unit vector in the deviatoric plane
I_1, I_2, I_3	Invariants of the stress tensor
J_1, J_2, J_3	Invariants of the deviatoric stress tensor
k	Material constant
K_1	Parameter in the Ottosen model, size factor
K_2	Parameter in the Ottosen model, shape factor
n_1, n_2, n_3	Principal axes
s_{ij}	Deviatoric stress field
s_1, s_2, s_3	Principal deviatoric stresses
δ	Kroneckers delta
θ	Angle in the deviatoric plane
ξ	Length of the hydrostatic part of the stress tensor
ρ	Length of the deviatoric part of the stress tensor
ρ_{com}	Length of the deviatoric part of the stress tensor (compression meridian)
ρ_{ten}	Length of the deviatoric part of the stress tensor (tensile meridian)
σ_1, σ_2, σ_3	Principal stresses (tension positive)
σ_m	Mean normal stress
σ_s	Separation strength
τ	Shear stress
μ	Coeficient of friction
φ	Internal-friction angle

Chapter 1

Introduction

A short historical outline of the development of the failure criterion for concrete, will be given in this chapter. Also presented is the scope of the investigation performed.

1.1 A short historical outline

The failure criterion for engineering materials in general, and for concrete in particular, has posed a challenging problem for scientists in the last 200 years.

It all started in 1773 when Coulomb formulated his very famous failure criterion. Although extremely simple, this failure criterion has been, and still is, much used, due to its simplicity, and relatively good accuracy when applied to concrete.

In the next 150 years the only major achievement in concrete failure criteria was the tension criterion proposed by Rankine in 1876. Although not nearly as accurate as the Coulomb criterion, it is still of some importance. This because, when combining the Rankine criterion with the Coulomb criterion, the accuracy of the resulting model is increased. In the same period failure criteria for other engineering materials, such as steel, were formulated. The best known of these is the von Mises' criterion (1913).

In the last 50 years formulation of a failure criterion for concrete has taken a giant step forward. Many researchers have proposed better and better failure criteria. The research has generally taken two paths. One path has been to modify the simple Coulomb criterion, like Hobbs [74.1]. The other path has been to propose more and more complex criteria, culminating with the 24 parameter constitutive model of Chen and Mau [89.1].

The last two decades have also seen developments in other areas of concrete research. When earlier a concrete strength of 30 MPa was looked upon as a strong concrete, we now have expanded the concrete strength to include 100 MPa concretes. These concrete strengths are far from theoretical laboratorial strengths. They are indeed used in many places all over the

world. The latest news is that Finland have expanded their code to include concrete up to 100 MPa in strength, and are now commercially using this strength in, among other things, prefabricated prestressed beams.

1.2 The scope of the investigation

In view of the development in the concrete strength, the scope of this investigation has been to determine the failure criterion for concrete, with an emphasis on concrete with a high uniaxial compressive strength. As stated earlier, many researchers have previously tested concrete triaxially for many years. However, the conclusions, and the failure criteria, developed from these investigations have a number of shortcomings. The major shortcoming is the lack of span in the concrete strength, along with the often small range of major principal stresses investigated.

The main part of the previous investigations have dealt with low and normal strength concrete, that is a uniaxial concrete strength between 10 and 30 MPa. These concretes have been extensively tested with the major principal stress in the range 0 to 2 times the concrete strength, and in some investigations up to 7 times the concrete strength.

The highest concrete strength, reported used in triaxial tests, has, to this author's knowledge, been 73 MPa, see also [90.1]. The best test series reported on any higher concrete strength, are the probably the investigation of Bellotti and Ronzoni [84.1]. They tested a 56 MPa concrete with the major principal stresses in the range 0 to 35 MPa.

Since we now are capable of producing, also on a commercial scale, concretes with compressive strength of more than 100 MPa. It is therefore imperative that this, in many ways new material, is investigated properly, rather than blindly extrapolating previous test results in order for the existing failure criteria to include high strength concrete.

On basis of the discussion above, it was decided that the investigation should center on the following problems:

1/ To investigate the triaxial strength of concrete, with the concrete strength varying from 10 to 100 MPa.

2/ To establish a simple failure criterion based on Coulomb's failure criterion for concrete. This modification is to be suitable for manual calculations.

3/ To establish a more accurate failure criterion based on Ottosen's failure criterion. This failure criterion is to be suitable for more complex calculations.

4/ To investigate the influence of aggregate size on the triaxial strength of concrete.

Chapter 2

Description of previous failure criteria

A failure criterion is not, as the name suggest, a criterion for determining when a material fails, but rather a criterion for determining the peak loading capacity of the material. Sometimes, when treating concrete under triaxial loading, a failure criterion is also a criterion for determining the yield stress of the concrete. This because when loading concrete under very high stresses, the deformations become very large, sometimes greater than 25%.

The names 'ultimate strength criterion', or 'yield criterion' might therefore be more appropriate than the name failure criterion. However, in order not to confuse things, the name 'failure criterion' will be used exclusively in this report.

Furthermore will the convention that tension is assumed positive, be used throughout the report. As a consequence, $0 > \sigma_1 > \sigma_2 > \sigma_3$ corresponds to a stress state where all stresses are compressive. The major principal stress is then σ_1, and the minor principal stress is σ_3.

This chapter will start with a brief introduction to the derivation of the stress invariants. Following this will be a list of the general accepted evidence concerning the failure envelope for concrete, and finally will the Mohr-Coulomb, and the Ottosen failure criteria be presented in detail.

2.1 Stresses and stress invariants

When dealing with failure criteria for concrete, it is usually assumed that the material is homogeneous and isotropic. When the size of the aggregate is considerably smaller than the dimension of the concrete specimen, this is normally also the case. In the basic sense the ultimate strength of concrete can then only be a function of the stresses.

$$f(\sigma_{ij}) = 0 \tag{2.1}$$

Since the stresses can be uniquely described by the principal stresses, σ_1, σ_2, σ_3, and the principal vectors, n_1, n_2, n_3, the failure criterion can then be written as in eq. (2.2).

$$f(\sigma_1, \sigma_2, \sigma_3, n_1, n_2, n_3) = 0 \tag{2.2}$$

Since it is assumed initially that concrete is isotropic, it follows that the failure criterion must be independent of the principal vectors. Eq. (2.2) therefore reduces to eq. (2.3).

$$f(\sigma_1, \sigma_2, \sigma_3) = 0 \tag{2.3}$$

Rather than expressing the failure criterion as a function of the principal stresses, it is possible to express the criterion as a function of the stress invariants, I_1, J_2, and J_3, as in eq. (2.4).

$$f(I_1, J_2, J_3) = 0 \tag{2.4}$$

These stress invariants can be calculated on basis of the actual stress field, whereas determination of the principal stresses requires solution of an eigenvalue problem. A failure criterion based on eq. (2.4) will therefore in many cases lead to more simplified calculations than a failure criterion based on eq. (2.3).

2.1.1 The stress invariants

Consider a stress field given by eq. (2.5).

$$\sigma_{ij} = \begin{pmatrix} \sigma_x & \tau_{xy} & \tau_{xz} \\ \tau_{yx} & \sigma_y & \tau_{yz} \\ \tau_{zx} & \tau_{zy} & \sigma_z \end{pmatrix} \tag{2.5}$$

The principal stresses can be found as the solution to eq. (2.6), where δ_{ij} is Kroneckers delta.

$$|\sigma_{ij} - \sigma\delta_{ij}| = 0 \tag{2.6}$$

Eq. (2.6) yields eq. (2.7), which is a cubic equation in σ.

$$\sigma^3 - I_1\sigma^2 + I_2\sigma - I_3 = 0 \tag{2.7}$$

In this equation, the roots are the principal stresses, σ_1, σ_2, σ_3, and I_1, I_2, and I_3, are called the invariants of the stress tensor, and are defined by eq. (2.8).

$$\begin{aligned} I_1 &= \sigma_{ii} = \sigma_x + \sigma_y + \sigma_z \\ I_2 &= \sigma_x\sigma_y + \sigma_y\sigma_z + \sigma_z\sigma_x - \tau_{xy}^2 - \tau_{yz}^2 - \tau_{zx}^2 \\ I_3 &= \begin{vmatrix} \sigma_x & \tau_{xy} & \tau_{xz} \\ \tau_{yx} & \sigma_y & \tau_{yz} \\ \tau_{zx} & \tau_{zy} & \sigma_z \end{vmatrix} \end{aligned} \tag{2.8}$$

The invariants can be written in a more simple form, by using that the shear stresses equal zero in the plane defined by the principal stresses. Eq. (2.8) then reduces to eq. (2.9).

$$\begin{aligned} I_1 &= \sigma_1 + \sigma_2 + \sigma_3 \\ I_2 &= \sigma_1\sigma_2 + \sigma_2\sigma_3 + \sigma_3\sigma_1 \\ I_3 &= \sigma_1\sigma_2\sigma_3 \end{aligned} \tag{2.9}$$

Instead of using the three principal stresses, it is possible to work with two stress fields. These are the 'hydrostatic' stress field, and the 'deviatoric' stress field. The hydrostatic stress field is defined as a stress field where the three principal stresses are equal, and the deviatoric stress field is defined as a state of pure shear. The definition of the two stress fields are given in eq. (2.10) and (2.11) respectively.

$$\sigma_m = \frac{1}{3}(\sigma_1 + \sigma_2 + \sigma_3) = \frac{1}{3} I_1 \tag{2.10}$$

$$s_{ij} = \sigma_{ij} - \sigma_m\delta_{ij} \tag{2.11}$$

Similar to deriving the invariants of the stress tensor, it is possible to derive the invariants of the deviatoric stress tensor. Consider eq. (2.12).

$$|s_{ij} - s\delta_{ij}| = 0 \tag{2.12}$$

The solution of eq. (2.12) follows the solution of eq. (2.6), and the invariants of the deviatoric stress tensor is then given in eq. (2.13).

$$J_1 = s_1 + s_2 + s_3 = 0$$

$$J_2 = \frac{1}{2}\left(s_1^2 + s_2^2 + s_3^2\right) = \frac{1}{6}\left[(\sigma_1 - \sigma_2)^2 + (\sigma_2 - \sigma_3)^2 + (\sigma_3 - \sigma_1)^2 \right]$$

$$J_3 = \frac{1}{3}\left(s_1^3 + s_2^3 + s_3^3\right) = s_1 s_2 s_3 \qquad (2.13)$$

where:

$$\begin{bmatrix} s_1 \\ s_2 \\ s_3 \end{bmatrix} = \begin{bmatrix} \sigma_1 - \sigma_m \\ \sigma_2 - \sigma_m \\ \sigma_3 - \sigma_m \end{bmatrix}$$

2.1.2 Using the stress invariants

The failure criterion describes a surface in a cartesian coordinate system with the axes σ_1, σ_2, and σ_3. Any point, **P**, on the failure surface, can either be described by the coordinates, σ_1, σ_2, and σ_3, or alternatively by two vectors **ON**, **NP**, and an angle θ, as shown in Fig. 2.1. The hydrostatic axis is now defined as the diagonal in the stress space, which has equal distances from the three axes. It then follows that every point on the diagonal is characterized by $\sigma_1=\sigma_2=\sigma_3$, and the unit vector **e** along the diagonal is given by eq. (2.14).

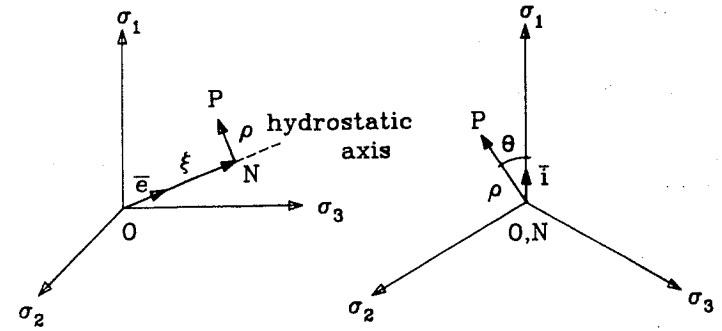

Fig. 2.1: Describing a point in the stress space by two vectors and an angle.

Any plane perpendicular to the hydrostatic axis is called a deviatoric plane. It is therefore

$$\bar{e} = \frac{1}{\sqrt{3}}[1 \quad 1 \quad 1] \qquad (2.14)$$

possible to resolve the vector **OP** into two vectors, **ON** along the hydrostatic axis, and **NP** in the plane perpendicular to the hydrostatic axis. The vector **ON** is lying on the hydrostatic axis, and the length of **ON**, ξ, is then given by eq. (2.15).

$$\xi = |\overline{ON}| = \overline{OP} \cdot \bar{e} = [\sigma_1 \ \sigma_2 \ \sigma_3] \cdot \frac{1}{\sqrt{3}} \begin{bmatrix} 1 \\ 1 \\ 1 \end{bmatrix} = \frac{1}{\sqrt{3}} I_1 \qquad (2.15)$$

The vector **NP** is situated in a deviatoric plane perpendicular to the hydrostatic axis, and the length, ρ, is given by eq. (2.16).

$$\overline{NP} = \overline{OP} - \overline{ON} = [\sigma_1 \ \sigma_2 \ \sigma_3] - [\sigma_m \ \sigma_m \ \sigma_m] = [s_1 \ s_2 \ s_3]$$
$$\rho = \sqrt{|\overline{NP}|^2} = \sqrt{s_1^2 + s_2^2 + s_3^2} = \sqrt{2\,J_2} \qquad (2.16)$$

If **i** is a unit vector in the deviatoric plane, and **i** is situated along the projection of the σ_1-axis on the deviatoric plane, as shown in Fig. 2.1, then **i** and θ will be given as stated in eq. (2.17).

$$\bar{i} = \frac{1}{\sqrt{6}}[2 \quad -1 \quad -1] \qquad (2.17)$$

$$\overline{NP} \cdot \bar{i} = \rho \cos\theta$$

Using eq. (2.16) and (2.17), $\cos\theta$ is then given by eq. (2.18).

$$\cos\theta = [s_1 \ s_2 \ s_3] \cdot \frac{1}{\sqrt{6}} \begin{bmatrix} 2 \\ -1 \\ -1 \end{bmatrix} \cdot \frac{1}{\sqrt{2\,J_2}} = \frac{2\sigma_1 - \sigma_2 - \sigma_3}{2\sqrt{3}\sqrt{J_2}} \qquad (2.18)$$

Finally it is possible to use the trigonometric identity, eq. (2.19), and thereby get the final equation for $\cos\theta$, as stated in eq. (2.20).

$$\cos 3\theta = 4\cos^3\theta - 3\cos\theta \qquad (2.19)$$

$$\cos 3\theta = \frac{3\sqrt{3}\,J_3}{2\,J_2^{3/2}} \qquad (2.20)$$

Another way of utilizing the identity (2.19), is to compare it with eq. (2.7) and (2.12). By doing so it is possible, se Chen [82.1], to define the three principal stresses of s_{ij} and σ_{ij} as in eq. (2.21).

$$\begin{bmatrix} s_1 \\ s_2 \\ s_3 \end{bmatrix} = \begin{bmatrix} \sigma_1 \\ \sigma_2 \\ \sigma_3 \end{bmatrix} - \begin{bmatrix} \sigma_m \\ \sigma_m \\ \sigma_m \end{bmatrix} = \frac{2}{\sqrt{3}} \sqrt{J_2} \begin{bmatrix} \cos\theta \\ \cos\left(\theta - \frac{2}{3}\pi\right) \\ \cos\left(\theta + \frac{2}{3}\pi\right) \end{bmatrix} \qquad \textit{for } 0 \le \theta \le \tfrac{1}{3}\pi \qquad (2.21)$$

2.2 Properties of the failure surface

The general shape of the failure surface in the σ_1, σ_2, σ_3, coordinate system, can best be described by the shape, or the cross-section, of the failure surface in the deviatoric plane, and the development of the cross-section along the hydrostatic axis.

Regarding the cross-section of the failure surface, the following argument can be applied. Assuming that concrete is an isotropic material, as stated earlier in this chapter, the labels attached to the coordinate axes are therefore arbitrary. It then follows that the failure surface must have a threefold symmetry, as shown in Fig 2.2, and it is therefore only of interest how the failure surface develops for θ in the interval $0 \le \theta \le 60°$.

In order to describe the development of the cross-section along the hydrostatic axis, meridians are used. A meridian is the intersection curve of the failure surface and a plane containing the hydrostatic axis. The plane is then characterized by a constant angle θ. Two meridians are of extreme importance, the compressive meridian, and the tensile meridian.

The stress state along the compressive meridian consists of a one-directional compressive stress superimposed upon a hydrostatic stress state. This corresponds to a stress state as given in eq. (2.22). Most of the test data so far lies on this meridian, and includes the uniaxial compressive strength, f_c, and the equal biaxial tensile strength, f_{tt}.

$$\sigma_1 = \sigma_2 > \sigma_3 \qquad \textit{tension positive} \qquad (2.22)$$

The other meridian of interest is the tensile meridian. The stress state along this meridian consists of a one-directional tensile stress superimposed upon a hydrostatic stress state. This corresponds to a stress state as given in eq. (2.23). Test data along this meridian are rather scarce, due to the difficulties in applying tensile loads to the concrete specimen. Data on the

tensile meridian includes the uniaxial tensile strength, f_t, and the equal biaxial compressive strength, f_{cc}.

$$\sigma_1 > \sigma_2 = \sigma_3 \qquad \textit{tension positive} \qquad (2.23)$$

These two meridians are important. This because for a given major principal stress, they give the extreme values of the load capacity for a varying intermediate principal stress. The compression meridian thereby gives the smallest load capacity, because the major and the intermediate principal stresses are equal. The tensile meridian gives the highest load capacity, because the minor and the intermediate principal stresses are equal.

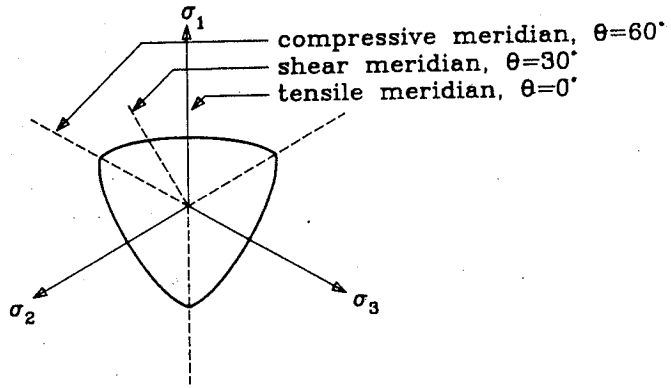

Fig. 2.2: Cross-section of the failure surface in the deviatoric plane.

Based on the symmetrical properties, the knowledge of the meridians, and the experimental results, the following general characteristics of the failure surface can be summarized, see also Ottosen [77.1]:

1/ The cross-section of the failure surface in the deviatoric plane is periodic, with a period of 60°, and a starting value of 0.
2/ The cross-section of the failure surface in the deviatoric plane is smooth.
3/ The cross-section of the failure surface in the deviatoric plane is convex, at least for compressive stresses.
4/ The cross-section of the failure surface in the deviatoric plane has a shape as shown in principle in Fig. 2.2.

5/ The cross-section of the failure surface in the deviatoric plane is nearly triangular for tensile and small compressive stresses, and becomes more and more circular for higher compressive stresses.

6/ The failure surface is open ended, so that pure hydrostatic pressures cannot cause failure. Tests have been reported up to I_1=-79 f_c, without any tendency for the meridian to approach the hydrostatic axis.

7/ The failure surface, when normalized by the uniaxial compressive strength, f_c, seems independent of f_c, when the stresses are compressive.

8/ The ratio ρ_{ten}/ρ_{com} increases from approximately 0.5 at low hydrostatic stresses, but remains less than unity.

Any proposed failure criterion must therefore respond to these properties. It is obvious that it is mathematically possible to develop a series of equations that together will result in a failure surface having all of the above properties. The particular choice of one model over the other will therefore depend on the following criteria

1/ The model should yield close fit of accepted experimental data in the range of stresses likely to occur in a structure. For more theoretical experimental test data, that is extremely large stresses, the model should respond without excessive deviations.

2/ The number of parameters should be kept low, and the parameters should be readily obtainable from standard concrete tests.

3/ The resulting failure surface should be continuously smooth, and differentiable.

4/ The cross-section of the failure surface in the deviatoric plane should be convex.

Furthermore should the resulting model be mathematically simple, and other more simple models, as the Drucker and Prager or the von Mises' models should be special cases of the proposed model. A more detailed description of these criteria can be found in Chen [82.1].

2.3 Mohr-Coulomb failure criterion

Formulated in 1773 the Mohr-Coulomb failure criterion is the classical failure criterion used in many applications. The Mohr-Coulomb failure criterion is developed from the friction hypothesis, which states that there exist only two different failure modes, the sliding failure, and the separation failure.

The sliding failure is assumed to occur, when the shear-stress, $|\tau|$, exceeds the sliding resistance. The sliding resistance is determined from two material constants, c, which is the

cohesion of the material, and μ, which is the coefficient of friction. Any stress normal to the failure plane will influence the ultimate shear stress, that is a compression stress will raise the sliding resistance, and a tensile stress will diminish the sliding resistance. The failure criterion can then be formulated as eq. (2.24).

$$|\tau| = c - \mu\sigma \tag{2.24}$$

Normally the internal-friction angle, φ, is used instead of μ. Using that φ is given by $\tan\varphi=\mu$, eq. (2.24) then becomes eq. (2.25).

$$|\tau| = c - \sigma \tan\varphi \tag{2.25}$$

The second failure type, the separation failure, is assumed to occur when the tensile stress, σ, reaches the separation strength, that is when

$$\sigma = \sigma_s \tag{2.26}$$

The failure envelope given by eq. (2.25) and (2.26) can be depicted in a (σ,τ) coordinate system, as shown in Fig. 2.3.

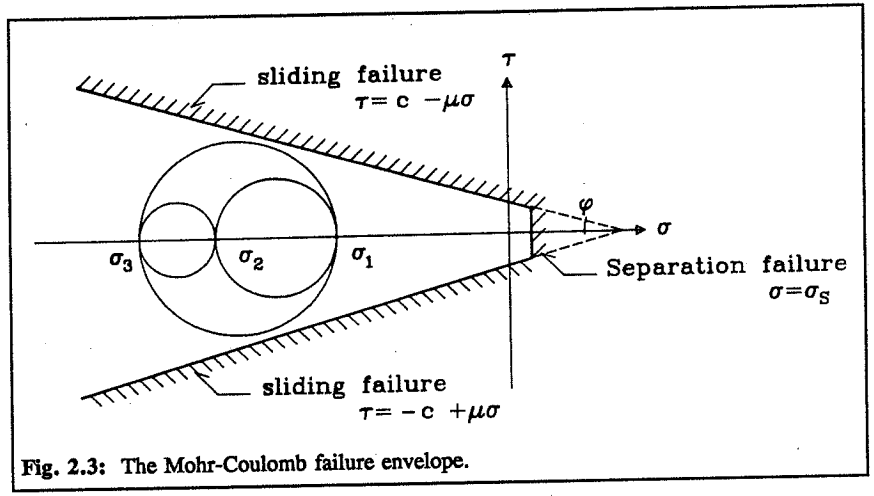

Fig. 2.3: The Mohr-Coulomb failure envelope.

If Mohr's circles are depicted together with the failure envelope, failure will occur when one of the straight lines becomes tangent to one of the circles. The worst possible combination of stresses is then seen to be when the intermediate principal stress is ignored. This gives the largest possible circle, and therefore the chance of failure is greatest. The Mohr-Coulomb failure criterion is doing exactly this, that is the influence of the intermediate principal stress

is neglected.

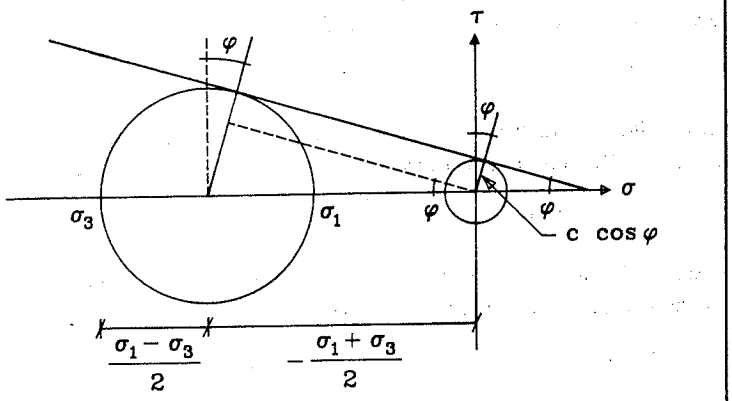

Fig. 2.4: Expressing eq. (2.25) as a function of the principal stresses.

By using Fig. 2.4, it is seen that eq. (2.25) can be expressed as a function of σ_1 and σ_3 as stated in eq. (2.27).

$$\frac{\sigma_1 - \sigma_3}{2} = c\cos\varphi - \frac{\sigma_1 + \sigma_3}{2}\sin\varphi \tag{2.27}$$

Introducing $\mu=\tan\varphi$ we get eq. (2.28),

$$\begin{aligned} &\frac{\sigma_1 - \sigma_3}{2} = c\,\frac{1}{\sqrt{1+\mu^2}} - \frac{\sigma_1 + \sigma_3}{2}\,\frac{\mu}{\sqrt{1+\mu^2}} \\ &\Updownarrow \\ &\left(\mu + \sqrt{1+\mu^2}\right)\sigma_1 + \left(\mu - \sqrt{1+\mu^2}\right)\sigma_3 = 2c \\ &\Updownarrow \\ &\left(\mu + \sqrt{1+\mu^2}\right)^2 \sigma_1 - \sigma_3 = 2c\left(\mu + \sqrt{1+\mu^2}\right) \end{aligned} \tag{2.28}$$

and if k is defined by eq. (2.29) then eq. (2.28) can be rewritten as eq. (2.30).

$$k = \left(\mu + \sqrt{1+\mu^2}\right)^2 \tag{2.29}$$

$$k\sigma_1 - \sigma_3 = 2c\sqrt{k} \tag{2.30}$$

Left now is to determine the material constants, k, $2c\sqrt{k}$, and σ_s.

The uniaxial compression test can be shown always to result in a sliding failure. Since the stress state is $\sigma_3=-f_c$, and $\sigma_2=\sigma_1=0$ we get from eq. (2.30) that

$$-\sigma_3 = 2c\sqrt{k} = f_c \tag{2.31}$$

meaning that eq. (2.30) can be written as eq. (2.32).

$$k\sigma_1 - \sigma_3 = f_c \tag{2.32}$$

The constant k, can only be determined from triaxial tests. The general accepted test data show that k=4, is a close approximation. Using k=4 it follows, that for a sliding failure to take place in the uniaxial tensile test, eq. (2.33) has to be fulfilled.

$$f_t = \frac{1}{k} f_c = \frac{1}{4} f_c \tag{2.33}$$

For concrete this is not true, and as a consequence, the failure mode for the uniaxial tensile test must be a separation failure, and eq. (2.26) then yields

$$\sigma_s = f_t \tag{2.34}$$

Eq. (2.34) is often referred to as the tension cut-off, or the Rankine criterion.

The complete Mohr-Coulomb failure criterion with tension cut-off is then (eq. (2.35))

$$k\sigma_1 - \sigma_3 = f_c \quad \wedge \quad \sigma_i = f_t \tag{2.35}$$

It is often more convenient to use the stress invariants in a failure criterion, rather than the principal stresses. Eq. (2.32) is therefore given below in two different forms, eq. (2.36) and (2.37). Eq. (2.32) is transformed into eq. (2.36) using eq. (2.21).

$$f(I_1, J_2, \theta) = \frac{1}{\sqrt{3}}\left[(2k+1)\cos\theta + \sqrt{3}\sin\theta\right]\sqrt{J_2} + \frac{1}{3}(k-1)I_1 - f_c = 0 \tag{2.36}$$

$$f(\xi, \rho, \theta) = \frac{\sqrt{2}}{2}\left[(2k+1)\cos\theta + \sqrt{3}\sin\theta\right]\rho + (k-1)\xi - \sqrt{3}\,f_c = 0 \tag{2.37}$$

The Mohr-Coulomb failure surface can then be shown, as in Fig. 2.5.

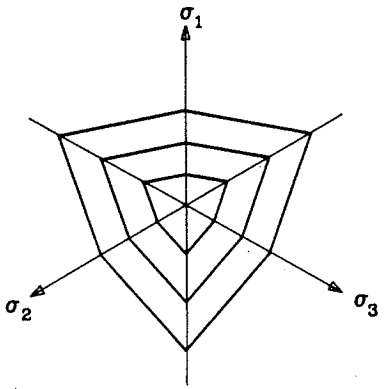

Fig. 2.5: The Mohr-Coulomb failure surface.

2.4 Ottosen failure criterion

One of the best models proposed, and yet not too complicated, is the model of Ottosen. The model was first published in 1977, see [77.1], and is extensively described in [82.1] and [89.2]. Lately the model has been included in the CEB model code 1990 [90.2].

The model is based on a membrane analogy in order to describe the development of the cross-section of the failure surface in the deviatoric plane. The analogy used, is that of a membrane simply supported along the sides of an equilateral triangle. When this membrane is loaded with an uniform pressure, the contour lines of the deflected membrane will vary between an equilateral triangle and a circle. These contour lines are used to describe the similar variation of the cross-section of the failure surface in the deviatoric plane.

The model incorporates all of the known features of the failure surface of concrete. The mathematical proof of this will not be included in this report, but can be found in [89.2]. The proposed model has the form as stated in eq. (2.38).

$$f(I_1, J_2, cos3\theta) = A\frac{J_2}{f_c^2} + \lambda\frac{\sqrt{J_2}}{f_c} + B\frac{I_1}{f_c} - 1 = 0 \qquad (2.38)$$

According to this model, a given state of stress does not lead to failure if the left side of eq. (2.38) is negative.

In the model, the parameters A and B are used for describing the meridians, and the function λ is used for describing the size and shape of the cross-section in the deviatoric plane. The function λ is defined in eq. (2.39).

$$\lambda = \begin{cases} K_1\cos\left[\frac{1}{3}\arccos(K_2\cos3\theta)\right] & \text{for } cos3\theta \geq 0 \\ K_1\cos\left[\frac{1}{3}\pi - \frac{1}{3}\arccos(-K_2\cos3\theta)\right] & \text{for } cos3\theta \leq 0 \end{cases} \qquad (2.39)$$

Where K_1 and K_2 are parameters.

Alternatively to using the invariants J_2 and I_1, ξ and ρ can be used. In that case the model becomes that of eq. (2.40).

$$\frac{A}{2}\left(\frac{\rho}{f_c}\right)^2 + \frac{\lambda}{\sqrt{2}}\frac{\rho}{f_c} + \sqrt{3}B\frac{\xi}{f_c} - 1 = 0 \qquad (2.40)$$

It can be shown, see [89.2], that K_1 is used for determining the size of the cross-section, and K_2 is used for determining the shape of the cross-section. These two parameters are therefore called the size-factor and the shape-factor respectively.

From eq. (2.38) and (2.39) it can also be seen that the model reduces to that of Drucker and Prager when A=0 and K_2=0, and it reduces to the classic von Mises' criterion when in addition B=0. The model therefore responds well to the demands stated in chapter 2.2. Furthermore are the parameters used for calibrating this model rather simple. Only four sets of data is used.

1/ The uniaxial compressive strength, f_c
2/ The uniaxial tensile strength, f_t
3/ The equal biaxial compressive strength, f_{cc}
4/ A point on the compressive meridian $(I_1, \sqrt{J_2}) = (x,y)$

Using the above, and after some tedious algebra, the parameters A, B, K_1, and K_2 can be found as stated in eq. (2.41).

$$M = \frac{\frac{x}{f_c} + \sqrt{3}\,\frac{y}{f_c}}{\frac{y}{f_c} - \frac{1}{\sqrt{3}}}$$

$$B = \frac{3\,\frac{y}{f_c}\,\frac{f_c^2}{f_t f_{cc}} - \sqrt{3}}{9\,\frac{y}{f_c}}$$
$$M + \frac{\frac{f_{cc}}{f_c} - \frac{f_t}{f_c}}{\frac{f_{cc}}{f_c} - \frac{f_t}{f_c}}$$

$$A = -\frac{\sqrt{3} + BM}{\frac{y}{f_c}} \qquad (2.41)$$

$$\lambda_c = \sqrt{3}\left(1 + B - \frac{A}{3}\right)$$

$$\lambda_t = \sqrt{3}\left(\frac{f_c}{f_{cc}} + 2B - \frac{f_{cc}}{f_c}\,\frac{A}{3}\right)$$

$$K_2 = \cos\left[3 \arctan \frac{2\frac{\lambda_c}{\lambda_t} - 1}{\sqrt{3}}\right]$$

$$K_1 = \frac{\lambda_t}{\cos\left[\frac{1}{3}\arccos\left(K_2\right)\right]}$$

Referring now to the four sets of data used for calibrating the model. The first parameter, f_c, poses no problem, since all data sets are normalized by f_c, and it has previously been stated that the failure surface seems independent of f_c. The uniaxial tensile strength, f_t, normalized by f_c might present a problem, since a fixed ratio, f_t/f_c=0.1, normally is used. Changing this fixed ratio have shown to have a large effect on the resulting values of A, B, K_1, and K_2. However, the influence on the failure surface in the triaxial stress space is very limited, and is only evident for very high triaxial stresses, se also Fig. 2.6.

In the case of the third parameter, f_{cc}/f_c, a ratio of 1.16 has been used. This ratio stems from the test result of Kupfer et.al. [69.1] and [73.1], which are widely accepted as probably the best biaxial tests performed until today.

For the last data set, the point on the compressive meridian, the data $(\xi,\rho)=f_c(-5,4)$ have been chosen from the experimental results of Richart et.al. [28.1], also widely regarded as being one of the best triaxial test programs performed. Using the data $(\xi,\rho)=f_c(-5,4)$ means that $(x,y)=(I_1, \sqrt{J_2})=(\xi\sqrt{3}, \rho/\sqrt{2})$.

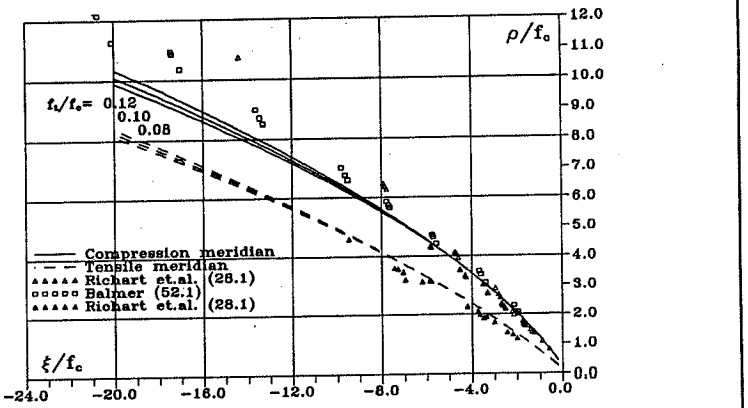

Fig. 2.6: Ottosen model with varying f_t/f_c ratio, compared to test data.

In Fig. 2.6 is the Ottosen model shown together with selected test data. Also in this figure are shown the result of changing the ratio f_t/f_c.

If the failure surface in the biaxial stress space is determined by the Ottosen failure criterion, it is seen that the f_t/f_c-ratio plays a major role in determining the shape of the failure surface. This is best seen in Fig. 2.7. In this figure the formula for the minimum tensile strength of concrete, as given by the CEB model code, has been used, see also chapter 3.2.5. It is clearly seen that the curvature of the failure surface increases for decreasing concrete strength, this seems also to conform well to the test data of Kupfer [73.1].

2.4.1 CEB model code 1990

The Ottosen model has been selected for the CEB model code 1990, [90.2]. The model is somewhat changed in that the parameters A, B, K_1, and K_2, is no longer determined by eq. (2.41), but rather as a function of the f_t/f_c-ratio, as stated in eq. (2.42).

Using the tensile strength to determine the compressive properties of concrete is inherently a bad practice. This because the tensile strength of concrete varies a lot, and is depending on

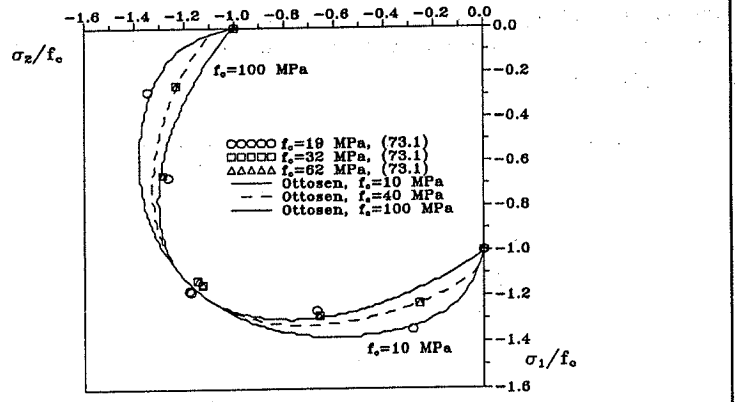

Fig. 2.7: Ottosen failure criterion in the biaxial stress space, varying f_t/f_c-ratio.

$$A = \frac{1}{9 \cdot k^{1.4}}$$

$$B = \frac{1}{3.7 \cdot k^{1.1}}$$

$$K_1 = \frac{1}{0.7 \cdot k^{0.9}} \qquad (2.42)$$

$$K_2 = 1 - 6.8\,(k - 0.07)^2$$

where

$$k = \frac{f_t}{f_c}$$

many more parameters than the compressive strength. Using eq. (2.42) for determining the parameters for the Ottosen model will therefore in some cases lead to very dubious results. The worst deviation between the CEB model and the original Ottosen model is found for high strength concretes having low tensile strengths.

If the CEB formula for the minimum tensile strength of concrete, see chapter 3.2.5, is used along with eq. (2.42) some difference will be seen in the failure curve in the triaxial stress space. The deviation is not excessive for low triaxial stresses but is very much increased for higher triaxial stresses. This, however, is not the worst case. If instead the failure surface in the biaxial stress space is shown, large deviation between facts and the model is evident. This is shown in Fig. 2.8.

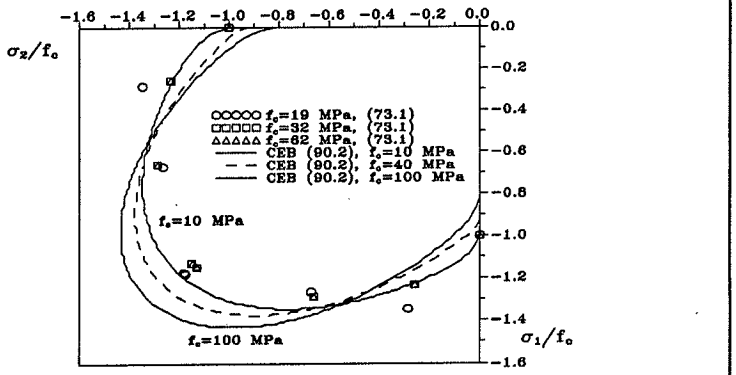

Fig. 2.8: Failure surface of the CEB model code in the biaxial stress space, varying f_t/f_c-ratio.

It can always be discussed how close a model should be to test data. However, the least expected from a model is, that is does not contradict known facts. For low strength concrete the CEB model seems to yield good agreement between fact and accepted test data. However, for normal and high strength concrete the model is clearly wrong. This is best seen when the model is used for determining the uniaxial concrete strength. The model will yield an answer which is up to 20% wrong. Using eq. (2.42) together with the CEB minimum tensile strength formula to determine the parameters for the Ottosen model, eq. (2.38), will therefore in many cases clearly result in erroneous results.

Chapter 3

Experimental program

In this chapter a more detailed description of the test program will be given. Also described in detail are the concretes used in this program.

3.1 The experimental program

In order to investigate the triaxial strength of concrete, a triaxial cell was used. This cell, and its calibration and use, has been extensively described by the author in [92.1]. Therefore no attempt will be made, in this report, to describe the cell or the use of it.

In order to investigate the influence of the uniaxial strength on the triaxial strength of concrete, 7 different concretes where used. The concretes were designed to have an uniaxial strength of 10, 35, 50, 70, 85, 100, and 110 MPa. The concretes were named 'Bnnn-m' where 'nnn' is the uniaxial strength level, and 'm' is the batch number. The concretes were designed to be like ordinary concretes, that is, the binder content was kept low, and the aggregate content kept high.

Each concrete was cast three times, except B110 which was only cast twice, and B035 which was cast four times. Each batch was tested with the major principal stresses ranging from 0 to 140 MPa. In order to compare concretes with different strengths, all the batches were tested with the major principal stress as follows:

$-0 \cdot f_c < \sigma_1 = \sigma_2 \leq -2 \cdot f_c$: $-\sigma_1/f_c$ = 0.2, 0.4, 0.6, 0.8, 1.0, 1.2, 1.4, 1.6, 1.8, 2.0
$-2 f_c < \sigma_1 = \sigma_2 \leq -4 \cdot f_c$: $-\sigma_1/f_c$ = 2.5, 3.0, 3.5, 4.0
$-4 \cdot f_c < \sigma_1 = \sigma_2 \leq -6 \cdot f_c$: $-\sigma_1/f_c$ = 5.0, 6.0
$-6 f_c < \sigma_1 = \sigma_2 \leq -14 \cdot f_c$: $-\sigma_1/f_c$ = 8.0, 10.0, 14.0

The different concretes were then tested as far as the capacity of the test equipment allowed, i.e. B100 were tested with the major principal stresses up to 140 MPa, that is $-\sigma_1/f_c = 1.4$.

In all the tests, the major and the intermediate principal stresses were equal. This means that the results of the test program lie exclusively on the compression meridian. This limitation is due to the limitations of the triaxial cell, as described in [92.1].

All the test specimens were tested using a 'normal' load path, that is loading along the hydrostatic axis, until a predetermined stress level is reached, hereafter increasing the deviator stress until failure.

The load speed was the same for all the tests, and was equal to 0.3 MPa/s.

In order to investigate the influence of the aggregate size, and -content, 2 mortars, and 1 paste were cast. The mix design for these paste and mortars was determined simply by removing one or more of the three aggregates in the mix design for B070. Hereby it was ensured that the uniaxial strength of the mortars and the paste was approximately the same as the uniaxial strength of B070.

The mix design for mortar B, M070-B, was established by removing all of the crushed granite from the mix design of B070. The mix design for mortar A, M070-A, was established by removing all of the Gravelit from the mix design of M070-B. Finally the mix design for the paste, P070, was established by removing all of the sand from the mix design of M070-A.

3.2 Description of the concretes

A total of seven concretes, 2 mortars, and 1 cement paste, were used in the investigation. In the following chapter the materials, the mix proportions, the handling of the concrete and the test specimens will be described.

3.2.1 Materials

The materials used have the following characteristics:

Binders:

Rapid hardening cement	ASTM type III, Danish classification PC(R).
White cement	A white, rapid hardening, low-alkali cement, ASTM type III or IV, Danish classification PC(R/L/S/H).
Low-alkali cement	ASTM type IV or V, Danish classification PC(A/L/S).
Fly Ash	Fly ash was supplied by Amagerværket, Copenhagen. Specific gravity was assumed to be 2200 kg/m^3.
Micro silica slurry	A solution of micro silica, with a dry-matter percentage of 51.6, and a density of 1391 kg/m^3.

Aggregate: (the grain size distribution graphs are shown in appendix 1)

Sand	Danish marine deposits (0-4 mm), free of calcium chloride, with a specific gravity of 2567 kg/m^3.
Gravelit	Danish marine deposits (4-8 mm), free of calcium chloride, with a specific gravity of 2627 kg/m^3. Gravelit consists of small rounded pebbles, free of flint and limestone.
Granite	Crushed Danish granite (4-16 mm), with a specific gravity of 2735 kg/m^3. The crushed granite had an oblong particle shape.

Admixtures:

Plasticizer	As plasticizer a product called CONPLAST 212 was used. CONPLAST 212 is a LIGNOSULFONAT based plasticizer, supplied by 4K Byggeteknik A/S. CONPLAST 212 has a density of 1170 kg/m^3, and a dry-matter percentage of 36.
Super-plasticizer	As super-plasticizer a product called PERAMIN F was used. PERAMIN F is a MELAMIN based super-plasticizer supplied by 4K Byggeteknik A/S. PERAMIN F has a density of 1210 kg/m^3, and a dry-matter percentage of 34.

The water used was ordinary tap water from the city's network.

3.2.2 Mix proportions

Seven different concrete mixes were used to produce the 7 different strength levels desired. Furthermore 2 different mortars, and 1 cement paste were produced. The mix design of the mortars and the paste, was based on the concrete B070, as described earlier.

The strengths of the concretes, mortars, and paste, varied from 10 to 110 MPa, as measured on Ø100·200 mm cylinders. Each concrete was cast 3 times. In table 3.1 are given the mix proportions, and in table 3.3 the uniaxial compressive strength of the concretes. It should be noted that the amount of superplasticizer was varied in the two concretes B100 and B110, in order to obtain a workable fresh concrete. The actual super-plasticizer used was between 100% and 150% of the amount stated in table 3.1.

Concrete Material	B010	B035	B050	B070	B085	B100	B110	P070	M070 A	M070 B
Cement (*)	129	247	260	309	320	375	390	1030	598	462
Fly ash	69	100	40	-	45	-	-	-	-	-
MS-slurry	-	-	36	55	60	75	76	183	106	82
Water	170	170	150	129	95	70	63	430	249	192
Sand (0-4 mm)	754	618	600	598	610	615	521	-	1157	904
Gravelit (4-8 mm)	246	244	257	265	186	188	247	-	-	395
Granite (4-16 mm)	985	977	1026	1061	1106	1120	989	-	-	-
Conplast 212	-	-	1.4	2.0	2.0	2.3	2.4	-	-	-
Peramin F	-	-	-	3.1	6.3	8.3	8.6	-	-	-

Table 3.1: Mix proportions for the different concretes, mortars, and paste, used in the investigation. All units are kg/m^3.

(*): The cement used was, B085: low-alkali cement, B100: white cement, the remaining: rapid hardening cement.

3.2.3 Mixing, casting and curing of the cylinders.

A 0.3 m^3 paddle mixer was used to mix the concrete in batches of 0.1 m^3. The mixing procedure was as follows.

1/ The dry aggregates, sand and coarse aggregate, were mixed together in the paddle mixer for 5 minutes.
2/ The cement and fly ash was added, and mixing continued for 5 minutes.
3/ The water, micro silica slurry, plasticizer, and approx. 70% of the super-plasticizer were blended together, and slowly added to the mixer. Mixing continued for 3 minutes.
4/ The concrete was examined, and if necessary more super-plasticizer was added until the fresh concrete had the desired workability.

Blending the fluids together prior to mixing has the advantages of, partly ensuring a better dispersal of the micro silica in the concrete, and partly of the plasticizers being more effective.

The slump and air content was measured on the fresh concrete, prior to casting. The results are given in table 3.2.

The cylinders were cast in plastic moulds, and compacted on a vibrator table. The moulds were filled with 3 layers of concrete, with a thorough compaction between each layer.

After approximately 24 hours, the cylinders were removed from the moulds. The cylinders were then cured 13 days in water, and 14 days at 20°C and 60% RH.

	Cast 1		Cast 2		Cast 3		Cast 4	
	slump (mm)	air (%)	slump (mm)	air (%)	slump (mm)	air (%)	slump (mm)	air (%)
B010	205	1.0	120	0.7	50	1.1	-	-
B035	120	0.6	100	0.6	90	n.m.	110	0.7
B050	90	0.6	85	0.7	70	n.m.	-	-
B070	70	1.5	120	0.7	90	0.7	-	-
B085	150	0.8	85	0.6	80	n.m.	-	-
B100	220	0.5	195	0.8	210	n.m.	-	-
B110	125	0.8	195	n.m.	-	-	-	-

Table 3.2: Properties of the fresh concretes.

Note: The abbreviation, n.m., means not measured. A dash means not cast.

3.2.4 Uniaxial compressive strength

For each batch 6 Ø100·200 mm cylinders were tested in order to determine the uniaxial compressive strength of that particular batch. All the cylinders were tested in a 200 tons MP MFL compression jack controlled by a Walter+Bai servo controller.

The test cylinders were ground accurately plane by means of a diamond cutting spindle. Wood fiber plates were used between the steel loading platens and the concrete. Previous studies at the Department of Structural Engineering have shown these fiber plates to have no influence on the strength measurements. The cylinders were tested at a rate of 0.7 MPa/s, as specified by the Danish National Code [84.2].

	Cast 1		Cast 2		Cast 3		Cast 4	
	f_c (MPa)	s.dev. (%)	f_c (MPa)	s.dev. (%)	f_c (MPa)	s.dev. (%)	f_c (MPa)	s.dev. (%)
B010	9.79	10.92	14.55	5.88	17.08	5.74	-	-
B035	37.39	2.82	42.95	1.83	40.41	3.54	42.11	2.19
B050	52.17	6.40	52.72	2.52	51.54	6.34	-	-
B070	64.12	3.41	71.65	2.23	76.73	4.74	-	-
B085	89.46	3.00	90.36	3.34	88.39	4.41	-	-
B100	106.20	1.75	107.12	5.47	99.82	2.95	-	-
B110	108.80	1.48	108.76	3.83	-	-	-	-
P070 (*)	30.42	14.88	-	-	-	-	-	-
M070-A	73.49	1.88	-	-	-	-	-	-
M070-B	69.61	3.33	-	-	-	-	-	-

Table 3.3: Uniaxial compressive strength of the concretes, mortars, and the paste. The compressive strengths are the average result of 6 test cylinders Ø100·200 mm.

Note: - No measurements, because casting did not take place.

(*) The paste cylinders failed due to the very severe shrinkage cracks that appeared shortly after the cylinders were removed from the water storage. The compressive strength shown here is therefore not the uniaxial compressive strength of the cement paste itself, but that of shrink-cracked cement paste.

3.2.5 Uniaxial tensile strength

To supplement the compressive strength measurements, uniaxial tensile strength measurements were also performed. The uniaxial tensile strength tests were performed in accordance with the Danish Standard DS 423.24 [84.3]. As specimen a concrete cylinder Ø100·200 was used. Prior to testing 5 mm were sawn from each end using a diamond saw, cooled with water. The resulting length of the specimens were then 190 mm. To each end a steel plate was glued. The sawing was performed in order for the glue to reach the aggregate.

The specimens failed in two different ways. Either the failure was a bond failure between the glue and the concrete, or the failure was a single crack running horizontal across the specimen. The placement of the single failure crack varied along the length of the specimen. In Fig. 3.1 are shown the test results. Specimens displaying bond failure have been disregarded.

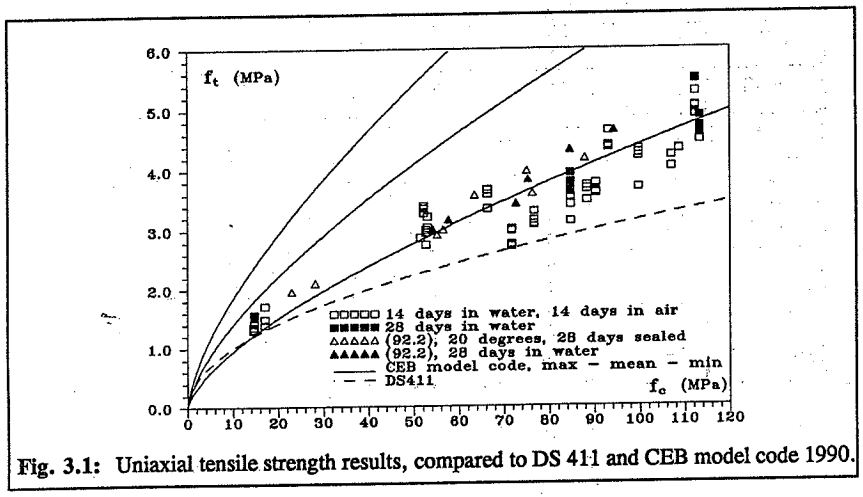

Fig. 3.1: Uniaxial tensile strength results, compared to DS 411 and CEB model code 1990.

The specimens were cured 14 days in water, and 14 days in the air, 60% RH, 20°C. Also in Fig. 3.1 are shown test result from [92.2]. These specimens were cured either 28 days in water, or 28 days sealed at 20°C.

The tensile strength results are compared partly to the Danish National Code [84.4], and partly to the CEB model code 1990 [90.2]. The uniaxial tensile strength formulas stated in [84.4] and [90.2] are given below in eq. (3.1).

$$f_t = 1.00\ MPa \cdot \sqrt{\frac{f_c}{10\ MPa}} \qquad \text{DS 411 [84.4]}$$

$$f_t = 0.95\ MPa \cdot \left(\frac{f_c}{10\ MPa}\right)^{2/3} \qquad \text{CEB minimum [90.2]} \qquad (3.1)$$

$$f_t = 1.40\ MPa \cdot \left(\frac{f_c}{10\ MPa}\right)^{2/3} \qquad \text{CEB mean [90.2]}$$

$$f_t = 1.85\ MPa \cdot \left(\frac{f_c}{10\ MPa}\right)^{2/3} \qquad \text{CEB maximum [90.2]}$$

It is seen that the water cured specimens generally had a slightly higher tensile strength than the specimens that were both water and air cured. This is opposed to the compressive strength where water curing leads to lower compressive strengths than air curing. It is also clearly seen that the CEB model code generally overestimates the tensile strength, however the CEB minimum value is very close to the mean of the test results, and will therefore be used in the following.

Chapter 4

Experimental results

Given in this chapter are the test results from the investigation concerning the triaxial strength of concrete. Also given is the definition of failure used in this investigation.

4.1 Definition of failure

Failure in uniaxial compression is rather straightforward, that is, failure occurs when the load carrying capacity is exhausted, meaning that the load supplied by the testing machine drops. In triaxial compression, the problem is more complex. For small values of the major principal stresses, failure can be defined the same way as for uniaxial compression. This is seen in the test result by a drop in the vertical load supplied by the hydraulic jack. However, for large values of the major principal stresses, 70 MPa or more, the material often behaves in a different way.

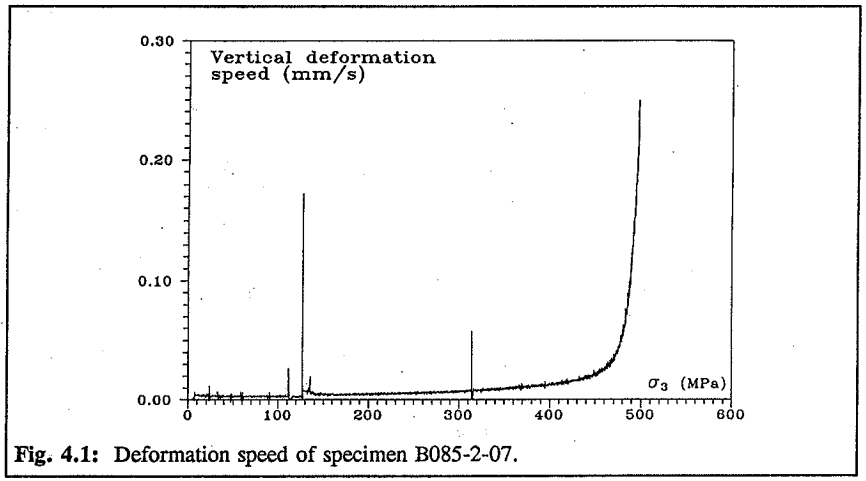

Fig. 4.1: Deformation speed of specimen B085-2-07.

Under these large major principal stresses the deformations also become very large. In some cases the deformation speed will exceed ~0.25 mm/s. This limit is the error limit for the hydraulic jack, and the test is therefore stopped automatically by the servo controller. It might be a problem that failure in this case is not defined the same way as when the vertical force drops. However, as seen in Fig. 4.1, the deformation speed rises very rapidly just before the error sensitivity of the jack is triggered, and failure in the concrete must therefore be imminent.

In Fig 4.1 is shown the deformation speed of specimen B085-2-07. The deformation speed was measured by a displacement transducer, as described in [92.1]. The specimen was loaded with a confining pressure of 126.6 MPa. It can be seen that there is a disturbance in the graph, for σ_3= 126 MPa. This is due to the way of loading, and the way of measuring the displacement. That is, when the desired hydrostatic pressure level (126.6 MPa) has been reached, the deviatoric stress is applied by the external jack. The piston therefore has to settle on top of the specimen. Since the transducer is measuring the total displacement of the piston, the settling of the piston can therefore be seen as a disturbance in the graph.

In some cases however the specimen never failed according to the above mentioned criterion. This sometimes happened for very large confining pressures, above 100 MPa. In these cases the deformation speed reached a maximum of ~0.2 mm/s. After reaching this value the deformation speed sometimes began to drop, even when the vertical load was increased. This decreasing of the deformation speed was always accompanied by a very large horizontal deformation. This behavior was experienced for all the concretes, except B010, B100, and B110.

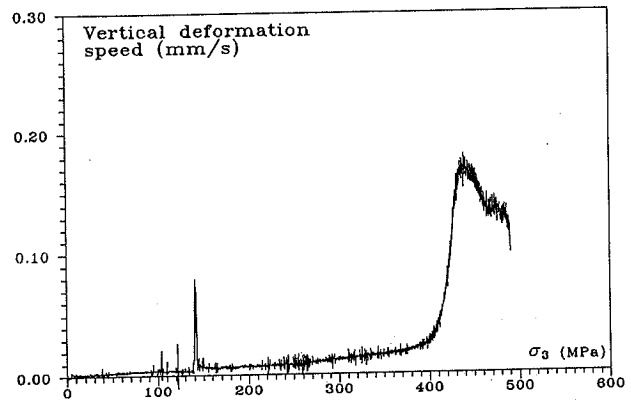

Fig. 4.2: Deformation speed of specimen B035-2-13.

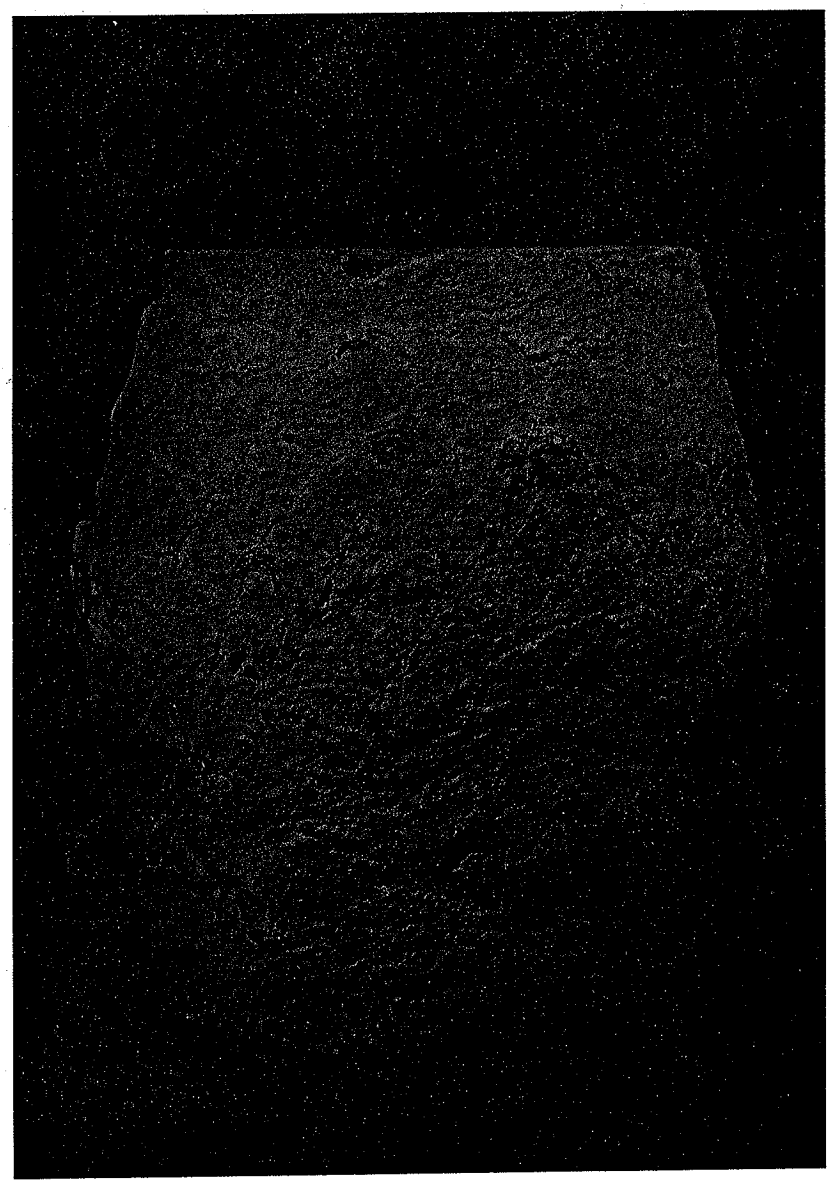

Fig. 4.3: Specimen B035-2-13 after testing.

These specimens did not fail, since the vertical jack was manually stopped due to the lack of deformation capacity of the triaxial cell. In table A.2.1 - A.2.24 these specimens are therefore marked with '***'.

An example of such a behavior is shown in Fig 4.2, and the deformed specimen is shown in Fig. 4.3. The total deformation of this specimen was ~60 mm vertically and ~30 mm horizontally.

4.2 Test results

The test results from this investigation are shown in appendix 2 and appendix 3. In appendix 2 are given the results from the individual tests. In the tables, '***' denotes a specimen which did not fail, as described previously in chapter 4.1.

In appendix 3 are the test results shown graphically. Along with the test data is shown the compressive meridian of both the original Mohr-Coulomb failure criterion and the original Ottosen failure criterion, as described previously in chapter 2.

Chapter 5

Discussion of the test results

In this chapter will the test results from this investigation be discussed, and compared to other investigations. Furthermore will the Ottosen failure criterion be modified to reflect the new knowledge found in this investigation. Also will a modification of the Mohr-Coulomb failure criterion be presented. This in order to present a simplified model fit for easy manual calculations.

5.1 Validation of the test results

The results from this investigation will in this chapter be compared to previous investigations. The comparison will be limited to other investigations where the test specimen also has been cylinders. Furthermore is the comparison for obvious reasons, see [90.1], limited to comparable concretes with similar curing and loading conditions.

The reason for limiting the comparison to cylindrical test specimens is as follows. The only practical alternative to the cylindrical tests are the cubical tests. The cubical tests offer an independent application of the three principal stresses, and are therefore more versatile than the cylindrical tests where two of the three principal stresses always are equal. In a large cooperative research project, promoted by Professor Gerstle, comparative tests using cubes and cylinders have been performed on identical concretes. The tests were performed using different test apparatus, and they showed some discordance in the results obtained. This discordance might be explained, partly by the influence of the test rig itself, and partly by the different geometry of the test specimens.

The discordance between the cubical and the cylindrical tests have not yet been fully explained nor understood. There is a global agreement that until this has happened the cylindrical tests are more suited for validation purposes than the cubical tests. This because in the cubical tests the load application are performed using steel rams in different sizes and shapes, whereas flexible membranes are used in the cylindrical tests. The use of membranes are widely regarded as being the best way of ensuring a friction free application of the load,

and hereby lessening the influence of the test equipment on the test results.

The tests in this investigation will therefore be validated using general accepted test results from the cylindrical tests of Richart et.al. [28.1], Hobbs [74.1], and Bellotti et.al. [84.1]. A further discussion of the influence of the test rig on the test results can be found in [91.1].

5.1.1 Comparison for $f_c < 40$ MPa

In Fig. 5.1 are the test results from this investigation compared to the famous results of Richart et.al. [28.1].

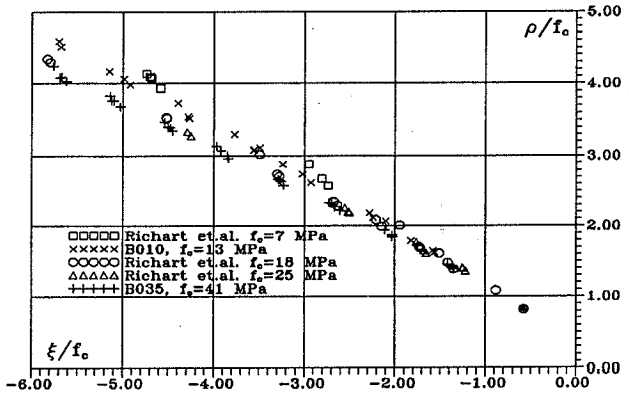

Fig. 5.1: Test results compared to Richart et.al. [28.1].

Examining Fig. 5.1 it is seen that the results from the different concretes are in agreement for $\xi < -2f_c$, with a very small scatter in the results. Beyond this point the results start to deviate from each other. However, beyond this point there is a clear layering of the test data. The low strength concretes are seen to be at the top, and the higher strength concretes at the bottom. It is also seen that this layering in the ultimate strength increases for increasing hydrostatic strength level.

A close examination reveals that the difference in the ultimate strength seems to diminish for increasing uniaxial concrete strength. The conclusion of this comparison must be that the test results compare well to the results of Richart et.al, and that the ultimate strength is depending on the uniaxial concrete strength.

5.1.2 Comparison for $f_c = 40$ MPa

In Fig. 5.2 are the test results from B035 compared to the results from Hobbs [74.1].

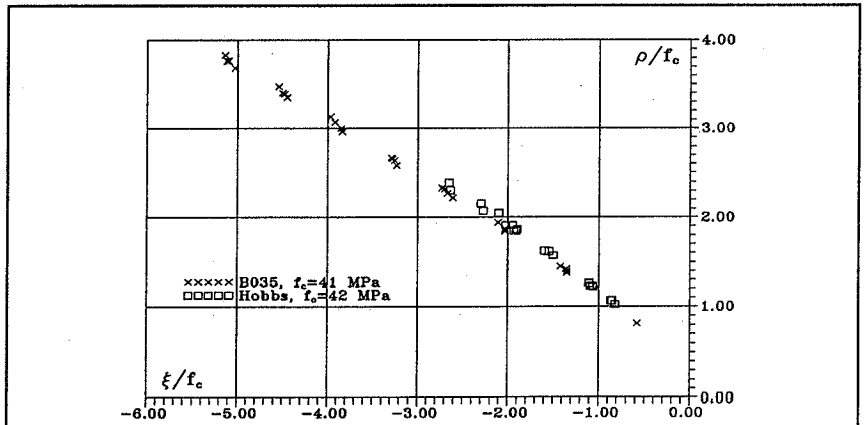

Fig. 5.2: B035 compared to Hobbs [74.1].

It is seen that the two sets of results for all practical purposes are identical. The small deviation in the ultimate strength that is seen for a few of Hobbs' results can only be ascribed to the normal scatter experienced in all concrete tests. It is also seen that there is a surprisingly small scatter when all of the results are considered.

5.1.3 Comparison for $f_c = 50$ MPa

The last comparison is made between the results of Hobbs, [74.1], Bellotti et.al., [84.1], and the test series B050. This comparison is shown in Fig. 5.3. Again it is seen that there is very little deviation between the different test series. The results from B050 are almost identical to the tests of Bellotti et.al., and only slightly lower than the results of Hobbs. This is perhaps even more remarkable because each of the results of Bellotti et.al. is the mean values of 8 tests.

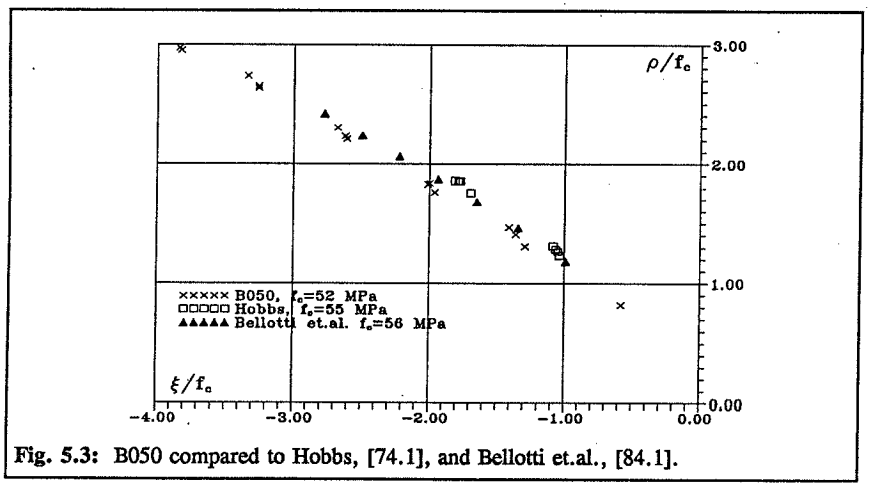

Fig. 5.3: B050 compared to Hobbs, [74.1], and Bellotti et.al., [84.1].

5.1.4 Validation, concluding remarks

Only some of the test results obtained in this investigation have been compared to other reported test results. This because high strength concretes have not been tested under triaxial stresses, and it is therefore not possible to compare the results from this investigation with other reported experimental results.

The comparison shows that for normal and low strength concrete the test results compare very well to other reported experimental results. None of the comparison tests, or the tests in this investigation, have used identical test equipment. This indicates that the test equipment, the preparation technique, and the general handling of the test specimens have only in a very minor way influenced the test results of the 4 investigations considered. Since the high strength concretes and the normal strength concretes have been prepared and tested identically, it therefore follows that there exists no indication of any significant outside influence on the test results of the high strength concretes.

5.2 Observations in the test results

The fact most clearly seen in the test results are the difference between the test results of B010 and the rest of the test results. The difference is best seen in Fig. A.3.9 and A.3.10. Here it can be observed that the results of B010 follows the failure criterion of Mohr-

Coulomb for a very long way. The rest of the results, however, is seen to deviate from this, in that they fall below the Mohr-Coulomb failure criterion for $\xi \sim -3.5f_c$, corresponding to a major principal stress of $\sigma_1 \sim -0.5f_c$.

It can be seen, apart from the concrete B010, that there is some layering of the test results with respect to the uniaxial compressive strength. The test results from the different concretes follow a failure curve of similar shape, but the value of ρ/f_c decreases for increasing concrete strength when ξ/f_c is kept constant. The layering seems to increase for increasing ξ/f_c. This is best seen in Fig. A.3.10 and A.3.11.

The difference between the results of B010 and the rest of the concretes is too obvious to be neglected. No other researchers have to this author's knowledge published results that indicates this behavior. Some researchers have commented that the failure curve is slightly depending on the uniaxial concrete strength. These researchers have disregarded this evidence on the grounds that the effect was too small to be significant. This is probably because the previous tests have mostly been performed on low and normal strength concretes with the major principal stress in the region $0 < \sigma_1/f_c < 1.0$, corresponding to $-0.58 < \xi/f_c < -4$. In this region the different low and normal strength concretes do not deviate significantly from each other, as can be seen in Fig. A.3.10 and A.3.11. However, as the major principal stress and the uniaxial concrete strength is increased, so does the dependency of the failure curve on the uniaxial concrete strength become clearer.

Almost all of the previous experiments with the major principal stress greater than $\sigma_1 = 1.0f_c$ have been performed on low strength concretes. When a failure criterion is formulated, it has to reflect the test results. If these results do not include tests of normal strength concrete in the high pressure region, then the proposed failure criteria will have to follow the low strength concrete results, and will therefore overestimate the ultimate strength of the normal and high strength concretes in the high pressure region. This is exactly what can be observed in Fig. A.3.1 to A.3.7.

In these figures it can be seen that the Ottosen failure criterion underestimates the ultimate strength for the low strength concrete, and, to some degree, overestimates the ultimate strength of the other concretes with uniaxial strengths between 40 and 110 MPa.

In the comparison tests of paste, mortar, and concrete, Fig. A.3.8, something very interesting can be observed. It is seen that the failure curve is not smoothly curved, but at some point rapidly approaches a maximum value of ρ/f_c. The value of ξ/f_c at which this change occurs is not constant, but is increasing by increasing aggregate content.

It is observed that the abruptness of the change also seems to soften for increasing aggregate

content. This softening behavior is most probably due to the stress concentrations that occurs around the aggregates.

In the concrete tests, something similar can be observed. Although not as dramatic as the paste result, there is some indication that a maximum level of ρ/f_c is approached. This maximum level seems to be increasing for decreasing uniaxial concrete strength.

It is very possible that the behavior here described is correlated to the 'yielding' observed in some of the tests, see also chapter 4.1. The 'yielding' took place when $\sigma_1 \sim 120$ MPa independently of the concrete strength. Since the only constant parameter in all of the tests are the aggregates, it therefore follows that the 'yielding' behavior somehow might be related to the aggregate properties.

In the comparison tests between concrete, mortar, and paste, the maximum value of ρ/f_c increased for increasing aggregate content, that is the specimen became more and more inhomogeneous.

In the concrete tests there are indications that the maximum level of ρ/f_c increases for decreasing uniaxial concrete strength. Since the properties of the matrix material approaches the properties of the aggregate material for increasing uniaxial concrete strength, it therefore follows that there also here is some indications that this maximum ρ/f_c level is depending on the homogeneity of the material tested.

The thesis that the maximum level of ρ/f_c is depending on the homogeneity of the material is supported by the behavior of steel. Steel is a very homogeneous material, and it is known that for steel the deviator stress, ρ, is independent of the hydrostatic stress ξ.

However, no definite conclusion can be made from these tests because of the limitations of the test equipment. This because the alleged change in failure happens when the capabilities of the test equipment with respect to the confining pressure is almost exhausted.

The observations here described makes it necessary to caution against extrapolating failure criteria beyond the test results they have been calibrated against. This because it is possible that a maximum value of the deviator stress is reached for stresses only slightly above the maximum values used in this investigation.

5.3 Modification of the Ottosen model

The Ottosen model is used in this investigation to describe the ultimate strength of concrete subjected to a triaxial stress field. Because of this the parameters used for the Ottosen model have also been studied. Three parameters need to be investigated, se also chapter 2.

1/ The uniaxial tensile strength
2/ The equal biaxial strength
3/ A point on the failure surface

5.3.1 The uniaxial tensile strength

The uniaxial tensile strength for the concretes used in this investigation, has been reported in chapter 3.2.5. It was found that the minimum value given by the CEB model code 1990, as stated in eq. (5.1), represents the test results well.

$$f_t = 0.95\ MPa \cdot \left(\frac{f_c}{10MPa}\right)^{2/3} \tag{5.1}$$

However, because of the rather large influence of the tensile strength on the failure surface in the biaxial stress space, and the difficulties in determining the tensile strength as a function of the compressive strength, eq. (5.1) will not be used. Instead of eq. (5.1), a fixed value of f_t/f_c, as given in eq. (5.2), will be used. This will of cause influence the shape of the failure surface in the triaxial stress space, but not to any noticeable degree.

$$\frac{f_t}{f_c} = 0.1 \tag{5.2}$$

5.3.2 The equal biaxial strength

Changing the equal biaxial strength does not influence the compressive meridian of the Ottosen failure criterion to any noticeable degree. Therefore only a cursory investigation of this parameter have been performed. It has been stated in [83.1] that the biaxial strength is not depending on the uniaxial concrete strength. This is mostly based on the works of Kupfer [73.1]. These results are shown in Fig. 5.4. In this figure it is seen that the biaxial strength is only somewhat influenced by the uniaxial concrete strength. A closer look reveals that although some discrepancies occur in the test results, the equal biaxial strength does not seem

to be influenced by the uniaxial concrete strength.

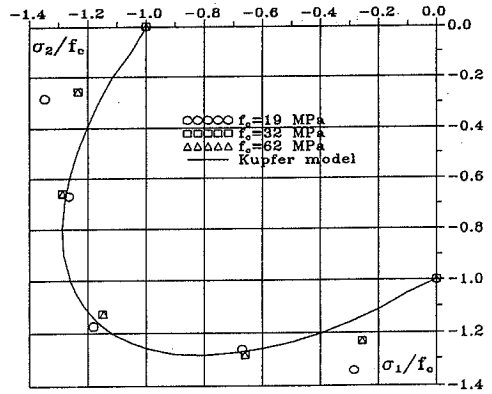

Fig. 5.4: Biaxial test results from Kupfer [73.1].

As a consequence of this, and because changes in the equal biaxial strength do not influence the failure surface in the triaxial stress space, the value for f_{cc} given in eq. (5.3) will be used.

$$f_{cc} = 1.16\, f_c \tag{5.3}$$

5.3.3 A point on the failure surface

Consider the figures A.3.1 to A.3.7. In these figures it is seen that the Ottosen model reflects the ultimate strength of concrete only for the low strength concretes, and then only for ξ less than approx. $-7f_c$. It is also seen that for the rest of the concretes tested, the Ottosen model always overestimates the ultimate strength. The only parameter left to change in order to achieve a closer agreement between the model and the test results is the point on the failure surface.

It is seen in the figures A.3.2 to A.3.7 that the point previously used, $(\xi,\rho)=(-5,4)f_c$, does not agree with the test results for concretes with a strength above ~20 MPa. It is also seen in Fig. A.3.10 and A.3.11 that no single point can be used as a common point for all the concretes here tested. Therefore the following points, given in table 5.1, have been used for determining the failure surface.

f_c (MPa)	ξ/f_c	ρ/f_c
10	-4.143	3.6
20	-4.389	3.6
30	-4.607	3.6
40	-4.796	3.6
50	-4.958	3.6
60	-5.091	3.6
70	-5.197	3.6
80	-5.275	3.6
90	-5.324	3.6
100	-5.345	3.6

Table 5.1: Points on the failure surface, used in the model.

Based on the points in table 5.1, the equal biaxial strength eq. (5.3), and the tensile strength ratio eq. (5.2), it is now possible to determine the parameters A, B, K_1, and K_2 using eq. (2.41). This has been done and it was seen that the parameters could be approximated using second degree polynomials. These polynomials are stated in eq. (5.4).

$$\begin{aligned} A &= -1.66\,x^2 + 3.49\,x + 0.73 \\ B &= -0.19\,x^2 + 0.41\,x + 3.13 \\ K_1 &= 0.46\,x^2 - 0.97\,x + 11.89 \\ K_2 &= -0.02\,x^2 + 0.04\,x + 0.974 \end{aligned} \tag{5.4}$$

where

$$x = \frac{f_c}{100\ MPa}$$

Using these polynomials it is now possible to show the failure surface in the triaxial stress space. This is done in Fig. 5.5 and 5.6. In Fig. 5.5 is shown the failure surface for $\xi/f_c > -40$ corresponding to the maximum stress level investigated in this investigation. In Fig. 5.6 is shown the part of Fig. 5.5 where ξ/f_c here is greater than -10. In both figures are the failure

curves for the different concretes stopped at a certain point. This represent the maximum stress level at which the failure criterion is valid for that particular concrete strength. The failure criterion is not extrapolated beyond this point, because no experimental evidence exists for larger stress levels.

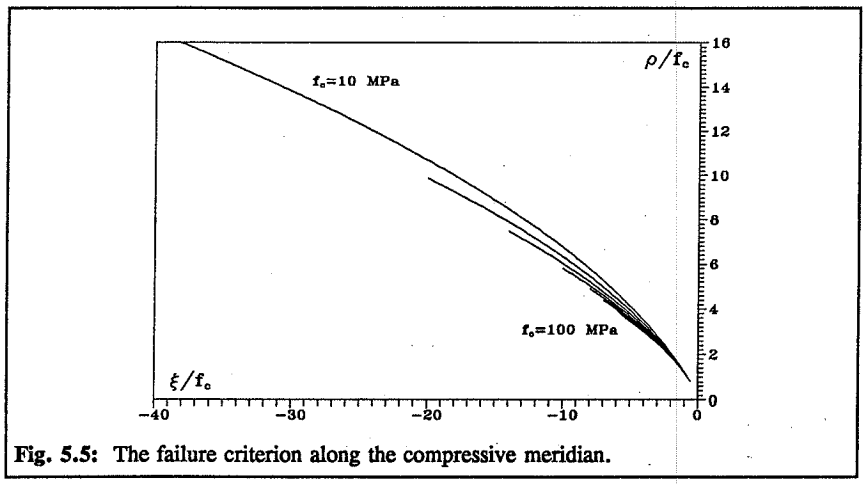

Fig. 5.5: The failure criterion along the compressive meridian.

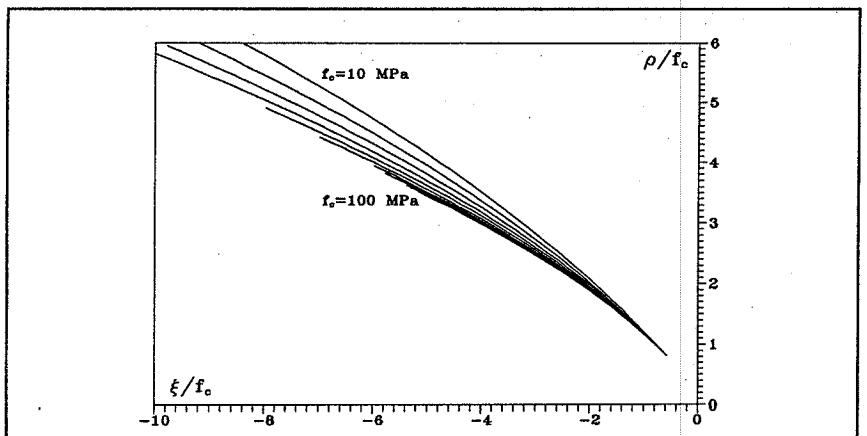

Fig. 5.6: The failure criterion along the compressive meridian, low stress levels.

5.3.4 Evaluation of the failure criterion

The failure surface resulting from this investigation is the one specified in eq. (2.38), where the parameters A, B, K_1, and K_2, are determined using eq. (5.4).

In order to validate the failure criterion a number of comparisons have been performed. Primarily the failure criterion is compared to the test results of this investigation. This is done in Fig. 5.7.

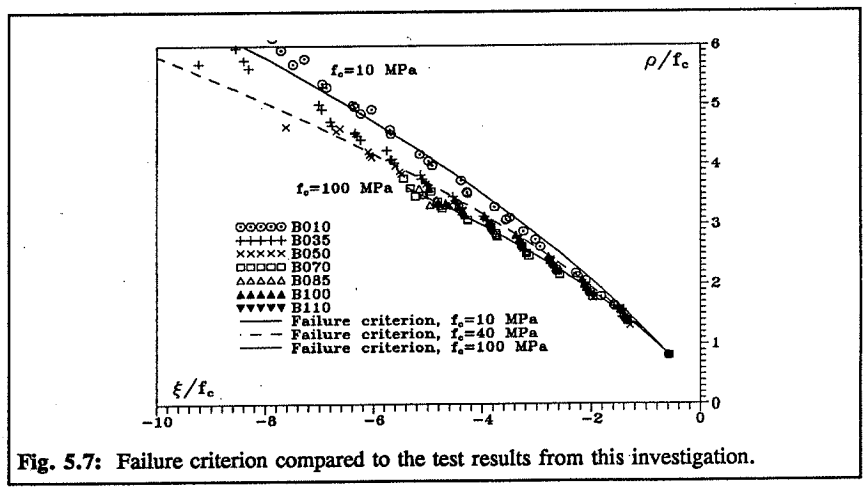

Fig. 5.7: Failure criterion compared to the test results from this investigation.

It is clearly seen, as expected, that the failure criterion is in good agreement with the test results. It is also seen that the failure criterion deviates from the low strength concretes, in that it underestimates the ultimate strength for very high hydrostatical stress levels, and that it, for all the concretes, tend to slightly overestimate the ultimate strength at low hydrostatic stress levels. However, all in all is the correlation between the model and the test results very good.

In Fig. 5.8 is the failure criterion compared to test data along the extension meridian. It is seen that the model is less depending on the uniaxial concrete strength along this meridian, than along the compression meridian. It can also be observed that the failure criterion tends to slightly overestimate the ultimate strength. However, test results along this meridian are scarce, and the spread in concrete strength is small, 10 to 40 MPa. All in all, however, there seems to be a good correlation between the test results and the failure criterion.

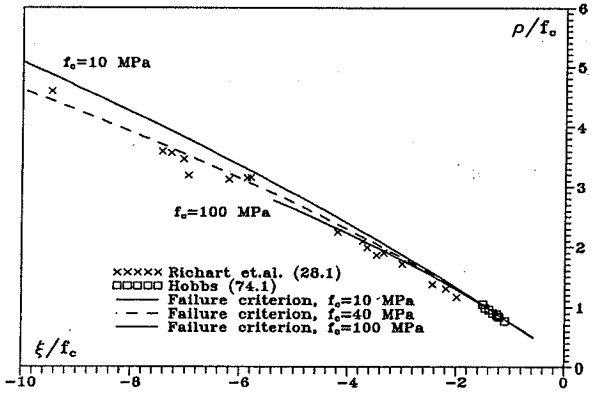

Fig. 5.8: Failure criterion compared to test results along the extension meridian.

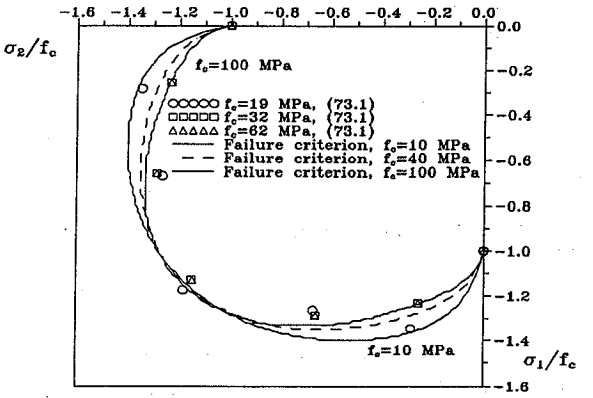

Fig. 5.9: The failure criterion compared to test results in the biaxial stress space.

In Fig. 5.9 is the failure criterion compared to test results in the biaxial stress space.

It can be observed that the dependency of the model on the compressive strength also here is slight. Also observed is that there is a good correlation between the test results and the failure criterion in the biaxial stress space.

Considering the above comparisons it is concluded that the proposed failure criterion correlate well with the test results of this, and other accepted, investigations. Is also clear from the

discussion in chapter 2, and in [90.1], that the model fulfill the general accepted characteristics of the failure surface for concrete. However, as with every model, there are some limitations to the model, and some areas where the investigation is not complete. The major limitations of the proposed failure criteria are presented below.

- The failure criterion is a failure criterion for normal weight ordinary concrete. It does not include heavy- or lightweight concrete, nor does it include very rich concretes, mortars or pastes. Likewise are fiber reinforced concretes neither included in the model.

- The failure criterion is only valid for concretes with a uniaxial compressive strength up to 100 MPa.

- The model is valid for compressive stresses only.

- Along the compression meridian the failure criterion is only valid for major principal stresses below approximate 120 MPa. The model should not be extrapolated to include higher stress levels. This because, as discussed in chapter 5.2, there are some indications of a changing failure mode when the hydrostatical stress level is increased, and the model does not include this change of failure mode.

- The model has not been compared to high strength concrete test results other than along the compression meridian. There are some indications that the influence of the uniaxial concrete strength is greater along the compression meridian than along the tensile meridian. If so the lack of high strength concrete test data along the tensile meridian is not serious, but more data are needed before a conclusion can be made.

5.4 Modification of the Mohr-Coulomb model

The main disadvantage of the Mohr-Coulomb failure criterion is the lack of smoothness. The failure criterion has a number of corners and singularities which makes the model difficult to handle in numerical analysis. Furthermore does the failure criterion ignore the intermediate principal stress. This is contrary to the experimental results, and results in a deviation up to 35% between the experimental results and the failure criterion in the biaxial stress space.

On the other hand the Mohr-Coulomb model is extremely simple to use, and the deviations

of the failure criterion from the test results are not prohibitive in the region of practical interest. As can be seen in Fig. A.3.1 to A.3.7 does the Mohr-Coulomb failure criterion follow the experimental results very well. It is only for higher stress levels that the model overestimates the ultimate strength of the concretes.

One way of handling this problem is to change the parameter k, and hereby increase the accuracy of the model for higher stress levels. This has been proposed by various researchers over the years. However, if k is changed (reduced) then the accuracy of the model will decrease in the low stress region.

In this report another way will be pursued. This new way is the two-stage model. The purpose of the two-stage model is to present a very simple failure criterion for concrete. This criterion has to be easy to use for manual calculations, as opposed to the Ottosen model, which is more suited for computer calculations. Furthermore should the two-stage model have an accuracy which is well within the normal engineering accuracy.

Consider again the figures A.3.1 to A.3.7. It is seen that the experimental results falls below the original Mohr-Coulomb model when the major principal stress reaches $\sim$-0.5f_c. In this, and in the following, are the results from B010 be disregarded. This because they behave unlike the rest of the concretes, and more importantly, the use of these low strength concretes is rather limited today.

Up to this point, σ_1=-0.5f_c, does the original Mohr-Coulomb failure criterion correlate very well with the experimental results. Beyond this point is the accuracy of the original model diminishing for increasing hydrostatical stress level. The idea was therefore to approximate the failure surface with two straight lines. The first line follows the original Mohr-Coulomb model up to σ_1=-0.5f_c, and the second line continues from this point but with a lower slope.

The original Mohr-Coulomb failure criterion (k=4) is given in eq. (5.5).

$$\sigma_3 = 4\ \sigma_1 - f_c \tag{5.5}$$

An analysis of the test results revealed that the second part of the two-stage model could be approximated as stated in eq. (5.6).

$$\sigma_3 = 3\ \sigma_1 - 1.5\ f_c \tag{5.6}$$

The resulting two-stage failure criterion is then given by eq. (5.7).

$$\sigma_3 = \max \begin{cases} 4\ \sigma_1 - f_c \\ 3\ \sigma_1 - 1.5\ f_c \end{cases} \qquad \text{tension positive} \tag{5.7}$$

$$\sigma = f_t$$

In Fig. 5.10 the two-stage model is shown along with the test results from this investigation.

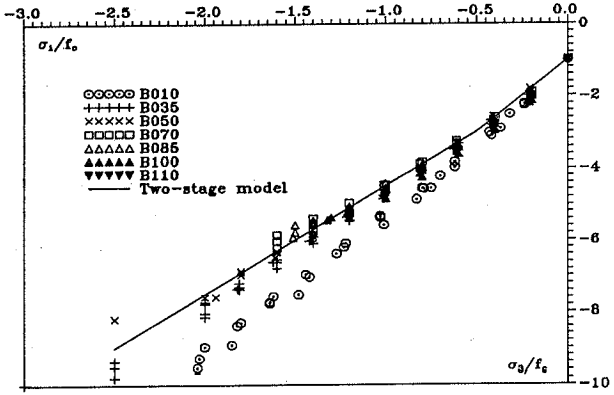

Fig. 5.10: The two-stage model compared to test data.

It is seen that the model correlates well with the test results. It is also seen that the model underestimates most of the test results, especially for the low and normal strength concretes. For the sake of simplicity the influence on the failure surface of the uniaxial concrete strength has been disregarded. In order for the two-stage model to cover the complete spectrum of concrete strength it has therefore been necessary to place the two straight lines so that the estimated failure surface is on the conservative side.

The physical explanation for the two-stage model is as follows. The reason for the change in the slope of the failure surface could be explained by a change in the internal friction angle φ. If φ decreases by increasing hydrostatic stress, then the failure surface will become more curved as the hydrostatic stress is increased. It has been attempted to measure the angles of the cracks in the specimens after they have been tested. These measurements are crude in nature, and can only be used as indicators. Furthermore are the specimens that display these cracks only the most severely loaded specimens. The measured angles between the cracks and the direction of the principal force varied between 24° and 28°. The theoretical angle corresponding to k=4 is 26.7°, and the theoretical angle corresponding to k=3 is 30°.

The theoretical change in the angle between the cracks and the direction of the minor principal stress from k=4 to k=3 is very small, and has been found to be of the same size as the scatter of the measured angles. No conclusions regarding the validity of the above argument can therefore at this time be made. However, the size of the measured angles is close to the theoretical sizes, and does therefore not contradict the argument.

5.4.1 Evaluation of the two-stage model

In the biaxial case is the two-stage model not different from the original Mohr-Coulomb model. As previously mentioned the model is therefore on the conservative side in the biaxial case.

As shown above is the model somewhat on the conservative side along the compression meridian. And because the influence of the intermediate principal strength is ignored it therefore follows that the model also is conservative along the extension meridian.

When tensile stresses are present, the two-stage model will behave like the original Mohr-Coulomb model. Since the original Mohr-Coulomb model, when combined with tension cutoff, yields a close fit to test data, it therefore follows that the two-stage model also can be used in the case of tensile stresses being present.

The presented simple two-stage model will therefore in all cases form a fair first approximation and is, due to its simplicity, very suitable for manual calculations. However, as with the modified Ottosen criterion there are some limitations to the model. These limitations are listed below.

- The two-stage model is a failure criterion for normal weight ordinary concrete. It does not include heavy- or lightweight concrete, nor does it include very rich concretes, mortars or pastes. Likewise are fiber reinforced concretes neither included in the model.

- The failure criterion is only valid for concretes with a uniaxial compressive strength up to 100 MPa.

- Along the compression meridian the failure criterion is only valid for major principal stresses below approximate 120 MPa. The model should not be extrapolated to include higher stress levels. This because, as discussed in chapter 5.2, there are some indications of a changing failure mode when the hydrostatical stress level is increased, and the model does not include this change of failure mode.

- The model has not been compared to high strength concrete test results other than along the compression meridian. There are some indications that the influence of the uniaxial concrete strength is greater along the compression meridian than along the tensile meridian. If so the lack of high strength concrete test data along the tensile meridian is not serious, but these test results are needed before a conclusion can be made.

- The model will in most cases yield a conservative value of the ultimate concrete strength. The deviation between the two-stage model and the test results is greatest in the biaxial stress space, where deviations up to 35% can be experienced.

Chapter 6

Conclusion

In this report the results from a large experimental program have been reported. The scope of the experimental program was partly to investigate the triaxial strength of high strength concrete, and partly to develop a failure criterion that is valid for all concrete strengths.

The experimental investigation was successfully undertaken, and the results have been compared to other experimental evidence. The comparison showed very good correlation between the test results here presented, and other accepted test results.

Also a number of comparison tests between concrete, mortar and pastes were performed. These results, along with the other concrete tests indicates that the maximum deviatoric stress concrete can carry is reached for a lesser hydrostatic stress level than previously thought. The relation between the concrete strength and this maximum deviatoric stress have not been determined. it was also found that the maximum deviatoric stress level seems to be depending on the homogeneity of the concrete. That is, the higher the uniaxial concrete strength, the more homogeneous is the concrete, and the lower is the maximum ratio of ρ/f_c.

The concrete tests show a large difference in the shape of the failure surface between low and normal strength concrete. The difference amounts to a much more curved failure surface for a normal strength concrete as compared to a low strength concrete. Between normal and high strength concrete the difference is not very large, but it is still noticeable.

In order to describe the failure surface for concrete, the Ottosen model was used. The model was changed somewhat in order partly to reflect the relation between the uniaxial concrete strength and the triaxial concrete strength, and partly to reflect the new knowledge of the increased curvature of the failure surface. The resulting model was validated, and found to be in close agreement with reported test data both in the triaxial, and also in the biaxial, stress space.

Since the Ottosen model is used in the CEB model code 1990 in a slightly different form, the CEB model was also compared to the test results. It was found that the determination of the parameters for the CEB model in some cases will lead to very erroneous results, especially

when determining the failure surface in the biaxial stress space.

Finally was the Mohr-Coulomb failure criterion compared to the test data. It was found that the failure criterion could be changed so also to include the ultimate strength of concrete for the higher stress levels. The resulting two-stage model was therefore introduced. The two-stage model is extremely simple to use and leads to results that are well within normal engineering accuracy.

References

[28.1] ***A Study of the Failure of Concrete under Combined Compressive Stresses.***
F.E. Richart, A. Brandzaeg, R.L. Brown, University of Illinois Engineering Station, Bulletin 185, 1928.

[52.1] ***A General Analytical Solution for Mohr's Envelope.***
G. Balmer, ASTM Proceedings, 1952, pp. 1260-1271.

[69.1] ***Behavior of Concrete under Biaxial Stresses.***
H. Kupfer, H.K. Hilsdorf, H. Rusch, Journal of the ACI, vol. 66, no. 8, 1969, pp. 656-666.

[73.1] ***Das Verhalten des Betons unter mehrachsiger Kurzzeitbelastung unter besonderer Berücksichtigung der zweiachsigen Beanspruchung.***
H. Kupfer, Deutscher Ausschuss für Stahlbeton, heft 229, 1973.

[74.1] ***Strength and Deformation Properties of Plain Concrete Subject to Combined Stress. Part 3: Results Obtained on a Range of Flint Gravel Aggregate Concretes.***
D.W. Hobbs, Cement and Concrete Association, report 42.497, July 1974.

[74.2] ***Apparatus for Testing Concrete under Multiaxial States of Stress.***
J.B. Newman, Magazine of Concrete Research, vol. 26, no. 89, December 1974, pp. 229-238.

[77.1] ***A Failure Criterion for Concrete.***
N.S. Ottosen, Journal of the Engineering Mechanics Division, ASCE, EM4, August 1977, pp. 527-535.

[82.1] ***Plasticity in Reinforced Concrete.***
W.F. Chen, McGraw-Hill Book Company, New York, 1982.

[83.1] ***Handbook of Structural Concrete.***
Pitman Advanced Publishing Program, 1983.

[84.1] ***Results of Tests Carried out on Cylindrical Concrete Specimens Subjected to Complex Stress States: A Critical Analysis.***
R. Bellotti and E. Ronzoni, Int. Conf. on Concrete under Multiax. Cond., RILEM, Press de l'Universite Paul Sabatier, Toulouse, May 1984, pp. 9 - 19.

[84.2] ***DS 423.23. Betonprøvning, Hærdnet beton, Trykstyrke.***
Dansk Standard, DS 423.23, 1984.

[84.3] ***DS 423.24. Betonprøvning, Hærdnet beton, Trækstyrke.***
Dansk Standard, DS 423.24, 1984.

[84.4] ***DS 411. Betonkonstruktioner.***
Dansk Standard, DS 411, 3. udgave, Marts 1984.

[89.1] ***Recalibration of Plastic-Fracturing Model for Concrete Confinement.***
B. Chen and S.T. Mau, Cement and Concrete Research, vol. 19, 1989, pp. 143-154.

[89.2] ***Review of Constitutive Models for Concrete.***
Y. Xiaoquin, N.S. Ottosen, S. Thelanderson, M.P. Nielsen, Report to the Commision of the European Comunities Joint Research Centre ISPRA, 1989.

[90.1] ***Preliminary State-of-the-art Report on Multiaxial Strength of Concrete.***
Kaare K. B. Dahl, Dept. of Struct. Engineering, Technical University of Denmark, Report R 262, 1990, also published in 'Højkvalitetsbetoner i 90'erne', Report 5.1

[90.2] ***CEB model code 1990.***
Comite Euro-International du Beton, Bulletin d'Information no. 203, 1991.

[91.1] ***Multiaxial Testing of Concrete.***
RILEM Technical Commitee, Final Report, Materials and Structures, vol. 24, no. 139, 1991, pp. 38-69.

[92.1] ***The Calibration and Use of a Triaxial Cell.***
Kaare K. B. Dahl, Dept. of Struct. Engineering, Technical University of Denmark, Report R 285, 1992. Also published in 'Højkvalitetsbetoner i 90'erne', Report 5.5

[92.2] ***Uniaxial Tensile Test Results.***
P.K. Nielsen, personal communications with the author, 1992.

Appendix 1

Sieve analyses

In the following appendix the sieve analyses of the aggregates, and the grain size distribution of the concrete mixes, will be presented. The sieve analyses have been performed on the three different aggregates, and both these analyses, and the total grain size distribution diagrams for the concretes are presented.

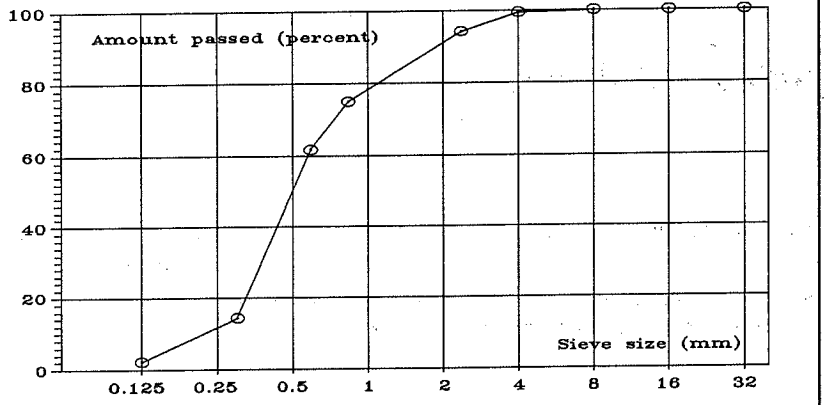

Fig. A.1.1: Sieve analysis of sand.

sieve size (mm)	amount remained (g)	amount passed (g)	amount passed (%)
32	0.0	715.8	100.0
16	0.0	715.8	100.0
8	0.0	715.8	100.0
4	4.1	711.7	99.4
2.360	37.7	674.0	94.2
0.833	137.8	536.2	74.9
0.589	95.4	440.8	61.6
0.300	338.5	102.3	14.3
0.125	86.3	16.0	2.2

Table A.1.1: Sieve analysis of the sand used in the concretes.

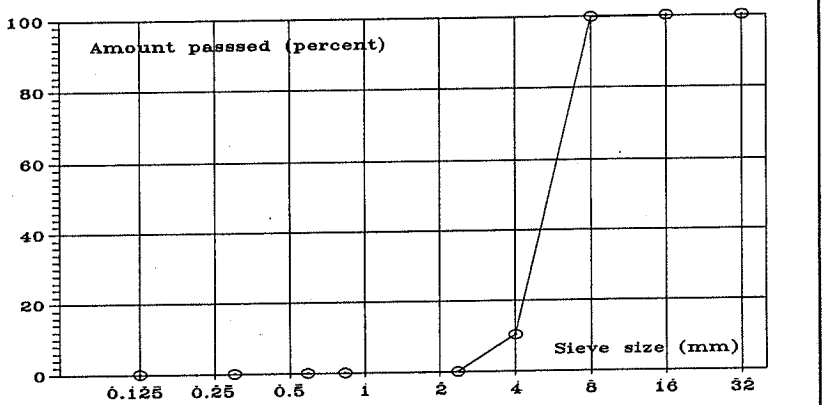

Fig. A.1.2: Sieve analysis of Gravelit.

sieve size (mm)	amount remained (g)	amount passed (g)	amount passed (%)
32	0.0	709.0	100.0
16	0.0	709.0	100.0
8	1.8	707.2	99.7
4	633.2	74.0	10.4
2.360	73.0	1.0	0.1
0.833	0.2	0.8	0.1
0.589	0.1	0.7	0.1
0.300	0.2	0.5	0.1
0.125	0.1	0.4	0.1

Table A.1.2: Sieve analysis of the Gravelit used in the concretes.

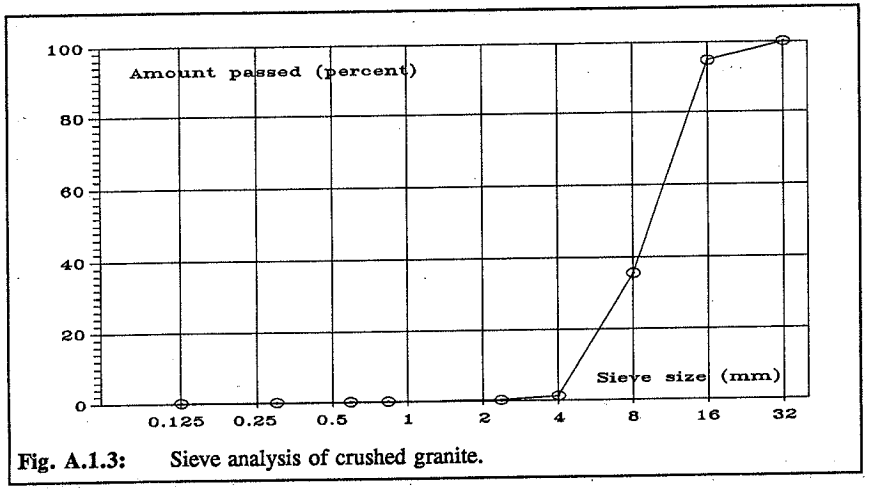

Fig. A.1.3: Sieve analysis of crushed granite.

sieve size (mm)	amount remained (g)	amount passed (g)	amount passed (%)
32	0.0	3489.5	100.0
16	186.3	3303.2	94.7
8	2063.9	1239.3	35.5
4	1196.5	42.8	1.2
2.360	37.0	5.8	0.2
0.833	1.9	3.9	0.1
0.589	0.1	3.8	0.1
0.300	0.8	3.0	0.1
0.125	0.2	2.8	0.1

Table A.1.3: Sieve analysis of the crushed granite used in the concretes.

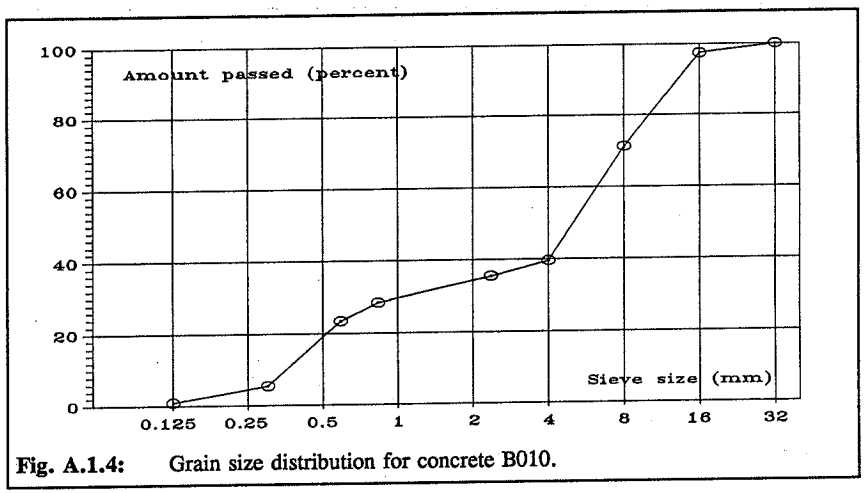

Fig. A.1.4: Grain size distribution for concrete B010.

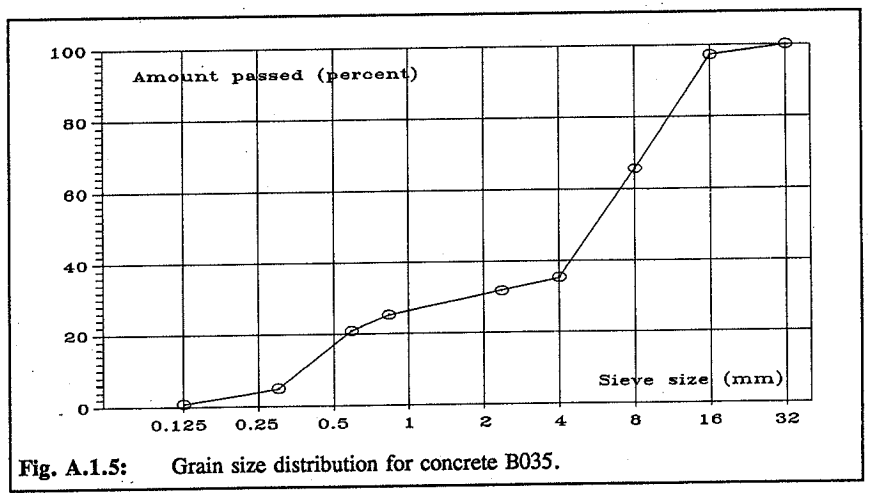

Fig. A.1.5: Grain size distribution for concrete B035.

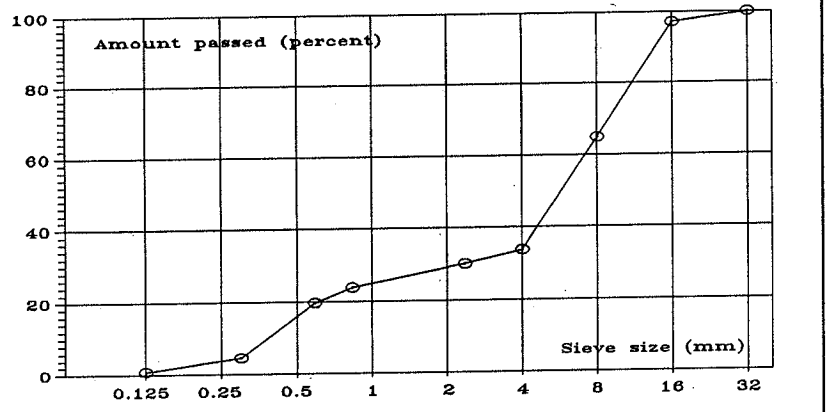

Fig. A.1.6: Grain size distribution for concrete B050.

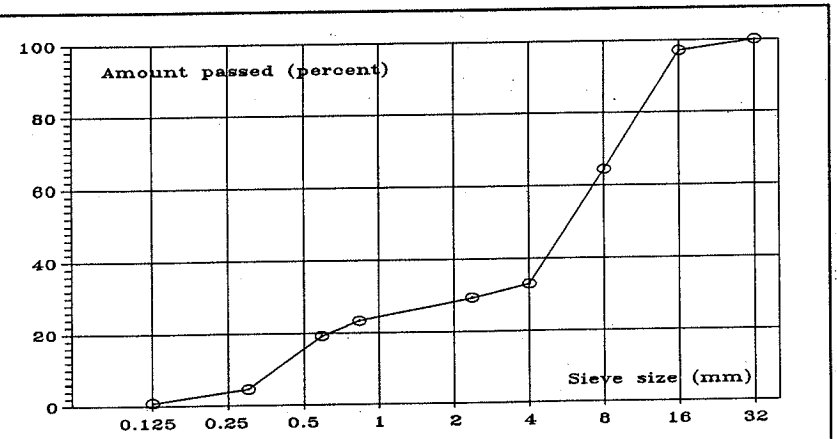

Fig. A.1.7: Grain size distribution for concrete B070.

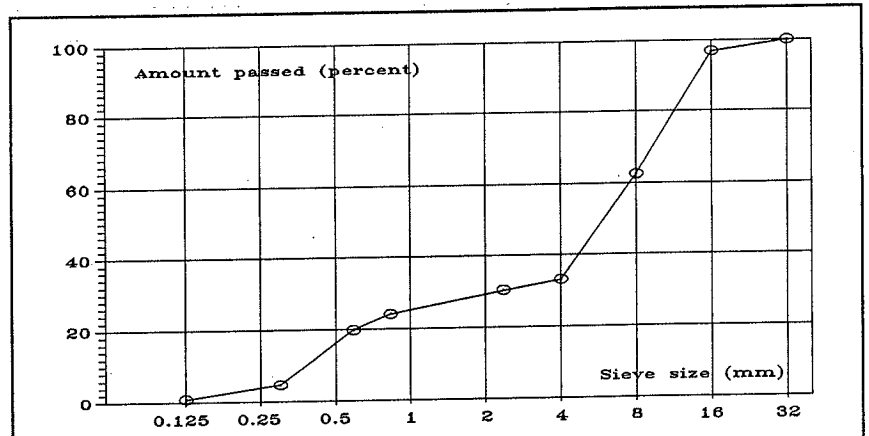

Fig. A.1.8: Grain size distribution for concrete B085.

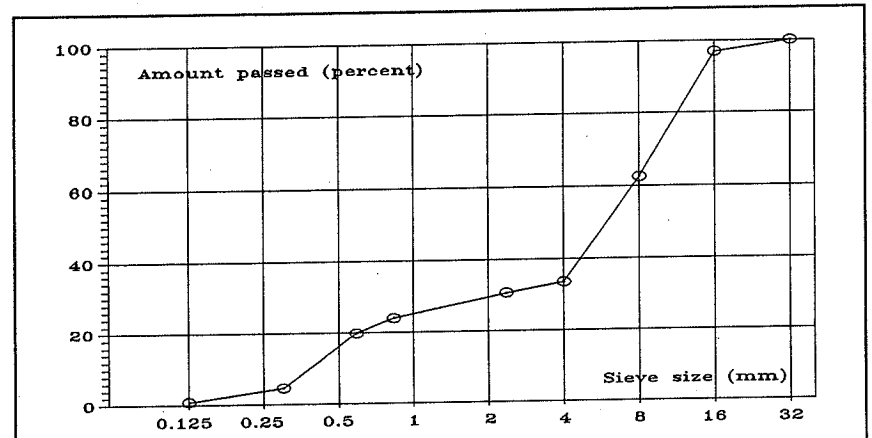

Fig. A.1.9: Grain size distribution for concrete B100.

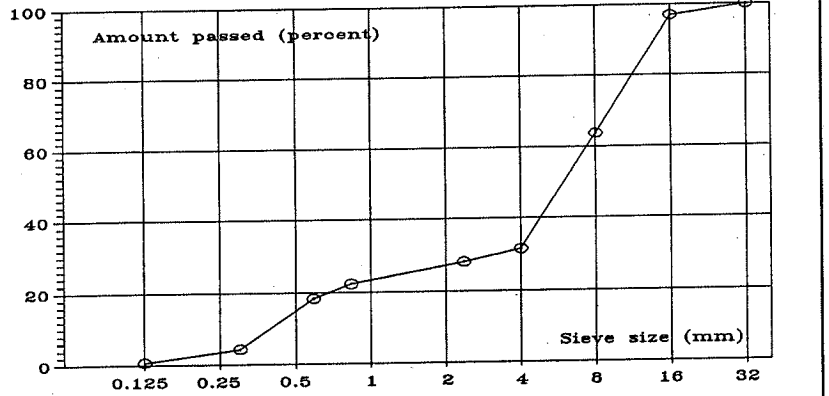

Fig. A.1.10: Grain size distribution for concrete B110.

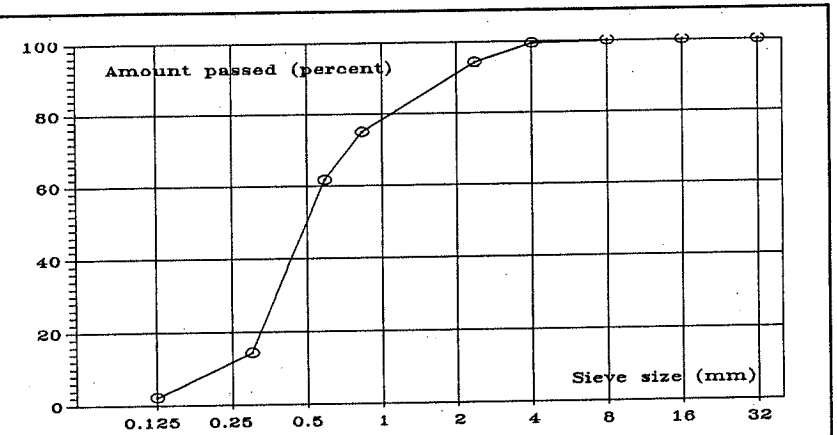

Fig. A.1.11: Grain size distribution for mortar M070-A.

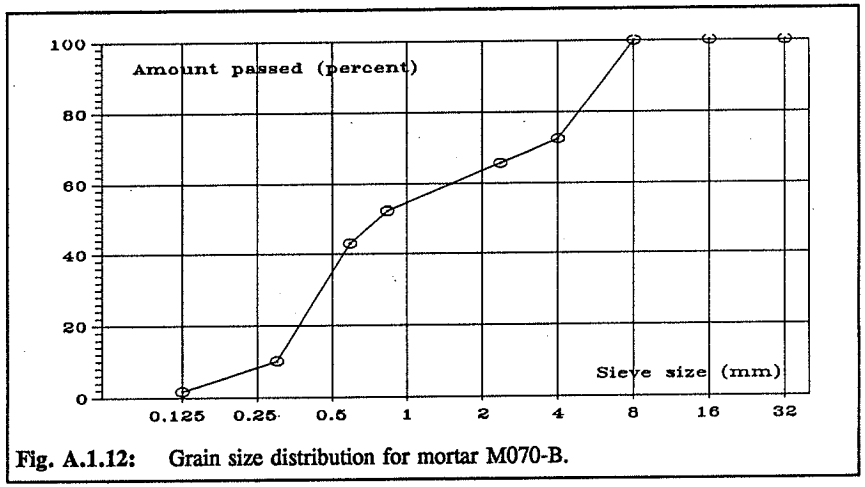

Fig. A.1.12: Grain size distribution for mortar M070-B.

Appendix 2

Triaxial test results

In table A.2.1 - A.2.24 are shown the results of the individual triaxial tests. In the tables, '***' denotes a specimen which did not fail, as described previously in chapter 4.1.

Concrete B010-1 f_c = 9.79 MPa						
Specimen	σ_1 MPa	σ_3 MPa	σ_1/f_c	σ_3/f_c	ξ/f_c	ρ/f_c
B010-1-01	-2.37	-21.76	-0.24	-2.22	-1.56	1.62
B010-1-02	-3.66	-28.37	-0.37	-2.90	-2.10	2.06
B010-1-03	-6.83	-41.33	-0.70	-4.22	-3.24	2.88
B010-1-04	-7.31	-44.63	-0.75	-4.56	-3.49	3.11
B010-1-05	-7.77	-44.72	-0.79	-4.57	-3.55	3.08
B010-1-06	-9.89	-54.58	-1.01	-5.58	-4.39	3.73
B010-1-07	-12.48	-62.45	-1.27	-6.38	-5.15	4.17
B010-1-08	-14.45	-73.60	-1.48	-7.52	-6.04	4.93
B010-1-09	-16.03	-75.63	-1.64	-7.73	-6.35	4.97
B010-1-10	-18.09	-87.35	-1.85	-8.92	-7.28	5.78
B010-1-11	-19.94	-93.51	-2.04	-9.55	-7.87	6.14
B010-1-12	-24.90	-114.20	-2.54	-11.66	-9.67	7.45
B010-1-13	-29.59	-128.81	-3.02	-13.16	-11.09	8.28
B010-1-14	-34.55	-144.02	-3.53	-14.71	-12.57	9.13
B010-1-15	-39.64	-165.23	-4.05	-16.88	-14.42	10.47
B010-1-16	-49.13	-199.08	-5.02	-20.34	-17.54	12.51
B010-1-17	-58.95	-228.85	-6.02	-23.38	-20.45	14.17
B010-1-18	-78.68	-301.34	-8.04	-30.78	-27.05	18.57
B010-1-19	-99.47	-383.12	-10.16	-39.13	-34.33	23.66
B010-1-20	-135.64	-495.95	-13.85	-50.66	-45.25	30.05

Table A.2.1: Test results, concrete B010-1.

Concrete B010-2 f_c = 14.55 MPa						
Specimen	σ_1 MPa	σ_3 MPa	σ_1/f_c	σ_3/f_c	ξ/f_c	ρ/f_c
B010-2-01	-4.64	-36.52	-0.32	-2.51	-1.82	1.79
B010-2-02	-6.20	-43.99	-0.43	-3.02	-2.24	2.12
B010-2-03	-9.03	-55.74	-0.62	-3.83	-2.93	2.62
B010-2-04	-11.67	-66.29	-0.80	-4.56	-3.56	3.07
B010-2-05	-14.92	-78.07	-1.03	-5.37	-4.28	3.54
B010-2-06	-17.68	-88.57	-1.22	-6.09	-4.92	3.98
B010-2-07	-20.91	-101.23	-1.44	-6.96	-5.68	4.51
B010-2-08	-23.55	-110.18	-1.62	-7.57	-6.24	4.86
B010-2-09	-26.53	-122.00	-1.82	-8.38	-6.95	5.36
B010-2-10	-29.55	-135.16	-2.03	-9.29	-7.71	5.93
B010-2-11	-43.97	-184.57	-3.02	-12.69	-10.81	7.89
B010-2-12	-58.44	-232.92	-4.02	-16.01	-13.88	9.79
B010-2-13	-73.11	-291.33	-5.02	-20.02	-17.36	12.25
B010-2-14	-87.51	-339.66	-6.01	-23.34	-20.42	14.15
B010-2-15	-116.97	-440.39	-8.04	-30.27	-26.76	18.15
B010-2-16	-140.57	-526.47	-9.66	-36.18	-32.05	21.66

Table A.2.2: Test results, concrete B010-2.

Concrete B010-2 f_c = 14.55 MPa						
Specimen	σ_1 MPa	σ_3 MPa	σ_1/f_c	σ_3/f_c	ξ/f_c	ρ/f_c
B010-2-01	-4.64	-36.52	-0.32	-2.51	-1.82	1.79
B010-2-02	-6.20	-43.99	-0.43	-3.02	-2.24	2.12
B010-2-03	-9.03	-55.74	-0.62	-3.83	-2.93	2.62
B010-2-04	-11.67	-66.29	-0.80	-4.56	-3.56	3.07
B010-2-05	-14.92	-78.07	-1.03	-5.37	-4.28	3.54
B010-2-06	-17.68	-88.57	-1.22	-6.09	-4.92	3.98
B010-2-07	-20.91	-101.23	-1.44	-6.96	-5.68	4.51
B010-2-08	-23.55	-110.18	-1.62	-7.57	-6.24	4.86
B010-2-09	-26.53	-122.00	-1.82	-8.38	-6.95	5.36
B010-2-10	-29.55	-135.16	-2.03	-9.29	-7.71	5.93
B010-2-11	-43.97	-184.57	-3.02	-12.69	-10.81	7.89
B010-2-12	-58.44	-232.92	-4.02	-16.01	-13.88	9.79
B010-2-13	-73.11	-291.33	-5.02	-20.02	-17.36	12.25
B010-2-14	-87.51	-339.66	-6.01	-23.34	-20.42	14.15
B010-2-15	-116.97	-440.39	-8.04	-30.27	-26.76	18.15
B010-2-16	-140.57	-526.47	-9.66	-36.18	-32.05	21.66

Table A.2.2: Test results, concrete B010-2.

Concrete B010-3 f_c = 17.08 MPa						
Specimen	σ_1 MPa	σ_3 MPa	σ_1/f_c	σ_3/f_c	ξ/f_c	ρ/f_c
B010-3-01	-4.06	-38.62	-0.24	-2.26	-1.58	1.65
B010-3-02	-7.24	-52.93	-0.42	-3.10	-2.28	2.18
B010-3-03	-10.66	-68.06	-0.62	-3.98	-3.02	2.74
B010-3-04	-14.25	-83.17	-0.83	-4.87	-3.77	3.29
B010-3-05	-17.53	-91.12	-1.03	-5.33	-4.27	3.52
B010-3-06	-20.97	-105.82	-1.23	-6.20	-4.99	4.06
B010-3-07	-24.20	-120.14	-1.42	-7.03	-5.70	4.59
B010-3-08	-28.04	-132.60	-1.64	-7.76	-6.38	5.00
B010-3-09	-30.74	-141.64	-1.80	-8.29	-6.87	5.30
B010-3-10	-34.14	-153.21	-2.00	-8.97	-7.49	5.69
B010-3-11	-51.47	-215.53	-3.01	-12.62	-10.77	7.84
B010-3-12	-69.00	-278.46	-4.04	-16.30	-14.08	10.01
B010-3-13	-85.82	-337.65	-5.02	-19.77	-17.22	12.04
B010-3-14	-103.63	-397.10	-6.07	-23.25	-20.43	14.03
B010-3-15	-138.11	-516.22	-8.09	-30.22	-26.79	18.08

Table A.2.3: Test results, concrete B010-3.

Concrete B010-3 f_c = 17.08 MPa						
Specimen	σ_1 MPa	σ_3 MPa	σ_1/f_c	σ_3/f_c	ξ/f_c	ρ/f_c
B010-3-01	-4.06	-38.62	-0.24	-2.26	-1.58	1.65
B010-3-02	-7.24	-52.93	-0.42	-3.10	-2.28	2.18
B010-3-03	-10.66	-68.06	-0.62	-3.98	-3.02	2.74
B010-3-04	-14.25	-83.17	-0.83	-4.87	-3.77	3.29
B010-3-05	-17.53	-91.12	-1.03	-5.33	-4.27	3.52
B010-3-06	-20.97	-105.82	-1.23	-6.20	-4.99	4.06
B010-3-07	-24.20	-120.14	-1.42	-7.03	-5.70	4.59
B010-3-08	-28.04	-132.60	-1.64	-7.76	-6.38	5.00
B010-3-09	-30.74	-141.64	-1.80	-8.29	-6.87	5.30
B010-3-10	-34.14	-153.21	-2.00	-8.97	-7.49	5.69
B010-3-11	-51.47	-215.53	-3.01	-12.62	-10.77	7.84
B010-3-12	-69.00	-278.46	-4.04	-16.30	-14.08	10.01
B010-3-13	-85.82	-337.65	-5.02	-19.77	-17.22	12.04
B010-3-14	-103.63	-397.10	-6.07	-23.25	-20.43	14.03
B010-3-15	-138.11	-516.22	-8.09	-30.22	-26.79	18.08

Table A.2.3: Test results, concrete B010-3.

Concrete B035-1 f_c = 37.39 MPa						
Specimen	σ_1 MPa	σ_3 MPa	σ_1/f_c	σ_3/f_c	ξ/f_c	ρ/f_c
B035-1-01	-8.46	-74.79	-0.23	-2.00	-1.42	1.45
B035-1-02	-15.86	-104.78	-0.42	-2.80	-2.11	1.94
B035-1-03	-23.00	-129.14	-0.62	-3.45	-2.70	2.32
B035-1-04	-30.07	-152.04	-0.80	-4.07	-3.28	2.66
B035-1-05	-37.85	-181.33	-1.01	-4.85	-3.97	3.13
B035-1-06	-44.94	-204.02	-1.20	-5.46	-4.54	3.47
B035-1-07	-52.50	-227.77	-1.40	-6.09	-5.14	3.83
B035-1-08	-59.80	-253.74	-1.60	-6.79	-5.76	4.24
B035-1-09	-67.56	-275.65	-1.81	-7.37	-6.34	4.54
B035-1-10	-74.82	-304.07	-2.00	-8.13	-7.01	5.01
B035-1-11	-93.54	-356.73	-2.50	-9.54	-8.40	5.75
B035-1-12	-112.20	***	***	***	***	***

Table A.2.4: Test results, concrete B035-1.

Concrete B035-1 f_c = 37.39 MPa						
Specimen	σ_1 MPa	σ_3 MPa	σ_1/f_c	σ_3/f_c	ξ/f_c	ρ/f_c
B035-1-01	-8.46	-74.79	-0.23	-2.00	-1.42	1.45
B035-1-02	-15.86	-104.78	-0.42	-2.80	-2.11	1.94
B035-1-03	-23.00	-129.14	-0.62	-3.45	-2.70	2.32
B035-1-04	-30.07	-152.04	-0.80	-4.07	-3.28	2.66
B035-1-05	-37.85	-181.33	-1.01	-4.85	-3.97	3.13
B035-1-06	-44.94	-204.02	-1.20	-5.46	-4.54	3.47
B035-1-07	-52.50	-227.77	-1.40	-6.09	-5.14	3.83
B035-1-08	-59.80	-253.74	-1.60	-6.79	-5.76	4.24
B035-1-09	-67.56	-275.65	-1.81	-7.37	-6.34	4.54
B035-1-10	-74.82	-304.07	-2.00	-8.13	-7.01	5.01
B035-1-11	-93.54	-356.73	-2.50	-9.54	-8.40	5.75
B035-1-12	-112.20	***	***	***	***	***

Table A.2.4: Test results, concrete B035-1.

Concrete B035-2 f_c = 42.95 MPa						
Specimen	σ_1 MPa	σ_3 MPa	σ_1/f_c	σ_3/f_c	ξ/f_c	ρ/f_c
B035-2-01	-9.18	-81.80	-0.21	-1.90	-1.35	1.38
B035-2-02	-18.09	-115.13	-0.42	-2.68	-2.03	1.84
B035-2-03	-26.46	-145.96	-0.62	-3.40	-2.67	2.27
B035-2-04	-34.81	-175.20	-0.81	-4.08	-3.29	2.67
B035-2-05	-43.32	-198.98	-1.01	-4.63	-3.84	2.96
B035-2-06	-51.70	-227.72	-1.20	-5.30	-4.45	3.35
B035-2-07	-60.27	-253.79	-1.40	-5.91	-5.03	3.68
B035-2-08	-68.74	-280.80	-1.60	-6.54	-5.62	4.03
B035-2-09	-77.55	-309.37	-1.81	-7.20	-6.24	4.41
B035-2-10	-85.86	-333.96	-2.00	-7.78	-6.80	4.72
B035-2-11	-107.51	-402.98	-2.50	-9.38	-8.31	5.62
B035-2-12	-129.02	-428.63	-3.00	-9.98	-9.23	5.70
B035-2-13	-140.00	***	***	***	***	***

Table A.2.5: Test results, concrete B035-2.

Concrete B035-2 f_c = 42.95 MPa						
Specimen	σ_1 MPa	σ_3 MPa	σ_1/f_c	σ_3/f_c	ξ/f_c	ρ/f_c
B035-2-01	-9.18	-81.80	-0.21	-1.90	-1.35	1.38
B035-2-02	-18.09	-115.13	-0.42	-2.68	-2.03	1.84
B035-2-03	-26.46	-145.96	-0.62	-3.40	-2.67	2.27
B035-2-04	-34.81	-175.20	-0.81	-4.08	-3.29	2.67
B035-2-05	-43.32	-198.98	-1.01	-4.63	-3.84	2.96
B035-2-06	-51.70	-227.72	-1.20	-5.30	-4.45	3.35
B035-2-07	-60.27	-253.79	-1.40	-5.91	-5.03	3.68
B035-2-08	-68.74	-280.80	-1.60	-6.54	-5.62	4.03
B035-2-09	-77.55	-309.37	-1.81	-7.20	-6.24	4.41
B035-2-10	-85.86	-333.96	-2.00	-7.78	-6.80	4.72
B035-2-11	-107.51	-402.98	-2.50	-9.38	-8.31	5.62
B035-2-12	-129.02	-428.63	-3.00	-9.98	-9.23	5.70
B035-2-13	-140.00	***	***	***	***	***

Table A.2.5: Test results, concrete B035-2.

Concrete B035-3 f_c = 40.41 MPa						
Specimen	σ_1 MPa	σ_3 MPa	σ_1/f_c	σ_3/f_c	ξ/f_c	ρ/f_c
B035-3-01	-8.47	-77.85	-0.21	-1.93	-1.35	1.40
B035-3-02	-16.53	-109.27	-0.41	-2.70	-2.03	1.87
B035-3-03	-24.26	-134.06	-0.60	-3.32	-2.61	2.22
B035-3-04	-32.57	-163.14	-0.81	-4.04	-3.26	2.64
B035-3-05	-40.79	-192.96	-1.01	-4.78	-3.92	3.07
B035-3-06	-48.57	-216.20	-1.20	-5.35	-4.48	3.39
B035-3-07	-56.89	-242.87	-1.41	-6.01	-5.10	3.76
B035-3-08	-64.81	-267.17	-1.60	-6.61	-5.67	4.09
B035-3-09	-73.00	-295.38	-1.81	-7.31	-6.31	4.49
B035-3-10	-81.02	-311.89	-2.00	-7.72	-6.77	4.66
B035-3-11	-101.13	-395.86	-2.50	-9.80	-8.55	5.96
B035-3-12	-101.00	***	***	***	***	***
B035-3-13	-121.20	***	***	***	***	***

Table A.2.6: Test results, concrete B035-3.

Concrete B035-4 f_c = 42.11 MPa						
Specimen	σ_1 MPa	σ_3 MPa	σ_1/f_c	σ_3/f_c	ξ/f_c	ρ/f_c
B035-4-01	-8.48	-81.96	-0.20	-1.95	-1.36	1.42
B035-4-02	-17.60	-113.07	-0.42	-2.69	-2.03	1.85
B035-4-03	-26.35	-146.45	-0.63	-3.48	-2.73	2.33
B035-4-04	-34.18	-167.47	-0.81	-3.98	-3.23	-2.58
B035-4-05	-42.05	-196.91	-1.00	-4.68	-3.85	3.00
B035-4-06	-50.86	-226.21	-1.21	-5.37	-4.50	3.40
B035-4-07	-59.72	-253.76	-1.42	-6.03	-5.12	3.76
B035-4-08	-68.13	-278.74	-1.62	-6.62	-5.69	4.08
B035-4-09	-76.68	-309.88	-1.82	-7.36	-6.35	4.52
B035-4-10	-84.39	-338.53	-2.00	-8.04	-6.96	4.93

Table A.2.7: Test results, concrete B035-4.

Concrete B050-1 f_c = 52.17 MPa						
Specimen	σ_1 MPa	σ_3 MPa	σ_1/f_c	σ_3/f_c	ξ/f_c	ρ/f_c
B050-1-01	-10.88	-100.76	-0.21	-1.93	-1.36	1.41
B050-1-02	-21.20	-138.57	-0.41	-2.66	-2.00	1.84
B050-1-03	-31.90	-178.67	-0.61	-3.42	-2.68	2.30
B050-1-04	-41.86	-211.04	-0.80	-4.05	-3.26	2.65
B050-1-05	-52.53	-242.15	-1.01	-4.64	-3.84	2.97
B050-1-06	-62.66	-275.95	-1.20	-5.29	-4.44	3.34
B050-1-07	-73.23	-307.85	-1.40	-5.90	-5.03	3.67
B050-1-08	-83.82	-338.40	-1.61	-6.49	-5.60	3.98
B050-1-09	-94.01	-363.38	-1.80	-6.97	-6.10	4.22
B050-1-10	-104.43	-395.90	-2.00	-7.59	-6.69	4.56
B050-1-11	-101.13	-395.86	-1.94	-7.59	-6.62	4.61
B050-1-12	130.40	***	***	***	***	***
B050-1-13	130.40	***	***	***	***	***

Table A.2.8: Test results, concrete B050-1.

Concrete B050-2 f_c = 52.72 MPa						
Specimen	σ_1 MPa	σ_3 MPa	σ_1/f_c	σ_3/f_c	ξ/f_c	ρ/f_c
B050-2-01	-10.99	-95.44	-0.21	-1.81	-1.29	1.31
B050-2-02	-21.59	-135.55	-0.41	-2.57	-1.96	1.76
B050-2-03	-31.88	-174.86	-0.60	-3.32	-2.61	2.21
B050-2-04	-42.50	212.35	-0.81	-4.03	-3.26	2.63
B050-2-05	-53.11	-243.77	-1.01	-4.62	-3.83	2.95
B050-2-06	-63.42	-274.57	-1.20	-5.21	-4.40	3.27
B050-2-07	-73.86	-307.16	-1.40	-5.83	-4.98	3.61
B050-2-08	-84.39	-335.02	-1.60	-6.35	-5.52	3.88
B050-2-09	-95.01	-363.89	-1.80	-6.90	-6.07	4.16
B050-2-10	105.40	***	***	***	***	***
B050-2-11	-131.87	-431.65	-2.50	-8.19	-7.62	4.64

Table A.2.9: Test results, concrete B050-2.

Concrete B050-3 f_c = 51.54 MPa						
Specimen	σ_1 MPa	σ_3 MPa	σ_1/f_c	σ_3/f_c	ξ/f_c	ρ/f_c
B050-3-01	-10.97	-103.53	-0.21	-2.01	-1.41	1.47
B050-3-02	-21.27	-136.54	-0.41	-2.65	-2.01	1.83
B050-3-03	-31.08	-171.96	-0.60	-3.34	-2.62	2.23
B050-3-04	-41.70	-214.73	-0.81	-4.17	-3.34	2.74
B050-3-05	-51.87	-246.67	-1.01	-4.79	-3.93	3.09
B050-3-06	-61.87	-270.74	-1.20	-5.25	-4.42	3.31
B050-3-07	-72.16	-300.81	-1.40	-5.84	-4.99	3.62
B050-3-08	-82.53	-325.21	-1.60	-6.31	-5.49	3.84
B050-3-09	-92.86	-353.67	-1.80	-6.86	-6.04	4.13
B050-3-10	103.10	***	***	***	***	***

Table A.2.10: Test results, concrete B050-3.

Concrete B070-1 f_c = 64.12 MPa						
Specimen	σ_1 MPa	σ_3 MPa	σ_1/f_c	σ_3/f_c	ξ/f_c	ρ/f_c
B070-1-01	-13.09	-129.00	-0.20	-2.01	-1.40	1.48
B070-1-02	-26.48	-178.23	-0.41	-2.78	-2.08	1.93
B070-1-03	-38.97	-215.24	-0.61	-3.36	-2.64	2.24
B070-1-04	-51.79	-258.05	-0.81	-4.02	-3.26	2.63
B070-1-05	-64.34	-296.55	-1.00	-4.62	-3.83	2.96
B070-1-06	-77.13	-337.24	-1.20	-5.26	-4.43	3.31
B070-1-07	-89.82	-368.95	-1.40	-5.75	-4.94	3.55
B070-1-08	-102.80	-399.25	-1.60	-6.23	-5.45	3.77

Table A.2.11: Test results, concrete B070-1.

Concrete B070-2 f_c = 71.65 MPa						
Specimen	σ_1 MPa	σ_3 MPa	σ_1/f_c	σ_3/f_c	ξ/f_c	ρ/f_c
B070-2-01	-14.68	-135.79	-0.20	-1.90	-1.33	1.38
B070-2-02	-28.95	-186.29	-0.40	-2.60	-1.97	1.79
B070-2-03	-43.73	-232.62	-0.61	-3.25	-2.58	2.15
B070-2-04	-57.86	-278.46	-0.81	-3.89	-3.18	2.51
B070-2-05	-72.02	-321.92	-1.01	-4.49	-3.75	2.85
B070-2-06	-86.20	-355.85	-1.20	-4.97	-4.26	3.07
B070-2-07	-100.27	-397.01	-1.40	-5.54	-4.82	3.38
B070-2-08	-114.66	-431.27	-1.60	-6.02	-5.32	3.61

Table A.2.12: Test results, concrete B070-2.

Concrete B070-3 f_c = 76.73 MPa						
Specimen	σ_1 MPa	σ_3 MPa	σ_1/f_c	σ_3/f_c	ξ/f_c	ρ/f_c
B070-3-01	-15.70	-148.09	-0.20	-1.93	-1.35	1.41
B070-3-02	-31.20	-205.24	-0.41	-2.67	-2.01	1.85
B070-3-03	-46.57	-253.88	-0.61	-3.31	-2.61	2.21
B070-3-04	-61.69	-293.74	-0.80	-3.83	-3.14	2.47
B070-3-05	-76.85	-341.85	-1.00	-4.46	-3.73	2.82
B070-3-06	-92.28	-381.67	-1.20	-4.97	-4.26	3.08
B070-3-07	-107.44	-414.40	-1.40	-5.40	-4.73	3.27
B070-3-08	-123.09	-449.33	-1.60	-5.86	-5.23	3.47
B070-3-09	-138.10	***	***	***	***	***

Table A.2.13: Test results, concrete B070-3.

Concrete B085-1 f_c = 89.46 MPa						
Specimen	σ_1 MPa	σ_3 MPa	σ_1/f_c	σ_3/f_c	ξ/f_c	ρ/f_c
B085-1-01	-17.90	-174.22	-0.20	-1.95	-1.36	1.43
B085-1-02	-36.48	-241.67	-0.41	-2.70	-2.03	1.87
B085-1-03	-54.24	-297.45	-0.61	-3.32	-2.62	2.22
B085-1-04	-71.83	-350.55	-0.80	-3.92	-3.19	2.54
B085-1-05	-89.80	-396.04	-1.00	-4.43	-3.72	2.80
B085-1-06	-107.57	-452.84	-1.20	-5.06	-4.31	3.15
B085-1-07	-125.36	-487.94	-1.40	-5.45	-4.77	3.31
B085-1-08	-125.19	-494.44	-1.40	-5.53	-4.81	3.37
B085-1-09	-134.28	-499.56	-1.50	-5.58	-4.96	3.33

Table A.2.14: Test results, concrete B085-1.

Concrete B085-2 f_c = 90.36 MPa						
Specimen	σ_1 MPa	σ_3 MPa	σ_1/f_c	σ_3/f_c	ξ/f_c	ρ/f_c
B085-2-01	-18.50	-179.83	-0.20	-1.99	-1.39	1.46
B085-2-02	-36.59	-246.59	-0.40	-2.73	-2.04	1.90
B085-2-03	-54.58	-310.81	-0.60	-3.44	-2.68	2.32
B085-2-04	-72.56	-360.84	-0.80	-3.99	-3.23	2.60
B085-2-05	-90.67	-410.00	-1.00	-4.54	-3.78	2.89
B085-2-06	-108.57	-462.70	-1.20	-5.12	-4.34	3.20
B085-2-07	-126.60	-497.37	-1.40	-5.50	-4.80	3.35
B085-2-08	-135.57	-522.65	-1.50	-5.78	-5.07	3.50

Table A.2.15: Test results, concrete B085-2.

Concrete B085-3 f_c = 88.39 MPa						
Specimen	σ_1 MPa	σ_3 MPa	σ_1/f_c	σ_3/f_c	ξ/f_c	ρ/f_c
B085-3-01	-18.11	-173.30	-0.20	-1.96	-1.37	1.43
B085-3-02	-36.09	-240.61	-0.41	-2.72	-2.04	1.89
B085-3-03	-53.42	-298.13	-0.60	-3.37	-2.65	2.26
B085-3-04	-71.11	-345.22	-0.80	-3.91	-3.18	2.53
B085-3-05	-88.72	-405.02	-1.00	-4.58	-3.80	2.92
B085-3-06	-106.48	-455.44	-1.20	-5.15	-4.37	3.22
B085-3-07	-123.78	-492.97	-1.40	-5.58	-4.84	3.41
B085-3-08	-133.03	-523.16	-1.51	-5.92	-5.16	3.60
B085-3-09	132.60	***	***	***	***	***

Table A.2.16: Test results, concrete B085-3.

Concrete B100-1 f_c = 106.20 MPa						
Specimen	σ_1 MPa	σ_3 MPa	σ_1/f_c	σ_3/f_c	ξ/f_c	ρ/f_c
B100-1-01	-21.95	-225.30	-0.21	-2.12	-1.46	1.56
B100-1-02	-43.12	-304.08	-0.41	-2.86	-2.12	2.01
B100-1-03	-64.62	-376.52	-0.61	-3.55	-2.75	2.40
B100-1-04	-85.57	-439.32	-0.81	-4.14	-3.32	2.72
B100-1-05	-107.09	-499.93	-1.01	-4.71	-3.88	3.02
B100-1-06	-128.02	-556.10	-1.21	-5.24	-4.42	3.29
B100-1-07	-140.26	-577.72	-1.32	-5.44	-4.67	3.36

Table A.2.17: Test results, concrete B100-1.

Concrete B100-2 f_c = 107.12 MPa						
Specimen	σ_1 MPa	σ_3 MPa	σ_1/f_c	σ_3/f_c	ξ/f_c	ρ/f_c
B100-2-01	-21.91	-228.15	-0.20	-2.13	-1.47	1.57
B100-2-02	-43.21	-298.85	-0.40	-2.79	-2.08	1.95
B100-2-03	-64.81	-372.67	-0.61	-3.48	-2.71	2.35
B100-2-04	-86.11	-435.73	-0.80	-4.07	-3.28	2.66
B100-2-05	-107.38	-493.66	-1.00	-4.61	-3.82	2.94
B100-2-06	-128.86	-545.53	-1.20	-5.09	-4.33	3.18
B100-2-07	-139.47	-575.46	-1.30	-5.37	-4.61	3.32

Table A.2.18: Test results, concrete B100-2.

Concrete B100-3 f_c = 99.82 MPa						
Specimen	σ_1 MPa	σ_3 MPa	σ_1/f_c	σ_3/f_c	ξ/f_c	ρ/f_c
B100-3-01	-20.71	-219.91	-0.21	-2.20	-1.51	1.63
B100-3-02	-40.40	-294.43	-0.40	-2.95	-2.17	2.08
B100-3-03	-60.39	-360.69	-0.60	-3.61	-2.78	2.46
B100-3-04	-80.12	-424.32	-0.80	-4.25	-3.38	2.82
B100-3-05	-100.29	-484.05	-1.00	-4.85	-3.96	3.14
B100-3-06	-120.09	-536.98	-1.20	-5.38	-4.50	3.41
B100-3-07	-139.71	-579.69	-1.40	-5.81	-4.97	3.60

Table A.2.19: Test results, concrete B100-3.

Concrete B110-1 f_c = 108.80 MPa						
Specimen	σ_1 MPa	σ_3 MPa	σ_1/f_c	σ_3/f_c	ξ/f_c	ρ/f_c
B110-1-01	-22.39	-232.28	-0.21	-2.13	-1.47	1.58
B110-1-02	-43.74	-305.84	-0.40	-2.81	-2.09	1.97
B110-1-03	-65.57	-383.01	-0.60	-3.52	-2.73	2.38
B110-1-04	-87.06	-454.01	-0.80	-4.17	-3.33	2.75
B110-1-05	-109.35	-509.01	-1.01	-4.68	-3.86	3.00
B110-1-06	-130.45	-560.71	-1.20	-5.15	-4.36	3.23

Table A.2.20: Test results, concrete B110-1.

Concrete B110-2 f_c =108.76 MPa						
Specimen	σ_1 MPa	σ_3 MPa	σ_1/f_c	σ_3/f_c	ξ/f_c	ρ/f_c
B110-2-01	-22.21	-224.02	-0.20	-2.06	-1.43	1.52
B110-2-02	-44.01	-307.01	-0.40	-2.82	-2.10	1.97
B110-2-03	-65.83	-385.17	-0.61	-3.54	-2.74	2.40
B110-2-04	-87.25	-445.97	-0.80	-4.10	-3.29	2.69
B110-2-05	-109.19	-510.36	-1.00	-4.69	-3.87	3.01
B110-2-06	-131.05	-560.04	-1.20	-5.15	-4.36	3.22

Table A.2.21: Test results, concrete B110-2.

Cement paste P070 f_c = 70(*) MPa						
Specimen	σ_1 MPa	σ_3 MPa	σ_1/f_c	σ_3/f_c	ξ/f_c	ρ/f_c
P070-1-01	-6.30	-88.44	-0.09	-1.26	-0.83	0.96
P070-1-02	-9.95	-98.65	-0.14	-1.41	-0.98	1.03
P070-1-03	-19.98	-127.45	-0.29	-1.82	-1.38	1.25
P070-1-04	-29.80	-146.07	-0.43	-2.09	-1.70	1.36
P070-1-05	-39.78	-158.97	-0.57	-2.27	-1.97	1.39
P070-1-06	-49.91	-168.48	-0.71	-2.41	-2.21	1.38
P070-1-07	-59.84	-179.87	-0.85	-2.57	-2.47	1.40
P070-1-08	-79.61	-196.92	-1.14	-2.81	-2.94	1.37
P070-1-09	-99.67	-216.44	-1.42	-3.09	-3.43	1.36

Table A.2.22: Test results, cement paste P070.

(*) The uniaxial strength is based on the triaxial tests 1 - 3, rather than the normal uniaxial tests. This due to heavy shrinkage cracks in the test cylinders.

Mortar M070-A f_c = 73.49 MPa						
Specimen	σ_1 MPa	σ_3 MPa	σ_1/f_c	σ_3/f_c	ξ/f_c	ρ/f_c
M070-1-01	-14.94	-122.48	-0.20	-1.67	-1.20	1.19
M070-1-02	-29.72	-163.36	-0.40	-2.22	-1.75	1.48
M070-1-03	-44.19	-198.00	-0.60	-2.69	-2.25	1.71
M070-1-04	-58.86	-226.86	-0.80	-3.09	-2.71	1.87
M070-1-05	-73.87	-240.79	-1.01	-3.28	-3.05	1.85
M070-1-06	-88.46	-255.70	-1.20	-3.48	-3.40	1.86

Table A.2.23: Test results, mortar M070-A.

Mortar M070-B f_c = 69.61 MPa						
Specimen	σ_1 MPa	σ_3 MPa	σ_1/f_c	σ_3/f_c	ξ/f_c	ρ/f_c
M070-2-01	-14.05	-122.71	-0.20	-1.76	-1.25	1.27
M070-2-02	-27.97	-162.36	-0.40	-2.33	-1.81	1.58
M070-2-03	-42.06	-201.79	-0.60	-2.90	-2.37	1.87
M070-2-04	-55.83	-228.47	-0.80	-3.28	-2.82	2.02
M070-2-05	-69.67	-253.77	-1.00	-3.65	-3.26	2.16
M070-2-06	-83.50	-270.60	-1.20	-3.89	-3.63	2.19
M070-2-07	-97.38	-290.28	-1.40	-4.17	-4.02	2.26
M070-2-08	-111.66	-303.60	-1.60	-4.36	-4.37	2.25

Table A.2.24: Test results, mortar M070-B.

Appendix 3

Triaxial strength diagrams

In this appendix the test results are shown graphically. The results are also compared to the original Coulomb model, chapter 2.3, and the original Ottosen model, chapter 2.4. Also shown are the results from the test of the mortars and the paste. These results are partly compared to the above mentioned models, and partly to the results of the concrete B070 tests.

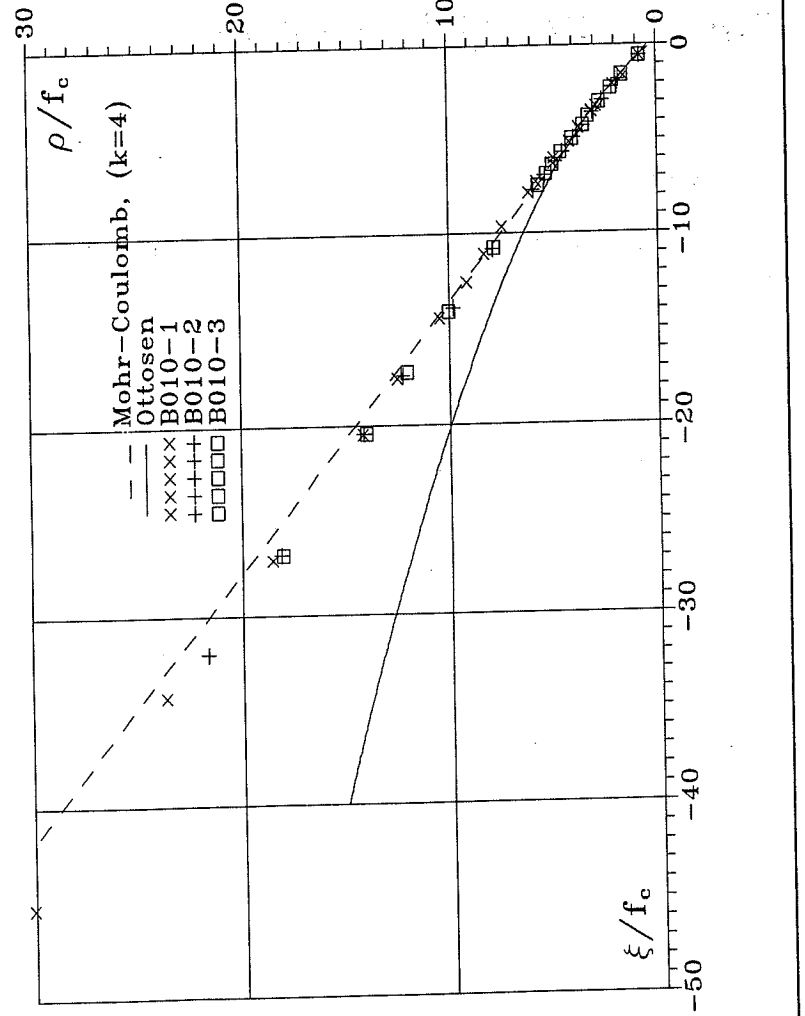

Fig. A.3.1: Test results from concrete B010, compared to the Mohr-Coulomb and the Ottosen model.

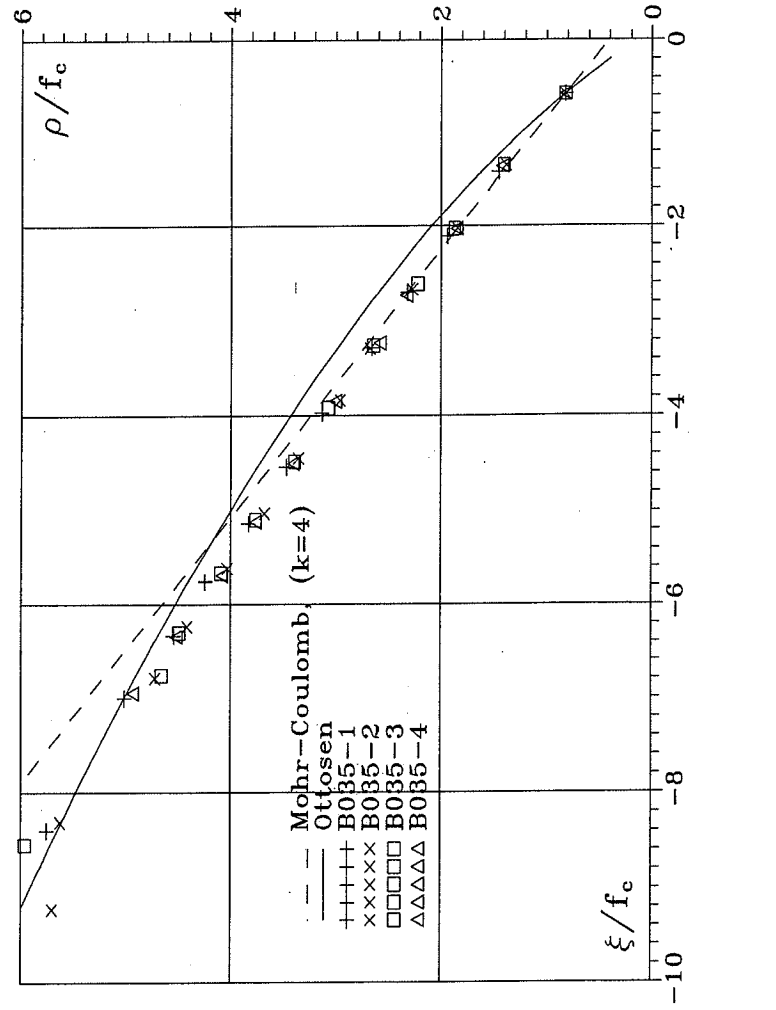

Fig. A.3.2: Test results from concrete B035, compared to the Mohr-Coulomb and the Ottosen model.

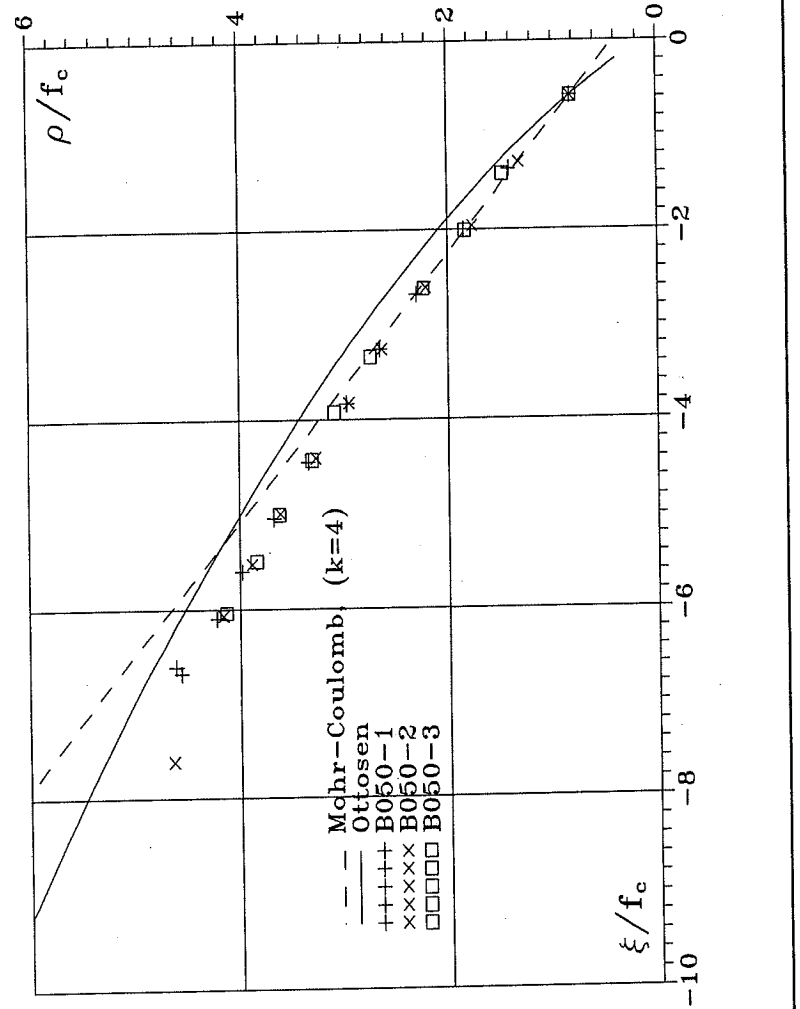

Fig. A.3.3: Test results from concrete B050, compared to the Mohr-Coulomb and the Ottosen model.

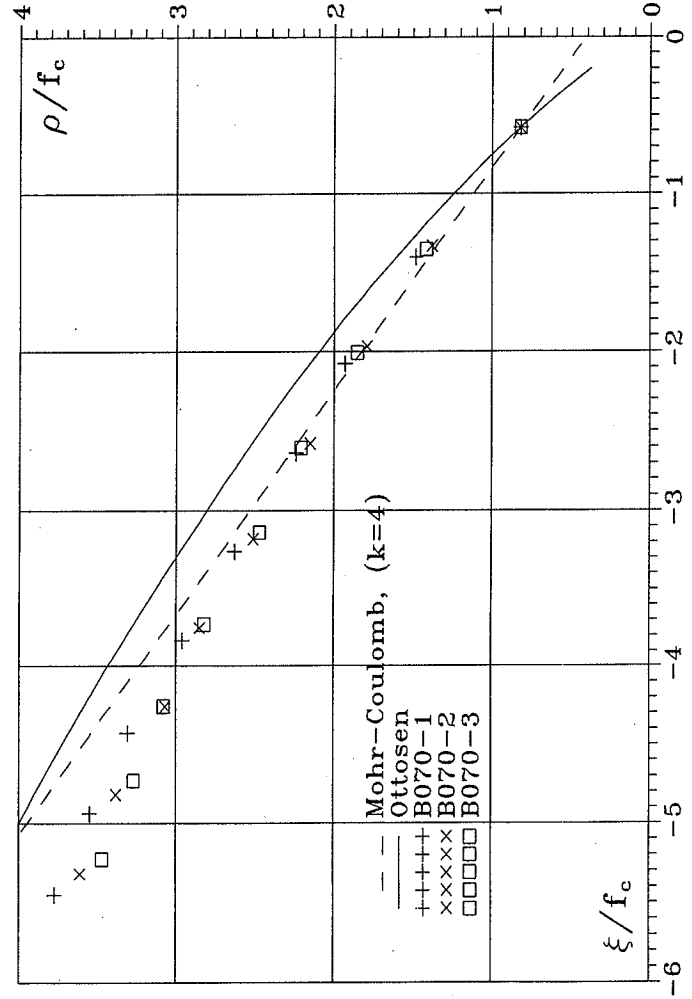

Fig. A.3.4: Test results from concrete B070, compared to the Mohr-Coulomb and the Ottosen model.

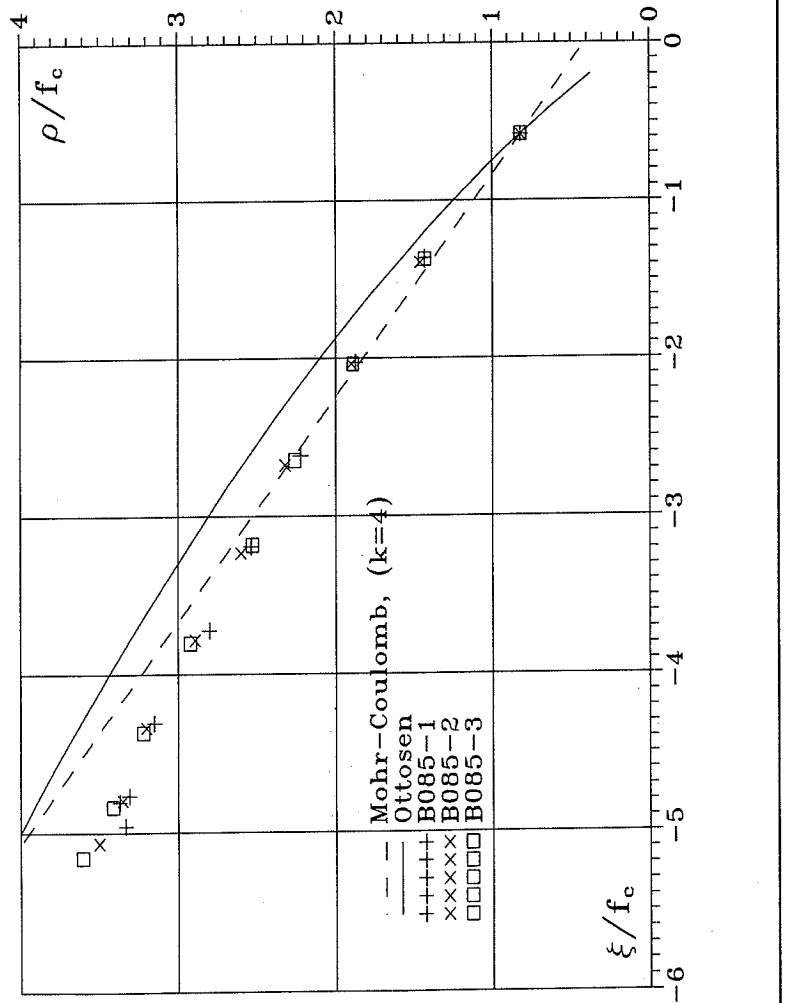

Fig. A.3.5: Test results from concrete B085, compared to the Mohr-Coulomb and the Ottosen model.

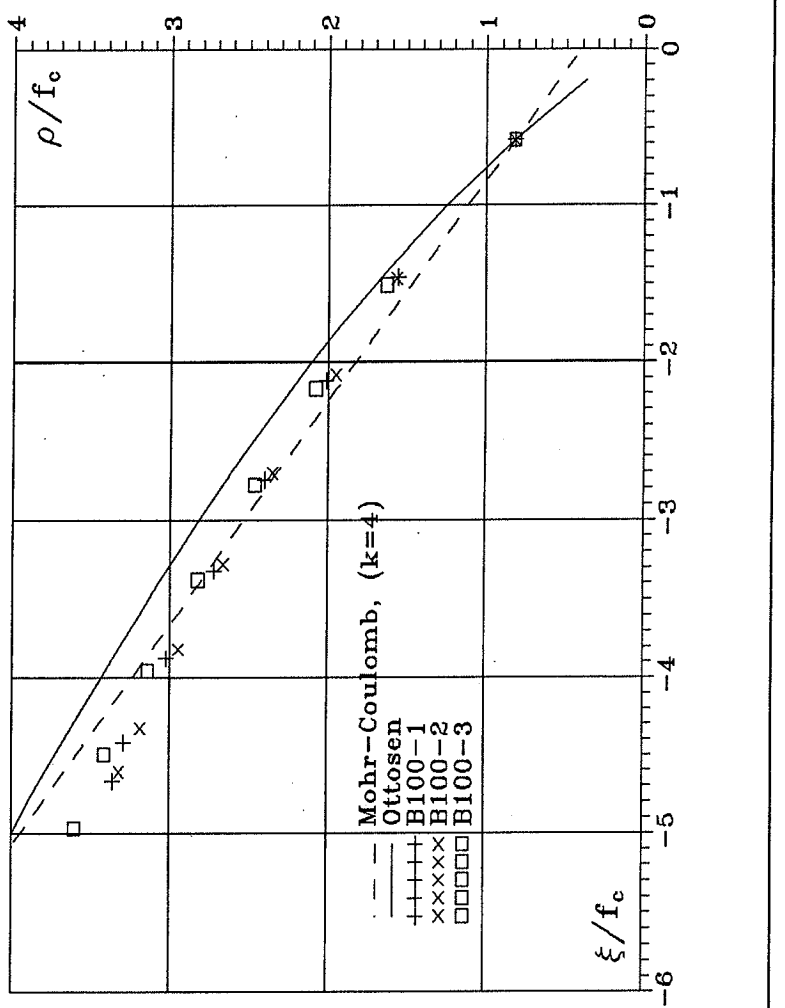

Fig. A.3.6: Test results from concrete B100, compared to the Mohr-Coulomb and the Ottosen model.

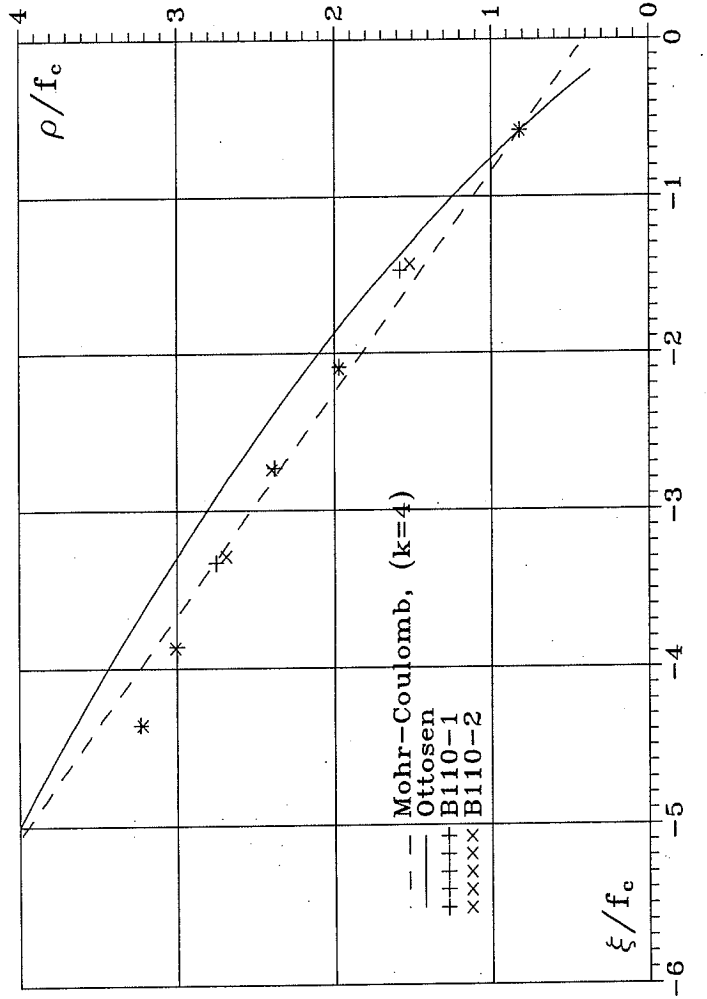

Fig. A.3.7: Test results from concrete B110, compared to the Mohr-Coulomb and the Ottosen model.

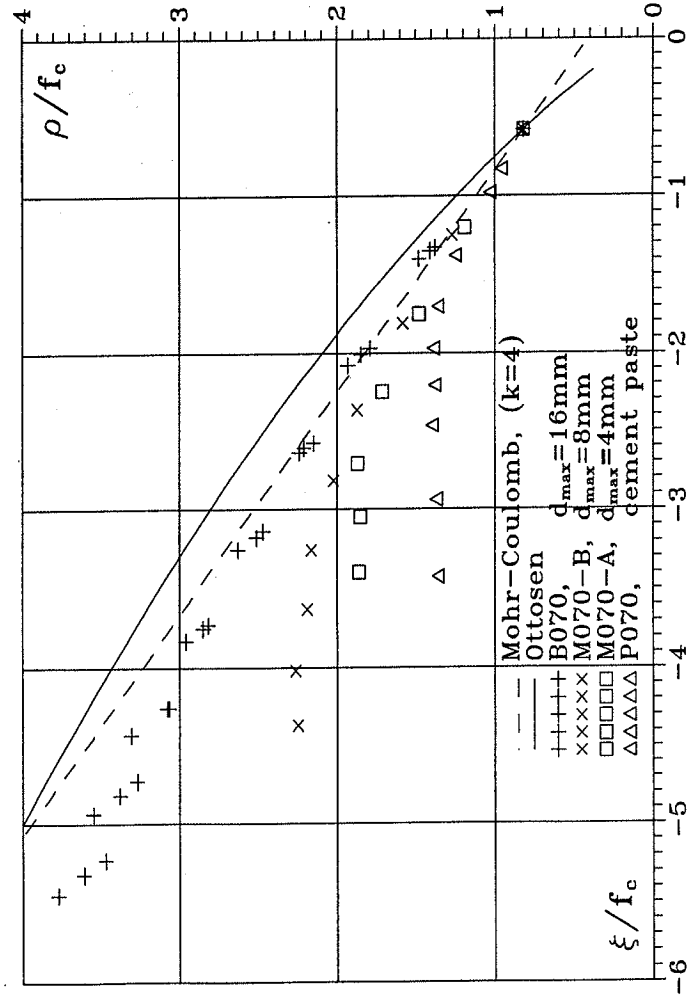

Fig. A.3.8: Test results from concrete B070, mortars M070-A and M070-B, and paste P070, compared to the Mohr-Coulomb and the Ottosen model.

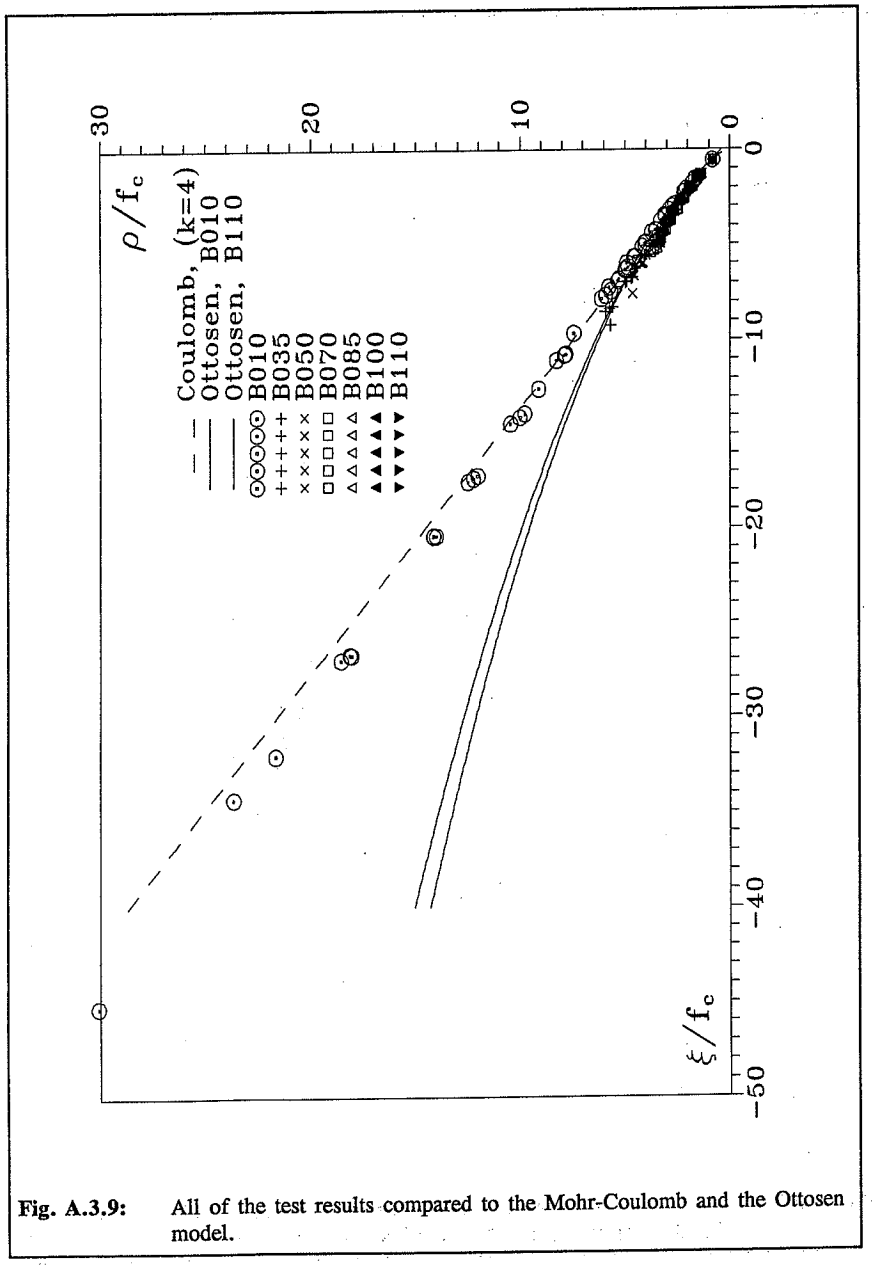

Fig. A.3.9: All of the test results compared to the Mohr-Coulomb and the Ottosen model.

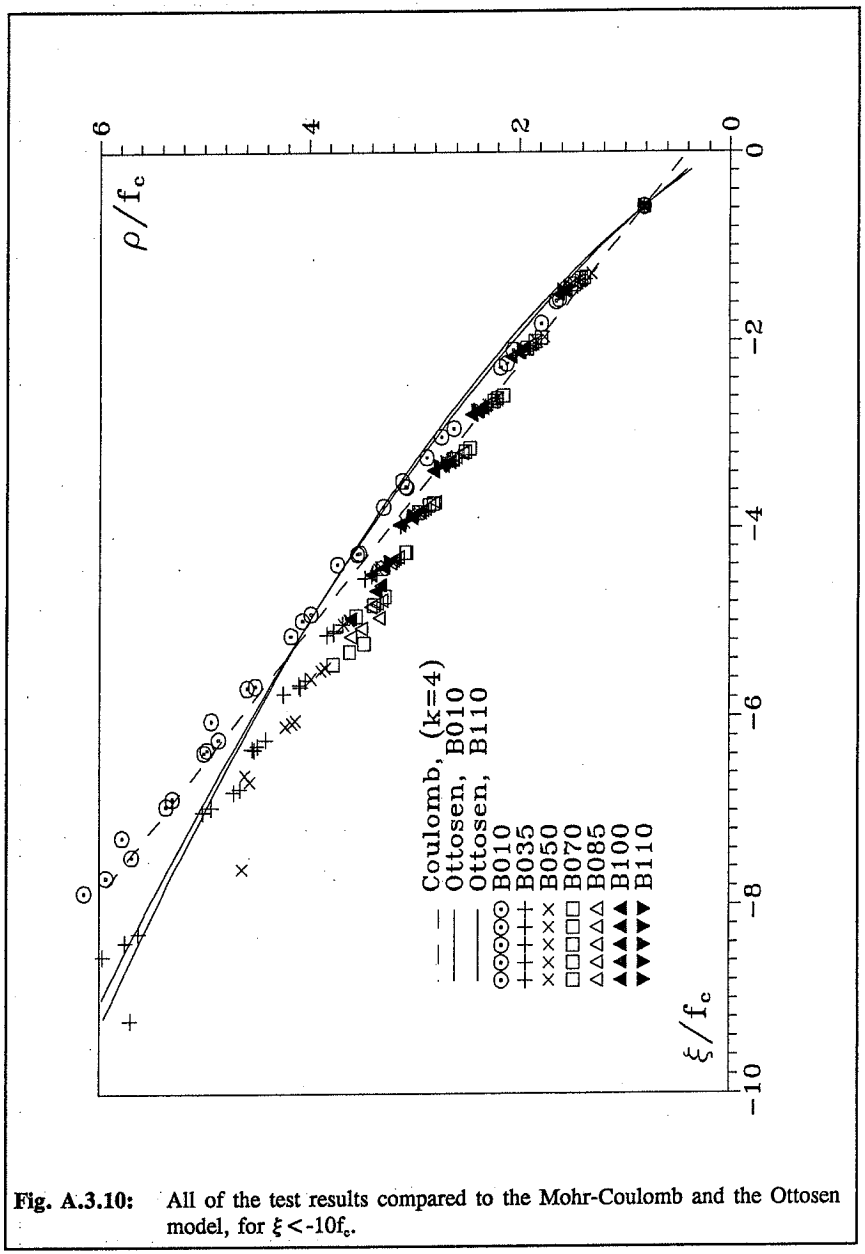

Fig. A.3.10: All of the test results compared to the Mohr-Coulomb and the Ottosen model, for $\xi < -10 f_c$.

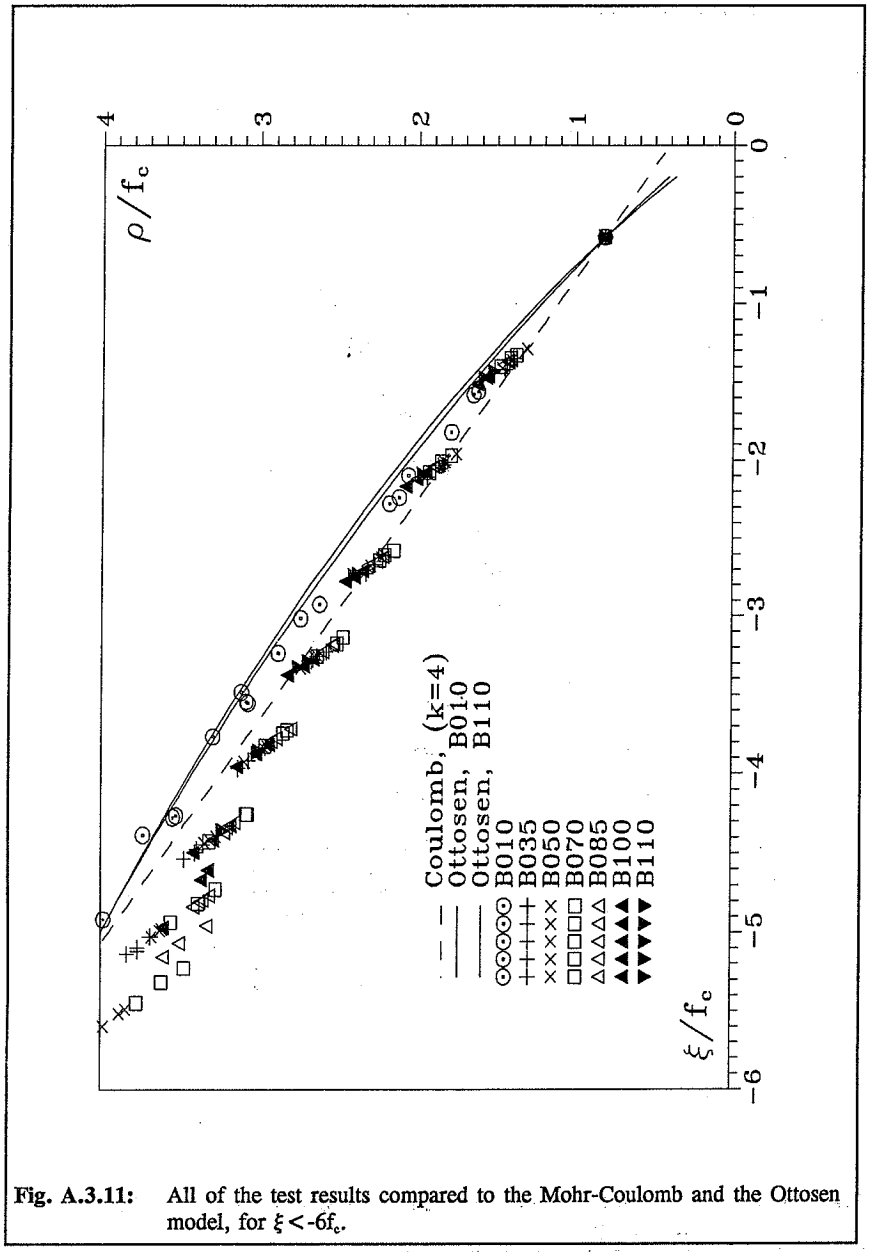

Fig. A.3.11: All of the test results compared to the Mohr-Coulomb and the Ottosen model, for $\xi < -6f_c$.

Appendix 4

Photos of the test specimens

In this appendix photos of the test specimens are presented as they look after being tested. In the case of the low and normal strength concretes, only some of the test specimens have been photographed, However those given in this appendix form a representative part of the test specimens.

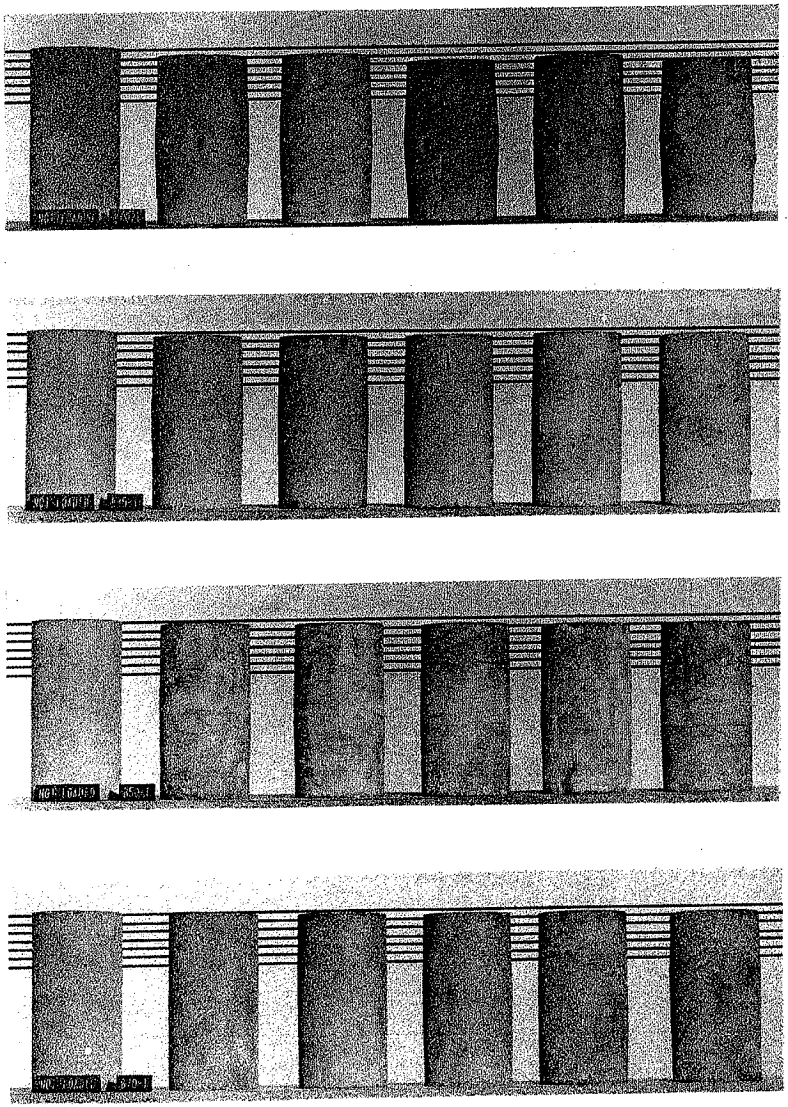

Fig. A.4.1: Test specimens B010-1 to B070-1, first part.

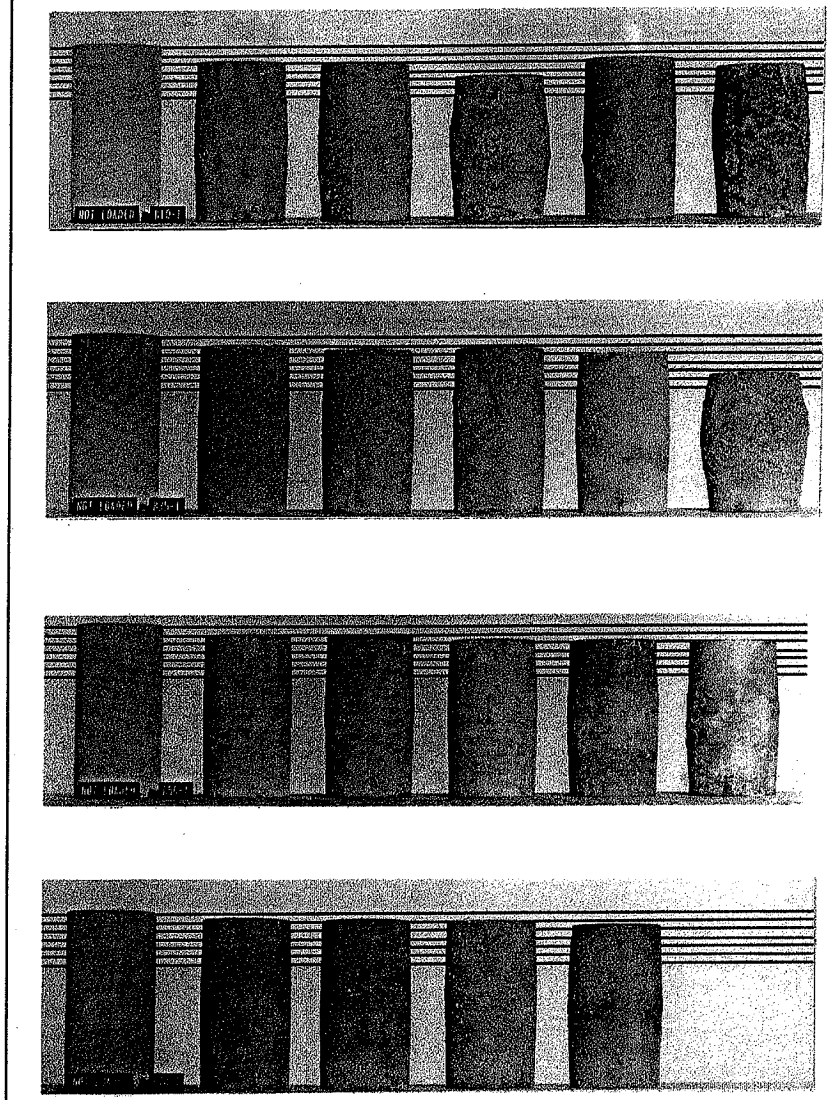

Fig. A.4.2: Test specimens B010-1 to B070-1, second part.

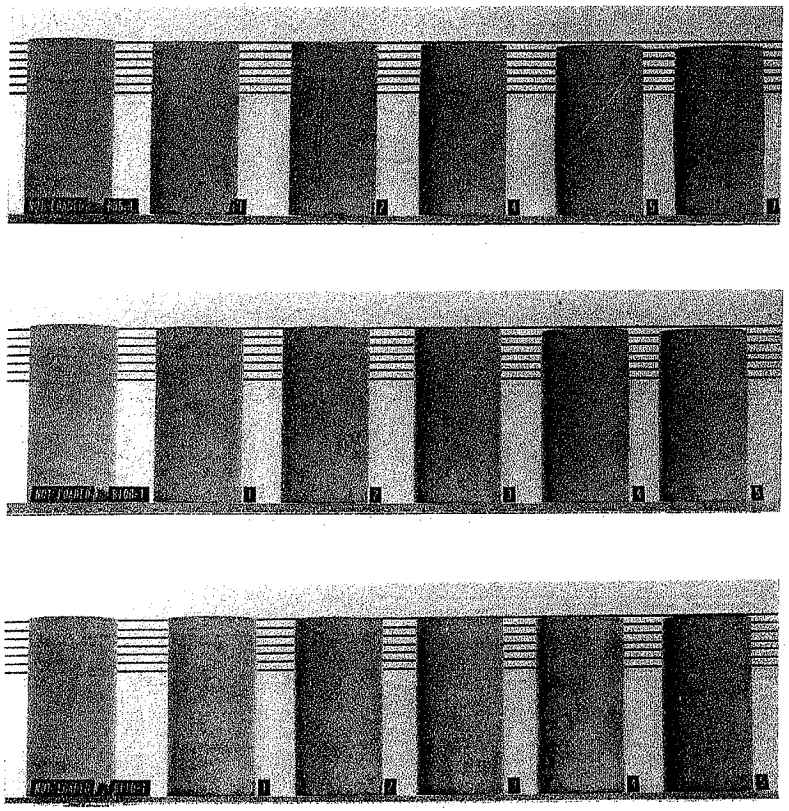

Fig. A.4.3: Test specimens B085-1 to B110-1, first part.

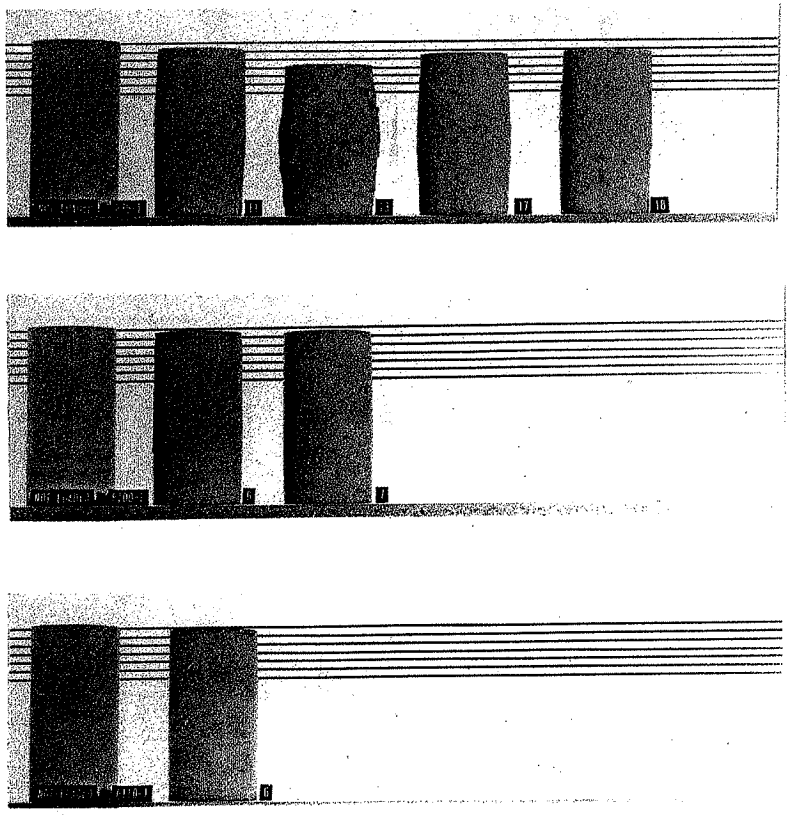

Fig. A.4.4: Test specimens B085-1 to B110-1, second part.

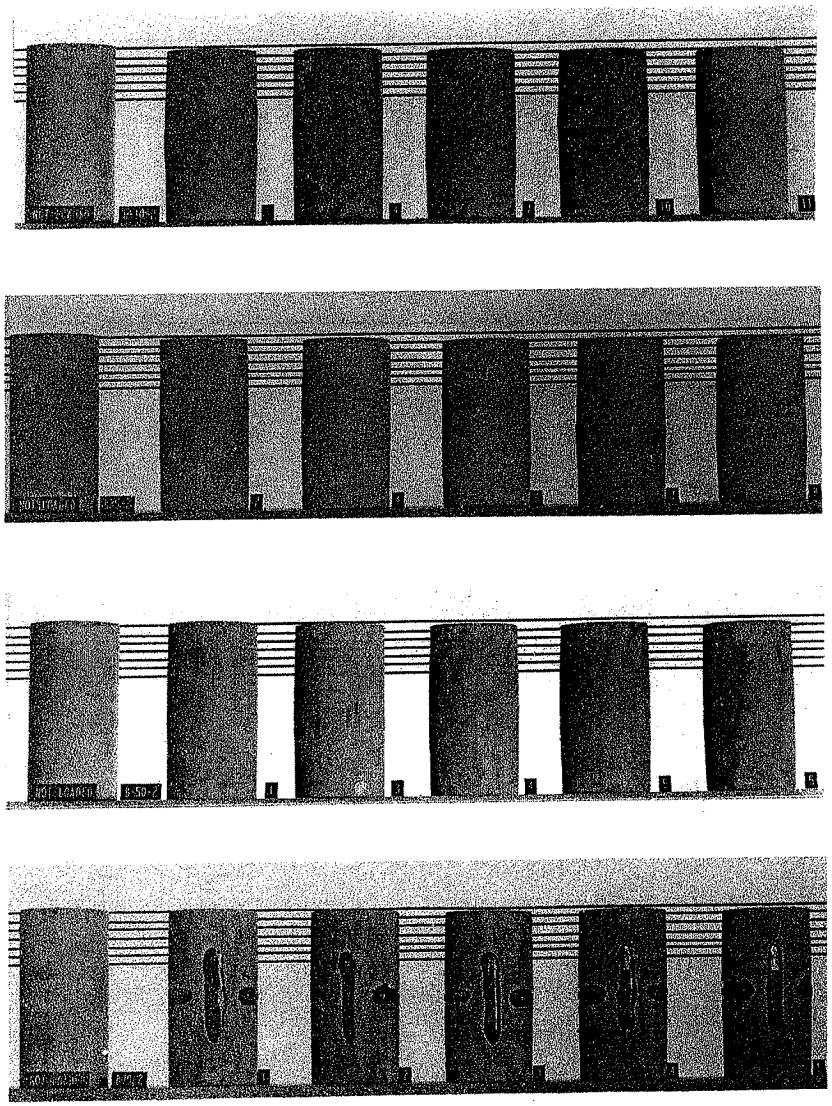

Fig. A.4.5: Test specimens B010-2 to B070-2, first part.

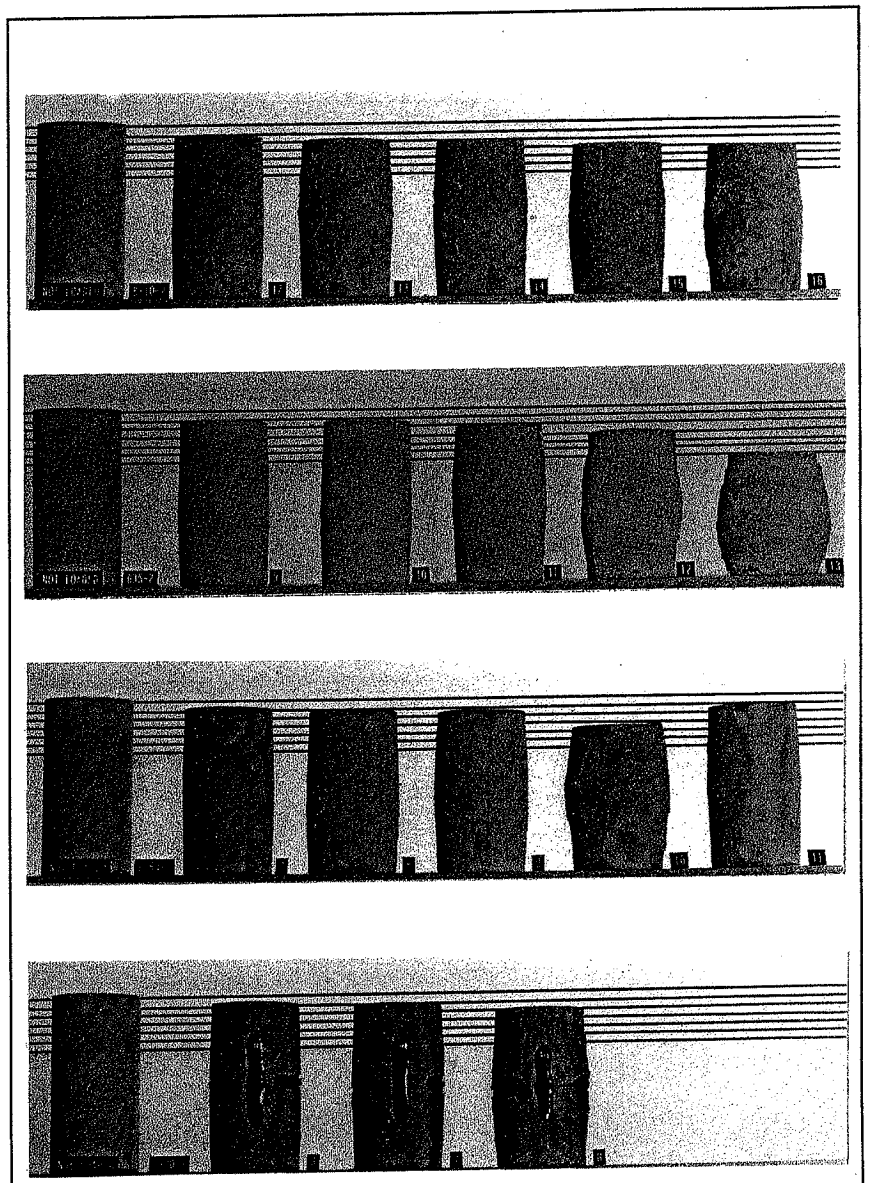

Fig. A.4.6: Test specimens B010-2 to B070-2, second part.

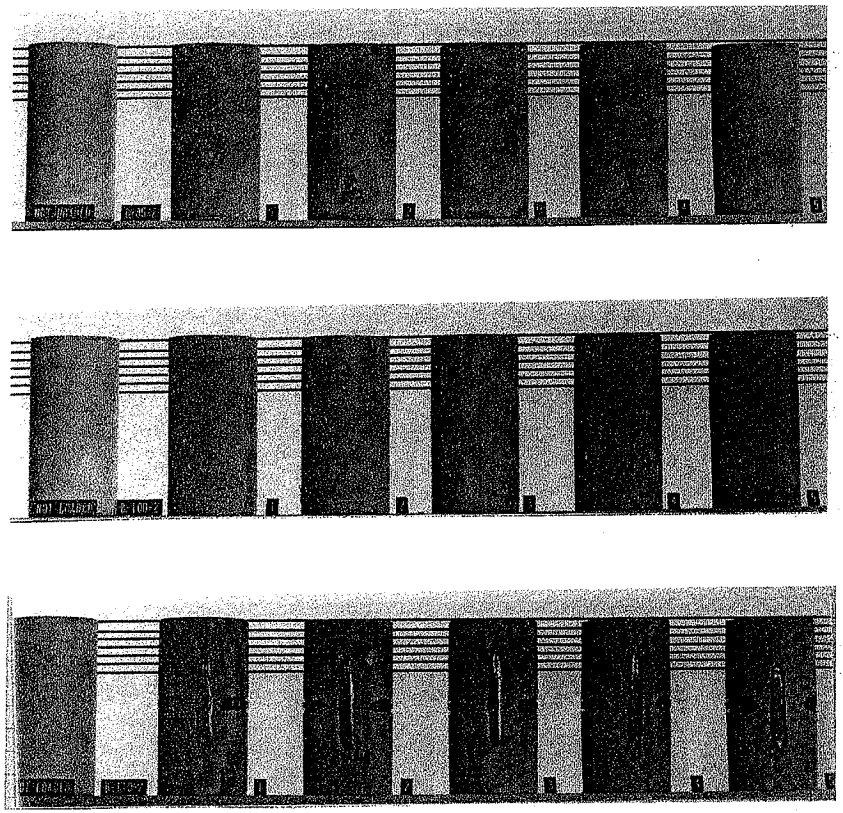

Fig. A.4.7: Test specimens B085-2 to B110-2, first part.

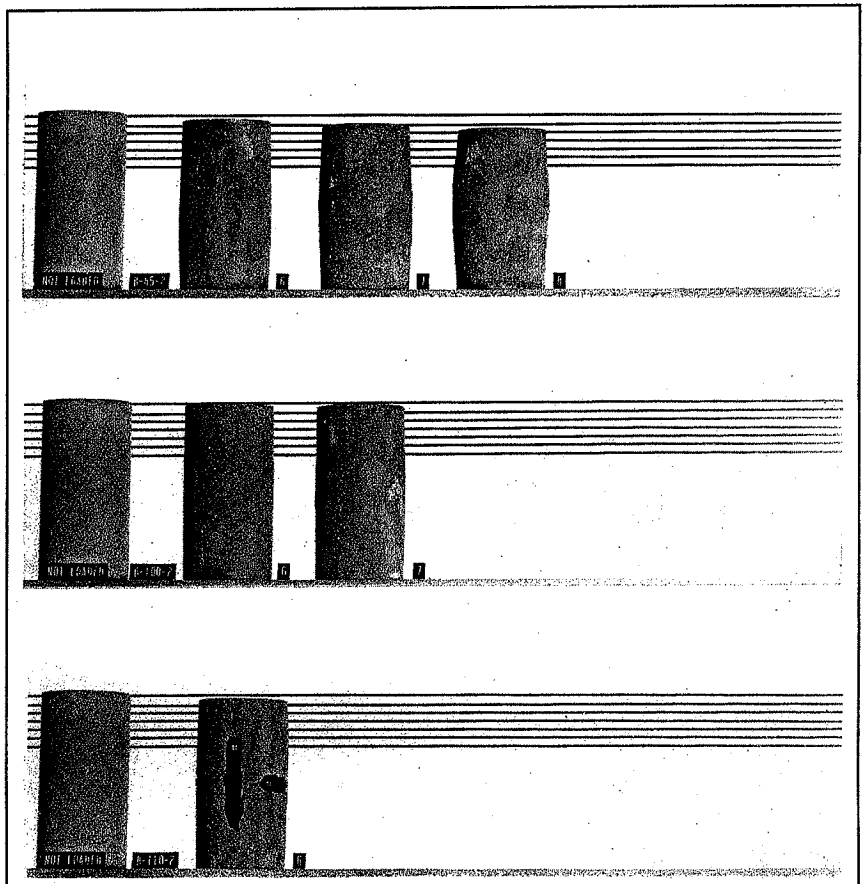

Fig. A.4.8: Test specimens B085-2 to B110-2, second part.

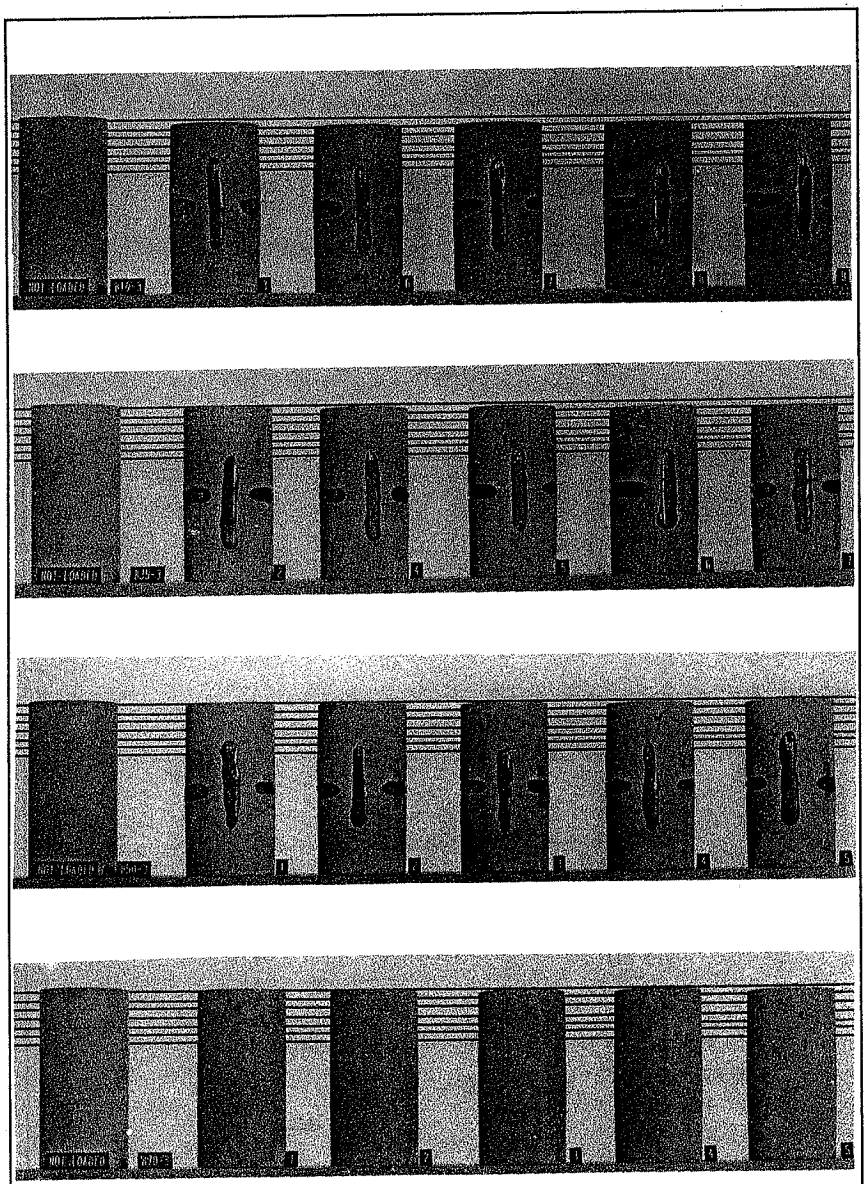

Fig. A.4.9: Test specimens B010-3 to B070-3, first part.

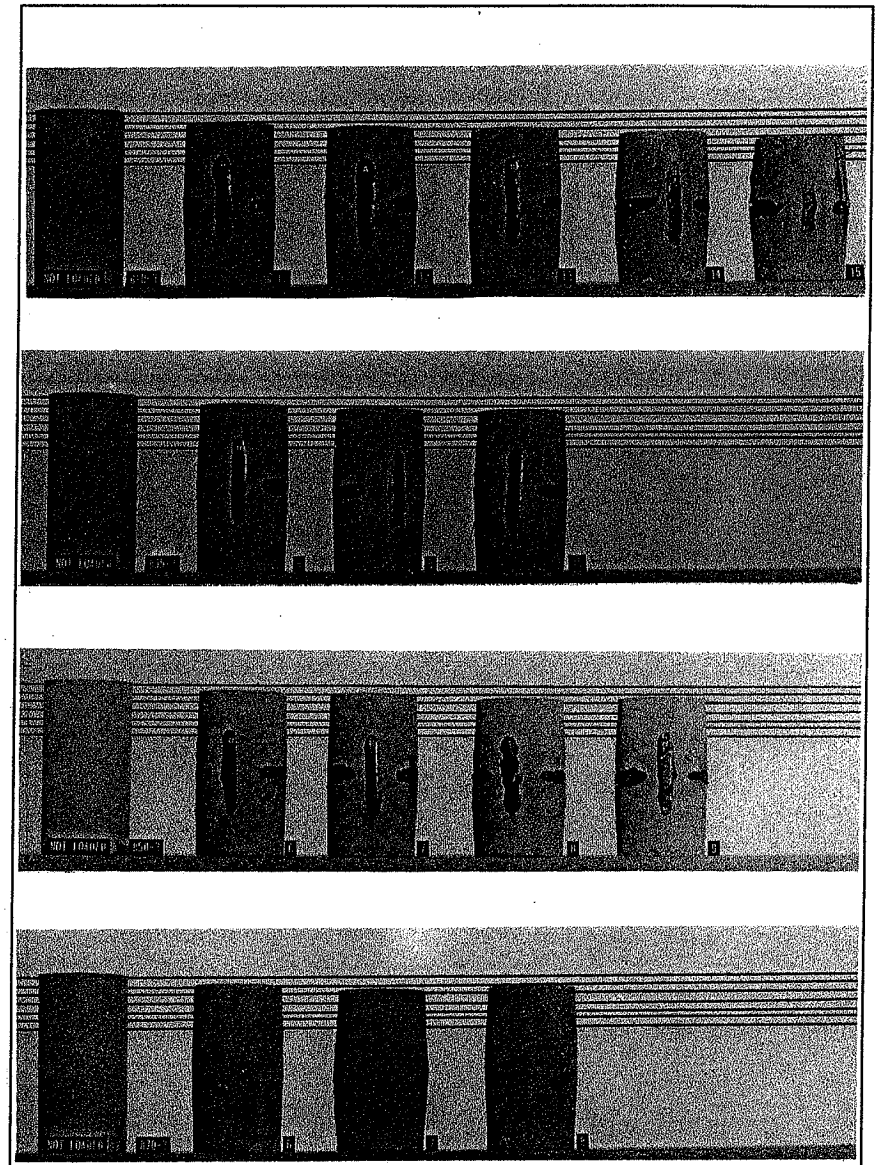

Fig. A.4.10: Test specimens B010-3 to B070-3, second part.

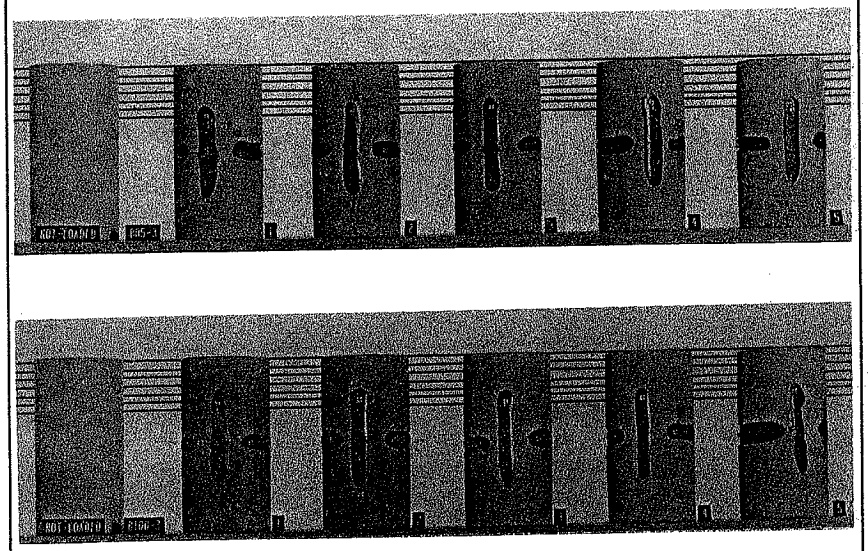

Fig. A.4.11: Test specimens B085-3 to B100-3, first part.

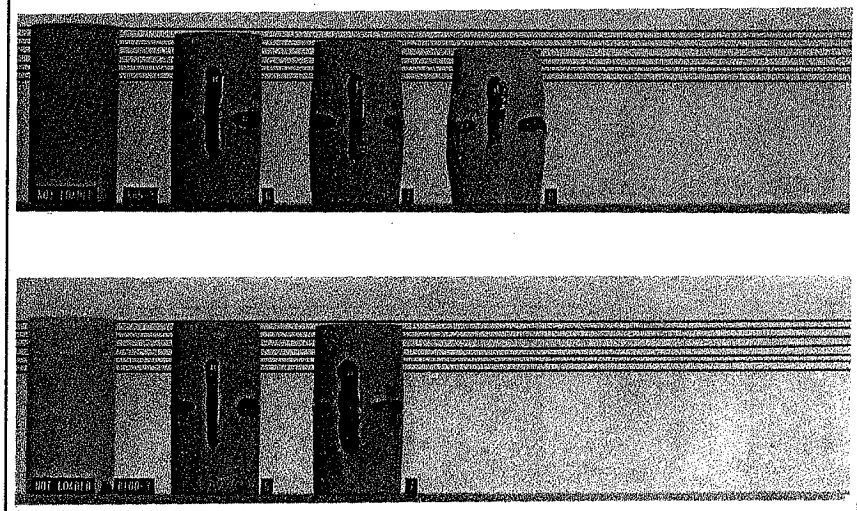

Fig. A.4.12: Test specimens B085-3 to B100-3, second part.

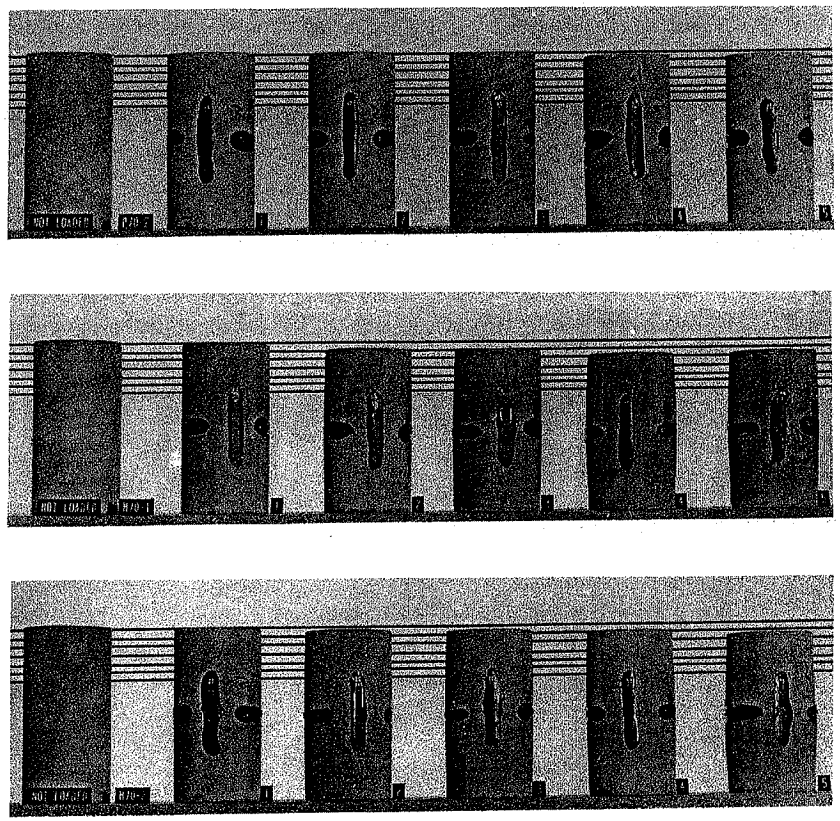

Fig. A.4.13: Test specimens paste and mortars, first part.

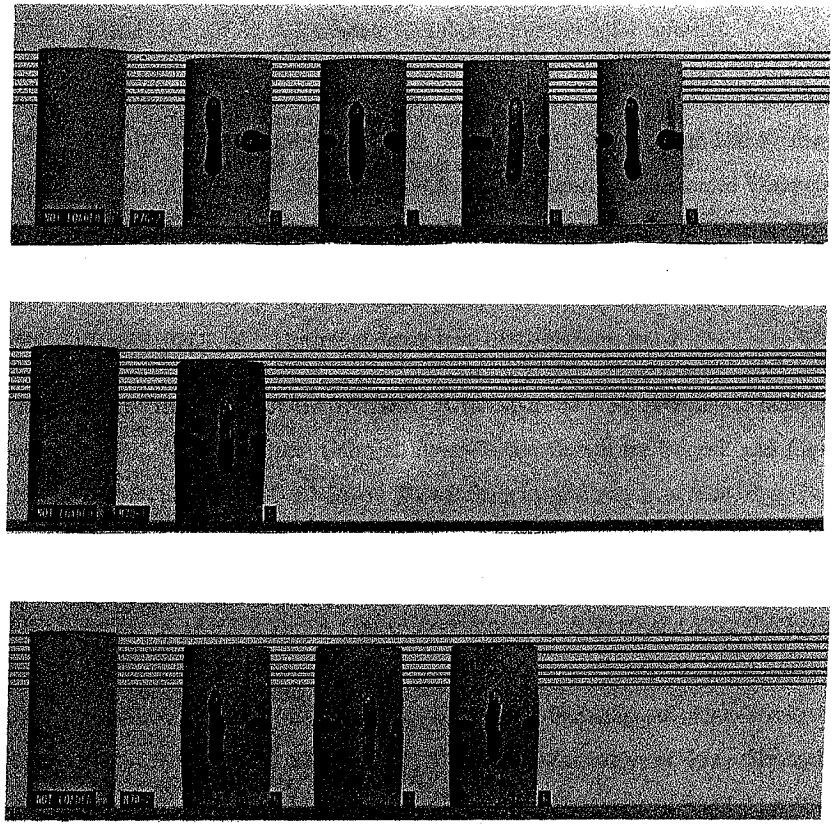

Fig. A.4.14: Test specimens paste and mortars, second part.

AFDELINGEN FOR BÆRENDE KONSTRUKTIONER
DANMARKS TEKNISKE HØJSKOLE

Department of Structural Engineering
Technical University of Denmark, DK–2800 Lyngby

SERIE R
(Tidligere: Rapporter)

R 271. VILMANN, OLE: A Harmonic Half–Space Fundamental Solution. 1991.
R 272. VILMANN, OLE: The Boundary Element Method applied in Mindlin Plate Bending Analysis. 1991.
R 273. GANWAY, CHEN, ANDREASEN, B.S., NIELSEN, M.P.: Membrane Actions Tests of Reinforced Concrete Square Slabs. 1991.
R 274. THOUGÅRD PEDERSEN, NIELS, AGERSKOV, H.: Fatigue Life Preduction of Offshore Steel Structures under Stochastic Loading. 1991.
R 275. ANDREASEN, B.S., NIELSEN, M.P.: Arch Effect in Reinforced Concrete one–way Slabs. 1991.
R 276. ASKEGÅARD, VAGN: Prediction of Initial Crack Location in Welded Fatigue Test Specimens by the Thermoelastic Stress Analysis Technique. 1991.
R 277. NIELSEN, KARSTEN: Analyse af Skråstagsbroers egenvægtstilstand, 1991.
R 278. NIELSEN, LEIF OTTO: Continuummechanical Lagrangian finite elements. 1991.
R 279. RIBERHOLT, H.: Limtræ af dansk træ, HQL–planker, Del 2.
R 280. RIBERHOLT, H., ENQUIST, B., GUSTAFSSON, P.J., JENSEN, RALPH BO: Timber beams notches at the support, December 1991.
R 281. RIBERHOLT, H., JOHANNESEN, JOHANNES M.: Fingerskarrede rammehjørner i limtræ. 1992.
R 282. DAHL, KAARE K.B.: Uniaxial Stress–Strain Curves for Normal and High Strength Concrete. 1992.
R 283. DULEVSKI, DAVID ENCHO: Global Structural Analysis of Steel Box Girder Bridges. 1992.
R 284. Resumeoversigt 1991 – Summaries of Papers 1991.
R 285. DAHL, KAARE K.B.: The Calibration and Use of a Triaxial Cell. 1992.
R 286. DAHL, KAARE K.B.: A Failure Criterion for Normal and High Strength Concrete. 1992.
R 287. DAHL, KAARE K.B.: A Constitutive Model for Normal and High Strength Concrete. 1992.
R 288. JENSEN, HENRIK ELGAARD: State–of–the–ark Rapport for Højstyrkebetons Svind og Krybning. 1992.
R 289. JENSEN, HENRIK ELGAARD: Creep and Shrinkage of High–Strength Concrete; A testreport. 1992.
R 290. JENSEN, HENRIK ELGAARD: Creep and Shrinkage of High–Strength Concrete; A testreport; Appendix A. 1992.
R 291. JENSEN, HENRIK ELGAARD: Creep and Shrinkage of High–Strength Concrete; A testreport; Appendix B. 1992.
R 292. JENSEN, HENRIK ELGAARD: Creep and Shrinkage of High–Strength Concrete; A testreport; Appendix C. 1992.
R 293. JENSEN, HENRIK ELGAARD: Creep and Shrinkage of High–Strength Concrete; A testreport; Appendix D. 1992.
R 294. JENSEN, HENRIK ELGAARD: Creep and Shrinkage of High–Strength Concrete; An Analysis. 1992.
R 295. JENSEN, HENRIK ELGAARD: State–of–the–art Rapport for Revnet Betons Styrke. 1992.
R 296. IBSØ, JAN BEHRENDT & RASMUSSEN, LARS JUEL: Vridning af armerede normal– og højstyrkebetonbjælker. 1992.
R 297. RIBERHOLT, HILMER, JOHANNESEN, JOHANNES MORSING & RASMUSSEN, LARS JUEL: Rammehjørner med indlimede stålstænger i limtræ. 1992.

Abonnement 1.7.1992 – 30.6.1993 kr. 130,–
Subscription rate 1.7.1992 – 30.6.1993 D.Kr. 130.–.

Hvis De ikke allerede modtager Afdelingens resumeoversigt ved udgivelsen, kan Afdelingen tilbyde at tilsende næste års resumeoversigt, når den udgives, dersom De udfylder og returnerer nedenstående kupon.

Returneres til
Afdelingen for Bærende Konstruktioner
Danmarks tekniske Højskole
Bygning 118
2800 Lyngby

Fremtidig tilsendelse af resumeoversigter udbedes af
(bedes udfyldt med blokbogstaver):

Stilling og navn: .....

Adresse: .....

Postnr. og -distrikt: .....

The Department has pleasure in offering to send you a next year's list of summaries, free of charge. If you do not already receive it upon publication, kindly complete and return the coupon below.

To be returned to:
Department of Structural Engineering
Technical University of Denmark
Building 118
DK-2800 Lyngby, Denmark.

The undersigned wishes to receive the Department's
List of Summaries:
(Please complete in block letters)

Title and name .....

Address.....

Postal No. and district.....

Country.....